

OAK RIDGE NATIONAL LABORATORY LIBRARY



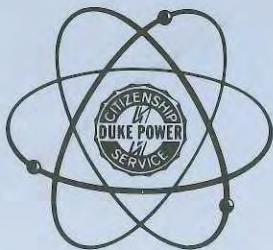
3 4456 0033863 1

DOE/ET/34212-41
BAW-1810
April 1984
UC-78

Urania Gadolinia : Nuclear Model Development and Critical Experiment Benchmark



OAK RIDGE NATIONAL LABORATORY
CENTRAL RESEARCH LIBRARY
CIRCULATION SECTION
4500N ROOM 175
LIBRARY LOAN COPY
DO NOT TRANSFER TO ANOTHER PERSON
If you wish someone else to see this
report, send in name with report and
the library will arrange a loan.
UCN-7969 (3-9-77)



Prepared For
U.S. Department Of Energy
Under Contract DE-AC02-78ET34212

Babcock & Wilcox
a McDermott company

DOE/ET/34212-41
BAW-1810

April 1984
UC-78

Urania-Gadolinia:
Nuclear Model Development and
Critical Experiment Benchmark

L. W. Newman
Project Engineer

Prepared For
U.S. Department of Energy
Under Contract DE-AC02-78ET34212

By

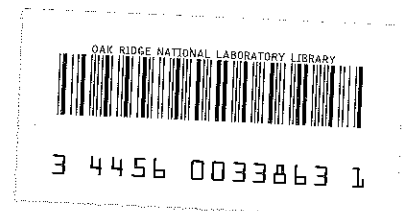
BABCOCK & WILCOX
Utility Power Generation Division
P. O. Box 1260
Lynchburg, Virginia 24505

BABCOCK & WILCOX
Research and Development Division
Lynchburg Research Center
P. O. Box 1260
Lynchburg, Virginia 24505

Submitted By

BABCOCK & WILCOX
Contract Research Division
P. O. Box 835
Alliance, Ohio 44601

DUKE POWER COMPANY
P. O. Box 33189
Charlotte, North Carolina 28482



Babcock & Wilcox
a McDermott company

ACKNOWLEDGEMENTS

The work reported herein is the product of the efforts of many individuals at The Babcock & Wilcox Company, Duke Power Company, and the U.S. Department of Energy. The authors gratefully recognize their help and efforts in the Extended-Burnup Program. In particular, the efforts of R. G. Snipes, J. D. Kortheuer, and T. Snead of Duke Power Company, and P. M. Lang of the Department of Energy are acknowledged.

Principal Authors

L. W. Newman
W. A. Wittkopf
W. G. Pettus
M. N. Baldwin
H. A. Hassan
V. O. Uotinen
J. D. Connell
P. S. Campbell

Babcock & Wilcox
Utility Power Generation Division
Lynchburg, Virginia

Report BAW-1810

April 1984

Urania-Gadolinia:
Nuclear Model Development and
Critical Experiment Benchmark

L. W. Newman

Key Words: Urania-Gadolinia Fuel, Critical Experiment,
Pressurized Water Reactor

ABSTRACT

The Babcock & Wilcox Company, Duke Power Company, and the U.S. Department of Energy are participating in an extended-burnup program for pressurized water reactors that will develop an advanced fuel assembly design. This advanced fuel assembly uses a UO_2 - Gd_2O_3 burnable absorber fuel mixture along with other state-of-the-art fuel performance and uranium utilization-enhancing design features including annular fuel pellets, annealed guide tubes, Zircaloy intermediate grids, and removable upper end fittings. As part of this program, a nuclear model for calculating the behavior of UO_2 - Gd_2O_3 was developed, and critical experiments were conducted to provide beginning-of-life data for benchmarking the model. This report describes the nuclear model, the critical experiments, and the comparison of data between the model and the experiments. This comparison confirmed the accuracy of the standard two-group, diffusion theory model for predicting global and discrete UO_2 - Gd_2O_3 effects provided the cross sections used in the model were generated with sufficiently detailed and sophisticated methods.

CONTENTS

	Page
1. INTRODUCTION	1-1
2. SUMMARY	2-1
3. DESCRIPTION OF CRITICAL FACILITY AND CORE COMPONENTS	3-1
3.1. Introduction	3-1
3.2. Critical Experiments Facility	3-1
3.3. 2.46 wt % Enriched Fuel Rod	3-2
3.4. 4.02 wt % Enriched Fuel Rods	3-3
3.5. Solid Urania-Gadolinia Fuel Rods	3-4
3.6. Annular Urania-Gadolinia Fuel Rods	3-4
3.7. Ag-In-Cd Rods	3-4
3.8. B ₄ C Rods	3-4
3.9. Void Tubes	3-5
4. EXPERIMENTAL MEASUREMENTS/RESULTS	4-1
4.1. Introduction	4-1
4.2. Core Loading Patterns	4-1
4.3. Reactivity Worth Measurements	4-3
4.4. Midplane Power Distribution Measurements	4-3
4.5. Incore Detector Measurements	4-5
4.6. Radial Power Profile Through a Fuel Pellet	4-6
4.7. U-238 Resonance Integral Measurements	4-6
4.7.1. Experimental Results	4-6
4.7.2. Evaluation of Resonance Integral Experimental Results	4-9
5. NUCLEAR MODEL DEVELOPMENT AND VERIFICATION	5-1
5.1. Introduction	5-1
5.2. Gadolinium Depletion Chains	5-1
5.3. Neutron Cross Section Data for Gadolinium	5-2
5.4. Developing an Adjustment Factor for Higher-Order Effects	5-2
5.5. Thermal Flux Factors	5-3
6. COMPARISON OF MEASURED AND CALCULATED RESULTS	6-1
6.1. Introduction	6-1
6.2. Measured and Calculated Reactivity Worths Comparison	6-1
6.3. Measured and Calculated Radial Power Comparisons	6-2
6.4. Summary and Conclusions	6-4
7. REFERENCES	7-1
APPENDIX	A-1

List of Tables

Table		Page
3-1.	Physical Properties of 2.46 wt % Enriched UO ₂ Fuel Rods	3-6
3-2.	Physical Properties of 4.02 wt % Enriched UO ₂ Fuel Rods	3-7
3-3.	Physical Properties of Ag-In-Cd Rods	3-8
3-4.	Certified B ₄ C Analysis for Total Boron and Total Carbon	3-8
4-1.	Cores Loaded During Experimental Program	4-15
4-2.	Measured Reactivity Worths of Gd Fuel Rods Using 2.46 wt % Enriched Fuel Region	4-18
4-3.	Measured Reactivity Worth of Ag-In-Cd and Void Pins Using 2.46 wt % Enriched Fuel Region	4-19
4-4.	Measured Reactivity Worths of Gd Fuel Rods Using 2.46/4.02 wt % Enriched Fuel Regions	4-20
4-5.	Measured Reactivity Worths of B ₄ C Rods Using 2.46/4.02 wt % Enriched Fuel Regions	4-21
4-6.	Basic Fuel Rod Scan Data from Core 1	4-22
4-7.	Basic Fuel Rod Scan Data from Core 5	4-23
4-8.	Basic Fuel Rod Scan Data from Core 12	4-24
4-9.	Basic Fuel Rod Scan Data from Core 14	4-25
4-10.	Basic Fuel Rod Scan Data from Core 18	4-26
4-11.	Basic Fuel Rod Scan Data from Core 20	4-28
4-12.	Core 1 Normalized Midplane Power Distribution Through Center Assembly	4-29
4-13.	Core 5 Normalized Midplane Power Distribution Through Center Assembly	4-30
4-14.	Core 5 Normalized Midplane Power Distribution Along Core Diagonal	4-31
4-15.	Core 12 Normalized Midplane Power Distribution Through Center Assembly	4-32
4-16.	Core 14 Normalized Midplane Power Distribution Through Center Assembly	4-33
4-17.	Core 14 Normalized Midplane Power Distribution Along Core Diagonal	4-34
4-18.	Core 18 Normalized Midplane Power Distribution Through Center Assembly	4-35
4-19.	Core 20 Normalized Midplane Power Distribution Through Center Assembly	4-36
4-20.	Core 20 Normalized Midplane Power Distribution Along Core Diagonal	4-37
4-21.	Comparison of Incore Detector Response	4-38
4-22.	Measured Fission Distribution Through UO ₂ -Gd ₂ O ₃ Fuel Pellet	4-39
4-23.	Measured Fission Distribution Through 2.46 wt % Enriched UO ₂ Fuel Pellet	4-40
4-24.	Dimensions of Pellets for Resonance Integral Measurements	4-41
4-25.	Resonance Integral Data Reduction	4-42
4-26.	Results of the Resonance Integral Measurements	4-43
4-27.	Parameters of Overlapping U-238 and Cd Resonances	4-44
4-28.	Estimate of Cadmium Shadowing Effect	4-45
5-1.	Characteristics of Natural Gadolinium	5-4
6-1.	Measured and Calculated Worths of Absorber Rods in Various Configurations	6-6

List of Tables

Table	Page
6-2. Measured and Calculated Worth of 16 Control Rods in Various Gd Configurations	6-7
6-3. Comparison of Normalized Relative Power Densities for Center Assembly, Core 1 - without UO_2 - Gd_2O_3	6-8
6-4. Comparison of Normalized Relative Power Density for Center Assembly, Core 5 - with Gd_2O_3	6-9
6-5. Comparison of Measured and Predicted Fuel Rod Relative Power Density Distribution Along Core Diagonal, Core 5	6-10
6-6. Comparison of Normalized Relative Power Densities for Center Assembly, Core 12 - without UO_2 - Gd_2O_3	6-11
6-7. Comparison of Normalized Relative Power Densities for Center Assembly, Core 14 - with Gd_2O_3	6-12
6-8. Midplane Relative Power Density Distribution Along Core Diagonal, Core 14	6-13
A-1. Measured and Calculated Reactivity Worths of Gadolinia-bearing Rods	A-5
A-2. RPDs on the Main Diagonals of Core 5	A-6

List of Figures

Figure	
3-1. Vertical Section Through Core Tank	3-9
3-2. CX-10 Moderator Fill System	3-10
4-1. Core 1 Loading Diagram	4-46
4-2. Core 2 Loading Diagram	4-47
4-3. Core 3 Loading Diagram	4-48
4-4. Core 4 Loading Diagram	4-49
4-5. Core 5 Loading Diagram	4-50
4-6. Core 5-A Loading Diagram	4-51
4-7. Core 5-B Loading Diagram	4-52
4-8. Core 6 Loading Diagram	4-53
4-9. Core 6-A Loading Diagram	4-54
4-10. Core 7 Loading Diagram	4-55
4-11. Core 8 Loading Diagram	4-56
4-12. Core 9 Loading Diagram	4-57
4-13. Core 10 Loading Diagram	4-58
4-14. Core 11, U-238 Resonance Integral Measurements Core Configuration	4-59
4-15. Core 12 Loading Diagram	4-60
4-16. Core 13 Loading Diagram	4-61
4-17. Core 14 Loading Diagram	4-62
4-18. Core 15 Loading Diagram	4-63
4-19. Core 16 Loading Diagram	4-64
4-20. Core 17 Loading Diagram	4-65
4-21. Core 18 Loading Diagram	4-66
4-22. Core 19 Loading Diagram	4-67
4-23. Core 20 Loading Diagram	4-68

List of Figures

Figure		Page
4-24.	Incore Detector Assembly	4-69
4-25.	All-Solid Incore Neutron Detector	4-70
4-26.	Radial Power Distribution Through Fuel Pellet	4-71
4-27.	Comparison of Solid and Annular Fuel U-238 Resonance Integral	4-72
4-28.	Neutron Spectrum in the Test Position	4-73
4-29.	Comparison of U-238 and Cd Resonance Structures	4-74
4-30.	Schematic of Actual and Ideal Sample Configurations	4-75
4-31.	Emergent Flux Cones from a Uniform Isotopic Source Region	4-76
4-32.	Linear Regression Results with all Points Equally Weighted	4-77
5-1.	U-235 Concentration Vs Pellet Radius and Burnup	5-5
5-2.	Gadolinium Worth Vs Burnup	5-6
5-3.	Gadolinium Multigroup Nuclear Library Generation	5-7
5-4.	Gd-157 Concentration Vs Pellet Radius and Burnup	5-8
5-5.	Gd-158 Concentration Vs Pellet Radius and Burnup	5-9
5-6.	Difference in k_{∞} Vs Time Step Size and Burnup	5-10
5-7.	Difference in Gadolinium Worth Vs Time Step Size and Burnup	5-11
6-1.	Gadolinia Worth Measured Vs Calculated - No CRAs In Core.	6-14
6-2.	Measured and Calculated Control Rod Worth	6-15
6-3.	Radial Power Distribution Through UO_2 Fuel Pellet	6-16
6-4.	Radial Power Distribution Through UO_2 - Gd_2O_3 Fuel Pellet	6-17
6-5.	Comparison of Measured and Predicted ² Fuel Rod Powers Along Core 5 Diagonal	6-18
6-6.	Comparison of Measured and Predicted Fuel Rod Powers Along Core 14 Diagonal.	6-19
A-1.	Boron Concentration Measured Vs Calculated.	A-7
A-2.	Gd Worth Measured Vs Calculated	A-8
A-3.	Comparisons of Measured and Predicted Normalized Relative Power Densities for Core 1.	A-9
A-4.	Comparisons of Measured and Predicted Normalized Relative Power Densities for Core 5.	A-10
A-5.	Comparison of Measured and Predicted Relative Fuel Rod Powers Along Core Diagonal.	A-11

1. INTRODUCTION

For light water reactors, increased fuel burnup is the most straightforward and readily employable way to reduce the number of spent fuel assemblies discharged each year. The pressurized water reactor (PWR) industry traditionally has discharged fuel with batch-average burnups of 33,000 MWd/mtU; however, increasing average burnups from 33,000 to 50,000 MWd/mtU reduces the generation of spent fuel assemblies by about 40% annually, uses about 15% less yellowcake (U_3O_8), and 1 to 3% fewer separative work units for U-235 enrichment.

In supporting extended burnup, the U.S. Department of Energy (DOE) has initiated programs to verify the burnup capability of various fuel assembly designs and collect fuel performance data at burnups above 50,000 MWd/mtU. One such program, which includes Duke Power Company (Duke) and The Babcock & Wilcox Company (B&W), combines state-of-the-art extended-burnup technology to design, fabricate, and irradiate an advanced PWR fuel assembly containing urania-gadolinia ($UO_2-Gd_2O_3$). As part of this DOE/Duke/B&W Extended-Burnup Program, a nuclear model was developed for calculating the behavior of $UO_2-Gd_2O_3$ in the PWR environment. To verify this model at beginning-of-life conditions, critical experiments were conducted. This report contains the data from the critical experiments, a description of the nuclear model, and comparisons of the experimental and calculational results.

Section 2 summarizes the information herein. The critical facility and core components are described in section 3. The core configurations and the measurements performed under this program are described in section 4. The nuclear models developed to analyze the behavior of $UO_2-Gd_2O_3$ are described in section 5, and the comparisons of calculated and measured results are presented in section 6. The Appendix contains a comparison of the measured results with predictions from the Electric Power Research Institute Advanced Recycle Methodology Program (EPRI-ARMP) code system.

2. SUMMARY

B&W, Duke, and the DOE are participating in a program to develop an advanced fuel assembly design incorporating $\text{UO}_2\text{-Gd}_2\text{O}_3$ for extended burnup in PWRs.¹⁻⁴ As part of this program, a nuclear model was developed for calculating the neutronics of PWRs using $\text{UO}_2\text{-Gd}_2\text{O}_3$, and an extensive program of measurements was performed to provide benchmark data for verifying the accuracy of the model.

A total of 23 different critical core configurations were studied. The measurements taken for benchmarking the nuclear models included:

1. Reactivity worths of $\text{UO}_2\text{-Gd}_2\text{O}_3$, control, and void rods,
2. Core radial power distributions (RPDs),
3. Radial power profiles within a $\text{UO}_2\text{-Gd}_2\text{O}_3$ pellet,
4. U-238 resonance integrals for solid and annular UO_2 and $\text{UO}_2\text{-Gd}_2\text{O}_3$ fuel pellets, and
5. Rhodium incore detector signals.

The nuclear cross-section generator developed to predict the behavior, reactivity worth, and depletion characteristics of $\text{UO}_2\text{-Gd}_2\text{O}_3$ fuel uses integral transport theory and has a cylindrical, multi-region geometry. Space- and energy-dependent cross sections are derived using this model and adjusted for higher-order, multi-group, and flux depression effects before use in the diffusion theory models for core design.

Comparisons of results obtained from the critical experiments with those predicted by the model showed that the model accurately predicts the beginning-of-life behavior of $\text{UO}_2\text{-Gd}_2\text{O}_3$ fuel.

Specifically, the results are as follows:

1. Gadolinium worths without control rods present for core configurations having 2.46 wt % enriched UO_2 were predicted within 1.35%, or 2 ppm boron, which is the experimental measurement uncertainty for individual moderator samples. For those cores containing an inner zone of 4.02 wt % enriched

UO₂ and an outer zone of 2.46 wt % enriched UO₂, the gadolinium worths were predicted within 4.5%, or 11 ppm boron, of those measured.

2. Gadolinium worths with Ag-In-Cd control rods present were predicted within 4.5%, or 4 ppm boron of those measured. Gadolinium worths with B₄C control rods present were predicted within 1.9%, or 9 ppm boron, of those measured.
3. Differences in the measured and predicted relative radial powers of rods within the center assembly for the reference cores without UO₂-Gd₂O₃ rods were small (RMS_{ΔRPD} = 0.015); cores with UO₂-Gd₂O₃ rods had larger relative power differences than those exhibited in the reference cores (RMS_{ΔRPD} = 0.022).
4. The RMS_{ΔRPD} of fuel rods on main diagonals are comparable to the values for the RMS_{ΔRPD} for the center assembly of the respective cores.
5. The difference between the measured maximum relative power and the power predicted for that location is 0.047 RPD, or 4.1%.
6. The radial power profiles through UO₂ and UO₂-Gd₂O₃ fuel pellets were predicted to within 5%.

The comparisons of measured and calculated data have verified that the modeling techniques and models used to predict the nuclear (nondepletion) characteristics of UO₂-Gd₂O₃ fuel and a core containing UO₂-Gd₂O₃ fuel are accurate. The two-group, diffusion theory methodology used in core design can accurately predict UO₂-Gd₂O₃ effects provided appropriate adjustments are made to the cross-section inputs. These adjustments should at least account for the differences between reaction rates predicted by detailed geometry, transport theory versus those predicted by coarse-mesh, diffusion theory, and include higher-order effects (P₁ versus P₀ scattering approximations) as well as the effect of a multi-epithermal group structure (31 versus 1). These results provide added assurance that the methods and model described herein can be used to design and analyze gadolinia-loaded PWR assemblies without impacting existing nuclear uncertainties.

3. DESCRIPTION OF CRITICAL FACILITY AND CORE COMPONENTS

3.1. Introduction

The critical experiments described in this report were conducted at B&W's Lynchburg Research Center. The critical experiments facility and the nuclear instrumentation and control system are described in section 3.2. Descriptions of the various fuel, control, and void rods are provided also. Specifically, UO_2 fuel rods having either 2.46 wt % or 4.02 wt % U-235 enriched fuel are discussed in sections 3.3 and 3.4, respectively. Fuel rods containing either solid or annular UO_2 - Gd_2O_3 fuel pellets are discussed in sections 3.5 and 3.6, respectively. Absorber rods, either Ag-In-Cd or B_4C , and void tubes are described in sections 3.7, 3.8, and 3.9, respectively.

3.2. Critical Experiments Facility

The various core configurations were constructed inside a 5-foot inside diameter (ID) by 6.5-foot high core tank with 0.5-inch thick aluminum walls (Figure 3-1). The core tank is located inside a steel tank 9 feet in diameter and is supported on a skirt that holds it about 30 inches above the base of the larger tank. The top and bottom "egg-crate" grid plates consist of 1.0-inch wide slotted aluminum strips interlocked to form a square matrix. The strips are 0.160-inch thick and are spaced on 0.644 ± 0.002 -inch centers. A 2-inch thick aluminum base plate, one inch above the bottom of the core tank, supports the fuel rods. Moderator heights are referenced from the top of this base plate.

Figure 3-2 shows the moderator fill system used. The maximum pump capacity is about 35 gpm. Except for the 4,500-gallon dump tank, which is constructed of amercoated carbon steel, the moderator system components are either aluminum or stainless steel.

The safety blades are 0.08-inch thick boral, 7.9 inches wide by 70.9 inches long. All blades are thin enough to pass between the rows of fuel rods, and webs are cut in the top grid to allow blade entry. During these experiments, the blades perform a safety function only and are fully withdrawn during operation.

The nuclear instrumentation and control system is basically the same as that used in earlier light water experiments.⁵ The neutron detectors are conventional pulse counters and ionization chambers located at the outside wall of the core tank in standpipes.

The moderator level in the core tank is sensed by a remotely operated conductivity probe. The probe is moved by a Selsyn motor driven by a manually operated Selsyn transmitter at the control console. The moderator level indicated at the console by a Veeder Root counter is calibrated to an accuracy of ± 0.1 inch. Incremental changes in moderator level can be measured to an accuracy of ± 0.01 inch.

Excess reactivity was controlled by dissolving boric acid (H_3BO_3) in the demineralized water moderator. The boron concentration in parts per million (ppm) is defined as the grams of natural boron per 10^6 cm³ of moderator at 25C. The boron concentration was determined by titration against a standard KOH solution.

3.3. 2.46 wt % Enriched Fuel Rod

These fuel rods are aluminum tubes filled with sintered pellets of 2.46 wt % U-235 enriched UO_2 . Aluminum plugs 0.125-inch thick are welded to the ends to seal the tubes. The one-inch space between the top pellet and the end plug is filled with Kaowool.

Table 3-1 is a summary of the physical properties of the fuel rods based on measurements of randomly selected samples. The standard deviation $\sigma(x)$ and standard deviation of the mean $\sigma(\bar{x})$ were computed from the equations:

$$\sigma^2(x) = \frac{\Sigma(x - \bar{x})^2}{N - 1}$$

$$\sigma^2(\bar{x}) = \frac{\Sigma(x - \bar{x})^2}{N(N - 1)}$$

The impurities are given as the summation of $N_i \sigma_i$ where N_i is the concentration of each impurity per cm^3 of the oxide fuel, and σ_i is the corresponding microscopic absorption cross section at 2200 m/s.

The physical and chemical properties of the fuel rods reported herein are taken from reports of an earlier experimental program at B&W.^{6,7} Additional details are given in the references.

3.4. 4.02 wt % Enriched Fuel Rods

These fuel rods are 4.02 wt % U-235 enriched UO_2 swaged in stainless steel tubes. The physical and chemical properties of these rods have been analyzed in prior experimental programs at B&W^{8,9} and are summarized in Table 3-2. The uncertainties are one standard deviation of the mean obtained from vendor quality control data and check measurements on randomly selected samples. The impurities are given as the summation of $N_i \sigma_i$, where N_i is the concentration of each impurity per cm^3 of the oxide fuel and σ_i is its microscopic absorption cross section.

Since the fuel rods were swaged and, thus, have no fuel gap, the fuel diameters were obtained by measuring the cladding outside and wall thicknesses. Although the outside diameter (OD) was constant, the wall thicknesses measured by a conductivity method were appreciably larger near the rod ends.⁹ The average cladding thickness between 15 and 55 inches was 15.9 ± 0.5 mils, but the average between 4 and 67 inches was 16.6 ± 0.6 mils. The value listed in Table 3-2 is the \cos^2 -weighted average between 4 and 67 inches.

The top and bottom end caps of the fuel rods are each approximately 2.35 inches long and consist of stainless steel thimbles filled with either aluminum or stainless steel plugs. Approximately 20% of the end caps are stainless steel. No distinction is being made in the experiments since the reactivity differences have been shown to be negligible.⁹

3.5. Solid Urania-Gadolinia Fuel Rods

The solid $UO_2-Gd_2O_3$ fuel rods are aluminum tubes filled with sintered fuel pellets containing approximately 4 wt % gadolinia and 96 wt % urania enriched in U-235 to 1.944 wt % nominal (variation was from 1.929 to 1.956 wt % U-235). The pellets are 0.4055 ± 0.001 -inch diameter by 0.59 ± 0.10 -inch long. The 63-inch long tubes are 0.475-inch OD by 0.032-inch wall, type 6063 aluminum. Aluminum plugs 1/8-inch thick are welded in the ends to seal the tubes. The minimum pellet stack length is 60.4 inches, and the space between the top pellet and the end plug is void.

3.6. Annular Urania-Gadolinia Fuel Rods

The annular $UO_2-Gd_2O_3$ fuel rods are identical to the solid $UO_2-Gd_2O_3$ fuel rods except that they contain annular pellets with an ID of 0.130 ± 0.005 inch.

3.7. Ag-In-Cd Rods

The Ag-In-Cd absorber rods are 0.400 inch in diameter by 62 inches long and have a nominal composition of 80 wt % Ag, 15 wt % In, and 5 wt % Cd. The calculated macroscopic thermal cross section is 13.6 cm^{-1} . The alloy rods are clad with 0.475-inch OD by 0.032-inch wall, type 6063 aluminum. The aluminum is sealed at the bottom by a 1/8-inch thick aluminum plug (welded in place) and at the top by a removable cork. Table 3-3 summarizes the physical properties of the Ag-In-Cd rods.

3.8. B_4C Rods

The B_4C absorber rods are 0.438-inch OD by 0.035-inch wall aluminum tubes filled with natural B_4C powder ranging from 30 to 50 mesh. The bottom ends are sealed with welded aluminum plugs and the tops with a removable cork plug. Each rod contains 156g of B_4C , which constitutes a column long enough to span the full core height. The space within the rod above the B_4C is void and extends about 1 foot above the moderator level. In all rods, the B_4C is compacted to 2.233 ± 0.003 g/inch. A certified chemical analysis of the B_4C is given in Table 3-4.

3.9. Void Tubes

These 63-inch long tubes are 0.475-inch OD by 0.032-inch wall, type 6063 aluminum. The tubes are sealed by a 1/8-inch thick aluminum plug welded in place at the bottom to exclude water. The tops are sealed by O-ring fitted lead weights, which also prevent the tubes from floating. These weights are located well above the moderator level in the core.

Table 3-1. Physical Properties of 2.46 wt % Enriched UO₂ Fuel Rods

<u>Parameter</u>	<u>Value</u>
Outside diameter, in.	0.4748 ±0.0006
Wall thickness, in.	0.032 ±0.001
Wall material	6061 aluminum
Pellet (fuel) diameter, in.	0.4054 ±0.0005
Total length, in.	61.59 ±0.16
Active fuel length, in.	60.37 ±0.35
Weight of fuel, g/rod	1305.5 ±1.0
U/UO ₂ , wt %	88.13 ±0.01
Enrichment, U-235/U, wt %	2.459 ±0.002
Weight of U-235, g/rod	28.29 ±0.02
Pellet (fuel) density, g/cm ³	10.24 ±0.04
$\sum N_i \sigma_i$ (summation of impurities), cm ² /cm ³ oxide	<10 ⁻³

Table 3-2. Physical Properties of 4.02 wt % Enriched UO₂ Fuel Rods

<u>Parameter</u>	<u>Value</u>
Outside diameter, in.	0.4755 ±0.0015
Wall thickness, in.	0.0160 ±0.0005 ^(a)
Wall material	Type 304 stainless steel
Fuel diameter, in.	0.444 ±0.002
Total length, in.	71.5
Active fuel length, in.	66.7 ±0.3
Weight of fuel, g/rod	1600 ±2
Weight of uranium, g/rod	1408 ±2
Weight of U-235, g/rod	56.61 ±0.10
Enrichment, U-235/U, wt %	4.020 ±0.005
Fuel density, g/cm ³	9.46 ±0.10
$\sum N_i \sigma_i$ (summation of impurities), cm ² /cm ³ oxide	<5 x 10 ⁻⁴

(a) Cos²-weighted average.

Table 3-3. Physical Properties of Ag-In-Cd Rods

<u>Parameter</u>	<u>Value</u>
Length, in.	62.03 ±0.00
Diameter, in.	0.400 ±0.000
Weight, g	1296 ±5
Analysis, wt %	
Silver	79.68
Indium	15.09
Cadmium	5.2
Copper	0.05
Zinc	0.016
Lead, nickel, tin, iron aluminum, bismuth	0.001

Table 3-4. Certified B₄C Analysis for Total Boron and Total Carbon

	<u>Sample</u>			<u>Average</u>
	<u>1</u>	<u>2</u>	<u>3</u>	
Total boron, %	78.1	77.7	77.6	77.8
Total carbon, %	20.8	20.9	20.8	20.8
Anhydrous B ₂ O ₃ , %	0.10	0.10	0.10	0.10
Boron plus carbon, %	98.9	98.6	98.4	98.6

Figure 3-1. Vertical Section Through Core Tank

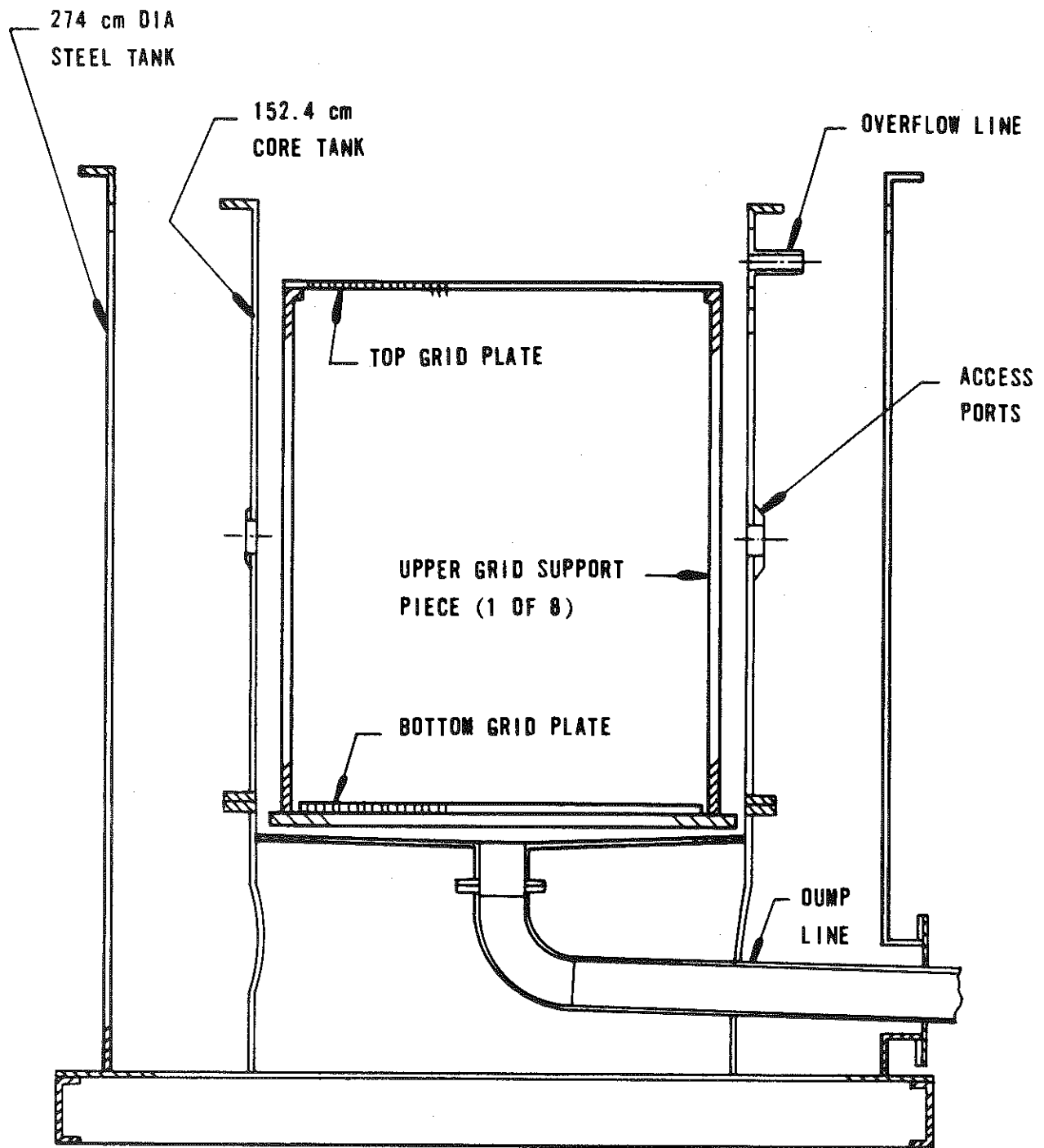
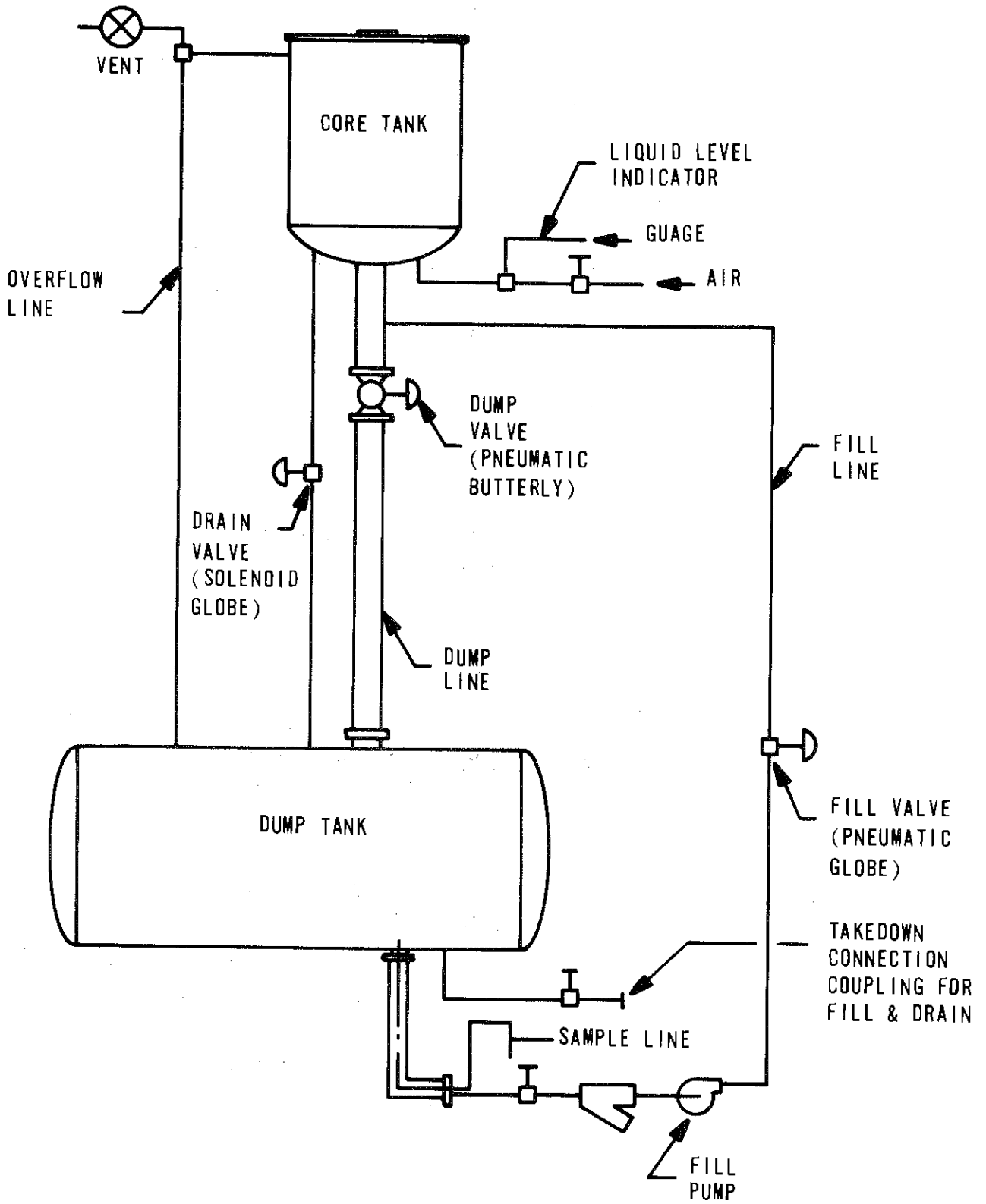


Figure 3-2. CX-10 Moderator Fill System



4. EXPERIMENTAL MEASUREMENTS/RESULTS

4.1. Introduction

Experimental data suitable for benchmarking the nuclear models used to license UO_2 - Gd_2O_3 fuel assemblies were generated under this task. In 22 of the 23 cores studied, UO_2 - Gd_2O_3 fuel rods (either solid and/or annular), Ag-In-Cd rods, B_4C rods, void tubes, and water holes were spaced on selected patterns in an otherwise uniform clean lattice to study their effect on reactivity, power distribution, and incore detector signal.

To study the effect on the U-238 resonance integral of removing the center of UO_2 pellets and adding gadolinia to UO_2 pellets, room temperature measurements were undertaken in a specially designed core. These measurements constitute the first known resonance integral measurements for hollow UO_2 pellets and for solid and hollow UO_2 - Gd_2O_3 pellets.

This section presents the experimental measurements and results. The core loading patterns for the 23 cores analyzed are described in section 4.2. Reactivity worth, midplane (radial) power, and incore detector measurements are discussed in sections 4.3 through 4.5. Section 4.6 describes measurements of the radial power profile through a fuel pellet (both UO_2 and UO_2 - Gd_2O_3). Section 4.7 presents the measurement and analysis of the U-238 resonance integral for UO_2 and UO_2 - Gd_2O_3 solid and annular fuel pellets.

4.2. Core Loading Patterns

A total of 23 cores were assembled under this task. (See Figures 4-1 through 4-23 for loading diagrams.) Table 4-1 includes a brief description of each core, the components, and the moderator boron required for each core to be critical when the moderator level is 57.1 inches (145.0 cm), and the temperature is 77F (25C).

A special core, designated core 11, was assembled for the resonance integral measurements. A loading diagram of this core is shown in Figure 4-14. The core contained a total of 554 2.46 wt % U-235 enriched fuel rods loaded on a square pitch of 0.644 inch. To provide a central water region, 36 fuel rod

positions in the center of the core are unoccupied by fuel rods. A 0.625-inch OD by 0.065-inch wall aluminum tube, sealed at the bottom to exclude water, is located along the core's axial centerline with the open end extending well above the moderator level.

The remaining 22 cores simulate a full PWR checkerboard loading of assemblies containing UO_2 - Gd_2O_3 fuel rods. The center of each of these cores can be divided by imaginary lines into nine "fuel assemblies." Five of these assemblies contain varying numbers of UO_2 - Gd_2O_3 fuel rods. To provide generic data germane to all domestic PWR designs, each core loading is a variation of two basic configurations:

1. Babcock and Wilcox Configurations

- 1a. 15x15 Fuel Rods per Assembly Using 2.46 wt % Enriched Fuel

The basic core (core 1) used for the 15x15 configuration measurements consists of 4808 fuel rods. Imaginary lines divide the center of the core into nine "fuel assemblies," 15 lattice pitches square. A pattern of vacant fuel rod positions in each "fuel assembly," simulates an instrument hole and 16 control rod guide tube positions. Cores 2 through 10 are variations of the basic core.

- 1b. 15x15 Fuel Rods per Assembly Using 2.46 and 4.02 wt % Enriched Fuel

The basic core (core 12) used is similar to the one described above except that the central zone contains 4.02 wt % U-235 fuel rods and the outer portion contains 2.46 wt % U-235 fuel rods. Cores 13 through 17 are variations of this basic core.

2. Combustion Engineering Configuration

The basic core (core 18) used is a 16x16 configuration and consists of 4620 fuel rods. Imaginary lines divide the center of the core into nine identical "fuel assemblies," 16 lattice pitches square. Large water holes have been created by omitting multiple fuel rods. Cores 19 and 20 are variations of this basic core.

4.3. Reactivity Worth Measurements

The change in the moderator boron concentration is used as a measure of reactivity change since boron concentration can be readily and accurately measured. Excess reactivity is controlled by dissolving boric acid (H_3BO_3) in the moderator (demineralized water). The boron concentration in parts per million (ppm) is defined as the grams of natural boron per million cm^3 of moderator at 25C; it is determined by titration against a standard KOH solution.

The moderator boron concentrations given in Table 4-1 are those that produce a critical condition when the moderator is at a height of 57.1 inches and the safety blades are fully withdrawn (i.e., they are above the moderator). In addition to the standard deviation shown for the boron concentration, a systematic bias which may be as large as 0.2% existed. This bias cancels when differences are calculated.

Reactivity worths for UO_2 - Gd_2O_3 , Ag-In-Cd, and B_4C rods and void tubes are determined by comparing the boron concentration of the moderator of the critical base core with that for the critical core loading of interest. These are tabulated in Tables 4-2 through 4-5.

4.4. Midplane Power Distribution Measurements

Relative midplane power distribution measurements were made for the base configuration having either 2.46 or 4.02 wt % U-235 in the 15x15 design, and the 16x16 design (cores 1, 12, and 18). Also measured were three cores similar to the base configuration but having UO_2 - Gd_2O_3 fuel, cores 5 and 14 with 12 UO_2 - Gd_2O_3 fuel rods per assembly, and core 20 with 16 UO_2 - Gd_2O_3 fuel rods per assembly. An incore detector assembly was loaded along the axial centerline of these cores. The incore detector assembly, similar to that used in B&W-designed PWRs, is illustrated in Figure 4-24. The assembly contains seven rhodium detectors (almost equally spaced along the vertical axis of the core), a background detector, a thermocouple, and a central calibration tube. Stainless steel filler rods are located between the end cap of the assembly and the ends of the detectors. The outer sheath is 0.316-inch OD and has a 0.031-inch wall thickness. The calibration tube is 0.125-inch OD by 0.093-inch ID.

The relative power profiles within the cores were determined by counting collimated fission product gammas from activated fuel rods with an NaI(Tl) scintillation counter. Gamma photons with less than 250 keV were discriminated out. The collimator consisted of a 1-inch diameter hole in a 2-inch thick lead shield placed between the fuel rod and the detector so that only the gammas from a 1.0-inch segment of the rod were counted. The detector was surrounded by at least 4 inches of lead, and other portions of the fuel rod were shielded from the detector by at least another 5 inches of lead. The rods were rotated while being counted to provide data that were independent of rod orientation. So that all fuel rod activations could be performed at a constant moderator height, the boron concentration was adjusted to make the core critical at a moderator height of approximately 55 inches. Activations were then made on an exponential period obtained by raising the moderator height to 57.10 ± 0.05 inches. The integrated exposure was about 1 kW minute. The background activity was kept low by always loading essentially unirradiated fuel rods in the positions to be studied.

Decay corrections were obtained from a "master" fuel rod, irradiated simultaneously with the rods to be scanned, and then counted in a second counting system. The second system was identical to the first in collimation and electronics. Counts were taken on the two systems simultaneously, and the master rod was never moved during the data acquisition of a given run. A standard fuel rod, recounted at frequent intervals, provided data to correct for any small changes in either system.

The basic rod scan data are presented in Tables 4-6 through 4-11. The average value for each fuel rod position tabulated is the result of three reactor runs. Locations of individual rods are identified by lattice coordinates indicating the number of rod pitches from the center of the core and the direction. For example, S6E7 indicates that the rod is located six rod pitches south by 7 rod pitches east of the core center. The standard deviation of the average value for each position averages 0.003. The results presented in Tables 4-6 through 4-11 have not been corrected for the difference in counting efficiency of the various types of fuel rods.

Counting efficiency difference is due to the differences in the radial power profile through the types of fuel pellets, cladding material, and thickness. This difference has been evaluated by dissolving fuel from each fuel rod type, determining the fission product activity of the solution, and comparing the results with a fuel rod scan. Correction factors derived from these comparisons were then applied to the fuel rod scan data. Thus, for core 5, the scan results from $\text{UO}_2\text{-Gd}_2\text{O}_3$ fuel had to be adjusted by a factor of 0.960 ± 0.010 to make it comparable with the scan results from 2.46 wt % enriched UO_2 fuel. Similarly for cores 14 and 20, the scan results from $\text{UO}_2\text{-Gd}_2\text{O}_3$ fuel had to be adjusted by 0.985 ± 0.017 , and the scan results from 2.46 wt % enriched UO_2 fuel had to be adjusted by a factor of 1.026 ± 0.014 to make them comparable with the scan results from 4.02 wt % enriched UO_2 fuel.

These correction factors have been applied to the data presented in Tables 4-12 through 4-20 and, in addition, the data have been normalized so that the average power of the fuel rods within the center assembly is unity.

4.5. Incore Detector Measurements

Incore detector measurements were collected for the base configurations (cores 1, 12, and 18) and the $\text{UO}_2\text{-Gd}_2\text{O}_3$ -bearing cores designated 5, 14, and 20 to determine the effect of $\text{UO}_2\text{-Gd}_2\text{O}_3$ fuel rods on the ratio of detector signal to assembly power. These measurements were made with a rhodium incore detector (Figure 4-25) located outside the calibration tube of the detector assembly as described in section 4.4. The rhodium emitter was located at a reproducible position at mid-core height. Background corrections were measured with a background detector identical in construction to the rhodium detector except that the Inconel lead wire extends into the region otherwise occupied by the rhodium emitter.

The ratio of measured background-corrected detector signal per unit of power in the standard fuel rod for the paired cores is presented in column 3 of Table 4-21. The last column of the table shows the ratio when the power in the paired cores is normalized (as in Tables 4-12 through 4-20) so that the total powers in the center assembly are identical.

4.6. Radial Power Profile Through a Fuel Pellet

Radial power profile measurements were made along the radii of both $\text{UO}_2\text{-Gd}_2\text{O}_3$ and 2.46 wt % enriched UO_2 fuel pellets to determine the degree to which the presence of Gd_2O_3 influences the profile in fresh fuel. For these measurements, unirradiated pellets were loaded at mid-core height along the axial centerline of core 5, within a special fuel rod which could be disassembled. On the day following each irradiation, the sample pellet was removed. Samples along the radii were taken in one of two ways: (1) drilling with a small diamond-core bit (producing a core of approximately 0.060-inch diameter) or (2) by surface etching with acid. These samples were dissolved in concentrated nitric acid and diluted to exactly 10 ml of volume for counting. Samples representing the average were made by dissolving the entire pellet in 200 ml of acid and taking a 10 ml aliquot for counting.

Counting was done with a Ge(Li) spectrometer, and La-140 to U-235 activity ratios, corrected for decay, were used as the measure of power. Data from different pellets were normalized by the activity of monitor foils which were present during each irradiation. Results are tabulated in Tables 4-22 and 4-23 and are plotted in Figure 4-26.

Based on the reproducibility of measurements in the interior of the pellets, each point-to-average fission ratio has an estimated standard deviation of approximately 3%. The scatter in the surface measurements of pellets containing Gd_2O_3 is believed to be due to actual differences in the Gd_2O_3 content at the pellet surfaces.

4.7. U-238 Resonance Integral Measurements

4.7.1. Experimental Results

Implementing extended-burnup fuel cycles will probably involve using annular fuel pellets and a gadolinium burnable absorber. Therefore, as part of this program, room-temperature measurements were undertaken to compare the uranium-238 resonance integral in solid and annular pellets with and without

the gadolinium burnable absorber. These measurements constitute the first known resonance integral measurements for hollow UO_2 pellets and for $UO_2-Gd_2O_3$ pellets. This task was performed to determine:

1. Whether or not the U-238 resonance integral of annular UO_2 pellets follows Hellstand's correlation for solid UO_2 pellets¹⁰, and
2. To what extent the addition of Gd_2O_3 to UO_2 pellets affects the U-238 resonance integral.

Six types of pellets were fabricated with various annulus sizes. Each pellet was 0.3685 ± 0.0005 -inch OD and was approximately 0.5 inch long. Four pellet types were composed exclusively of UO_2 depleted in U-235 (0.2 wt % U-235), while the remaining two types also contained 7.99 wt % Gd_2O_3 . Table 4-24 gives the dimensions of the pellets for which resonance integral measurements were made.

A special core configuration, designated core 11, was assembled for these measurements. A loading diagram of this special core is shown in Figure 4-14. Sample pellets inside a cadmium-lined capsule were irradiated at mid-core height in the test location. At least 1.75 inches of water isolated the sample pellets from the nearest fuel rod of the lattice, thus eliminating Dancoff shielding and providing a 1/E neutron spectrum in the resonance region.

As a test to assure that negligible thermal flux was present inside the cadmium-lined capsule, bare and cadmium-covered gold foils were irradiated inside the capsule, and a cadmium ratio of 1.006 ± 0.005 for the 0.005-inch thick foils was obtained. A comparison of the thermal-to-resonance capture cross sections of the foils and the UO_2 pellets shows that between 0.1 and 0.7% of the U-238 captures occurring in the UO_2 pellets of this experiment are from thermal neutrons. Thermal captures by U-238 in the pellets containing 7.99 wt % Gd_2O_3 are assumed to be zero since the Gd_2O_3 will further suppress the thermal neutron flux within these pellets.

A column of five pellets was loaded inside a tight-fitting, cadmium-lined aluminum capsule that was precisely positioned at core center inside the

open-ended aluminum tube. Cadmium thickness was 0.020 inch nominal and 0.019 inch minimum. Of the five pellets loaded, the three central pellets were of the same type, and the end pellets were always solid UO_2 to prevent neutron streaming along the fuel annulus. The pellets were activated by bringing the core to a power level of 500 watts.

Following activation, the center pellet was removed, dissolved in nitric acid, diluted to precisely 200 ml of solution, transferred to a counting bottle, and counted on an NaI scintillation spectrometer. The background-corrected and decay-corrected 106 keV photopeak was a measure of the relative U-238 capture rate. Three half-life determinations and an examination of the spectra with a Ge(Li) spectrometer confirmed the spectral purity of the sample over the area of interest that extended from 94.5 to 115.5 keV.

Background counts were determined from an unirradiated pellet that had been dissolved in nitric acid. The background correction for each sample was assumed proportional to its UO_2 content.

Counts under the photopeak were collected for three separate 1,000-second counting intervals, then corrected for UO_2 background and decay using a half-life of 2.35 days. These corrected counts are tabulated in the second column of Table 4-25. Division by the UO_2 pellet mass and the core power during activation resulted in the relative resonance integral values given in the last column of this table. The uncertainties listed are one standard deviation of the average. Table 4-26 summarizes the measurements. The resonance integral measurements have been normalized by a factor of 9.0244 so that an unweighted linear least-squares fit of the UO_2 data agrees with the Hellstrand correlation for the solid UO_2 pellets.

An additional normalization factor of 1.004 ± 0.003 has also been applied to the UO_2 - Gd_2O_3 pellet data to correct for the small thermal flux inside the cadmium-lined capsule during the UO_2 pellet irradiation. Normalized results are presented in Table 4-26 and Figure 4-27. The Hellstrand correlation for solid UO_2 pellets agrees very well with the measured values for UO_2 annular pellets. The U-238 resonance integral for pellets containing 7.99 wt % Gd_2O_3 , however, is approximately 6% lower than the Hellstrand correlation prediction.

This heretofore unrecognized effect was observed for both solid and annular $\text{UO}_2\text{-Gd}_2\text{O}_3$ pellets and is not due to the reduced UO_2 content of the pellet since all data were normalized to the actual UO_2 content. Although the cause of the difference has not been positively established, it is believed to be due to a partial overlap in several U-238 resonances by gadolinium resonances (the U-238 resonance is overlapped by Gd-155 resonance at 6.7 eV; the U-238 resonance is overlapped by both Gd-155 and Gd-157 resonances at 20.9 eV), and to the reduction of the $1/V$ component of the U-238 resonance integral by several low-energy gadolinium resonances (from the thermal energy range up to 6.67 eV).

4.7.2. Evaluation of Resonance Integral Experimental Results

Normal experimental corrections for exposure time, decay time, relative counting efficiency, etc., have been applied previously. This section evaluates several additional second-order effects.

Spectrum Effects

An ANISN¹¹ calculation with 111 energy groups was run to obtain the neutron spectrum in the test thimble. From this spectrum shown in Figure 4-28 and appropriate group cross sections generated by NULIF¹² for a solid UO_2 rod, the total U-238 absorption rate in the test position was calculated to be approximately 2.5% higher than an ideal $1/E$ spectrum with a sharp cutoff at 0.49 eV. Most of this excess absorption occurs in the high-energy region rather than in the thermal leak-through peak at about lethargy $u = 19$. A similar correction for the annular UO_2 samples is calculated under the assumption that the "surface" component is the same for all samples. The result is that the change in the spectrum correction from the solid sample to the 15% void sample is only about 0.03%. Since only the relative absorption is of interest in these experiments, the spectrum correction is negligible. This conclusion applies also to the $\text{UO}_2\text{-Gd}_2\text{O}_3$ samples except that a small relative correction, as described in section 4.7.1., is applied to account for the fact that the thermal leak-through component is annihilated by the gadolinium.

Interference From Cadmium Resonances

A comparison of the resonance structures for natural Cd and U-238 is given in Figure 4-29. An examination of the respective resonance parameters¹³ reveals only three significant resonances in U-238 that are partially overlapped by cadmium resonances. The basic parameters of these resonances are given in Table 4-27. Also given is the peak capture cross section and the resonance integral for each resonance to generally indicate the relative importance of these resonances and their overlap effects. These quantities do not account for isotopic abundance, self-shielding, or Doppler broadening. Also, the resonance integrals are calculated in the symmetric resonance approximation. The isotopic abundances of Cd-111 and Cd-112 are 12.75 and 24.07%, respectively; these factors reduce the shadowing effects proportionately.

As shown in Table 4-28, the estimated reduction of the total resonance absorption due to cadmium shadowing of the three resonances above is on the order of 1%. The additional cadmium shadowing in other regions should be much less than 1%. Since only the relative absorption of the various samples with respect to that of the solid UO₂ sample is of interest, the cadmium resonance shadowing correction is about the same for all samples; thus, this correction is negligible.

Scattering From The End Buffer Regions

The experimental samples were configured with a solid pellet at each end to prevent neutron streaming down the center hole from the outside medium. The resonance absorption rate at the inner surface of the sample pellet in this configuration is essentially the same as that for an ideal infinitely long annular rod.

The two configurations are illustrated in Figure 4-30. The incident resonance neutron contributions arriving through identical solid angles $d\Omega$ at an arbitrary point on the inner surface of the sample pellet are

formulated below. Uniform isotropic scattering is assumed and the absorption mean free path of the scattered neutrons (in the resonance peaks) is assumed to be much less than the pellet wall thickness.

For the test configuration, the contribution entering $d\Omega$ through da , is given by

$$dQ_1 \approx c \phi\left(\frac{\pi}{2} - \theta\right) \frac{da_1 \sin\theta}{r_1^2}$$

and for the infinitely long annular rod, it is

$$dQ_2 \approx c \phi(\theta) \frac{da_2 \cos\theta}{r_2^2}$$

where the constant c is the same in both relations. But considering the same solid angle in both cases,

$$\frac{da_1 \sin\theta}{r_1^2} \approx \frac{da_2 \cos\theta}{r_2^2} = d\Omega.$$

Also, $\phi\left(\frac{\pi}{2} - \theta\right) = \phi(\theta)$ for a uniform isotropic source in an infinite half-space. This can be seen from the diagram in Figure 4-31, where $d\Omega$ and $d\Omega'$ have equal magnitudes. Clearly, the emergent flux per unit solid angle is the same in any direction since the source in each case comes from identical cones. Therefore, $dQ_1 = dQ_2$ and the scattering contribution is the same at the sample pellet for both cases. The effect of scattering from the end buffer regions is essentially the same as that from the corresponding regions of an infinitely long hollow rod, and no correction is necessary.

Effect of Excess Potential Scattering

In the case of the UO_2 samples, the potential scattering σ_p differs slightly from the ideal value due to a non-stoichiometric oxygen-to-uranium (O/U) ratio. The O/U ratio for the UO_2 samples is 2.0067, which implies a value of the potential scattering per U-238 nucleus of $\sigma_p = 18.065$ barns. This is compared with a value of 18.00 barns for natural UO_2 and gives a change of $\sigma_p = 0.065$ barns.

From NULIF calculations, the rate of change of the UO_2 resonance integral with σ_p was determined to be approximated by

$$\frac{1}{RI} \frac{\partial RI}{\partial \sigma_p} \approx 5.26 \times 10^{-2} \text{ %/barn.}$$

Therefore, the effect of the excess potential scattering in the UO_2 samples is only about $5.26 \times 10^{-4} \times 0.065 = 0.0034\%$, which is clearly negligible.

Similar analysis for the UO_2 - Gd_2O_3 samples show the potential scattering per U-238 nucleus to be 19.83 barns. This is 1.83 barns greater than for the UO_2 samples and should result in a relative increase in the resonance integral of $5.26 \times 10^{-4} \times 1.83$, or 0.1%, which is also considered negligible in comparison with the other uncertainties.

Extraneous Activity

Fission product activity could potentially contribute to the observed integral counts from which the U-238 capture rates were deduced. Experiments confirmed this effect to be small because of the use of depleted uranium in the samples. The correction was found to be less than 0.3% in the worst case and was therefore neglected.

Error Analysis

The $\sqrt{S/M}$ and relative resonance integral values for each experimental sample are given in Table 4-26. For the UO_2 - Gd_2O_3 cases, the measured relative resonance integral values have been multiplied by a factor of 1.004 to compensate for the thermal leak-through component in the spectrum. All values of the relative resonance integrals were determined to be about the same precision (on the order of 0.5%), and they are given equal weight in the following error analysis.

Two different procedures can be used to determine the best linear correlations of the data: (1) use each measured relative resonance integral as a separate data point with equal weight in a least-squares fit, and (2) average the resonance integral values for each pellet type and perform a linear least-squares fit to the average values with each weighted by the reciprocal of its variance. These methods give slightly different but consistent results. The first procedure is adopted here since the $\sqrt{S/M}$ values for pellets of a given type are not all identical and since the second method does not permit the determination of finite confidence limits for the UO_2 - Gd_2O_3 case where there are only two different pellet types and the number of degrees of freedom ($n-2$) appears in the denominator of the expressions for the variance.

The regression analysis was performed according to the relations given by Birge¹⁴. Since the UO_2 and UO_2 - Gd_2O_3 data were distinctly different, they were analyzed separately. The results are shown in Figure 4-32.

For the UO_2 case, the regression line is given by

$$RI_{UO_2} = (3.06 \pm 2.07) + (28.7 \pm 3.1) \sqrt{S/M}$$

where the uncertainties are 1σ values. A 95% confidence interval¹⁵ about the regression line is also shown in Figure 4-32. These results are consistent with the Hellstrand correlation, which gives a slope of 26.3.

In the $UO_2-Gd_2O_3$ case, the regression line is given by

$$RI_{UO_2-Gd_2O_3} = (3.70 \pm 1.97) + (25.8 \pm 2.8) \sqrt{S/M}$$

The slope is consistent with that for UO_2 , but the regression line is shifted down by 6%.

Note that the uncertainty in the regression line at an arbitrary point is not determined by the uncertainties in the linear fitting parameters, but by equation 4.0 in reference 15.

Conclusions

A systematic analysis of the measured resonance integral data has been carried out and all known perturbing effects have been estimated. No significant corrections were found beyond those previously applied to the measured data. A final regression analysis of the data gives resonance integral correlations of

$$RI_{UO_2} = 3.06 + 28.7 \sqrt{S/M}$$

as the recommended expression for annular UO_2 fuel, and

$$RI_{UO_2-Gd_2O_3} = 3.70 + 25.8 \sqrt{S/M}$$

as the recommended expression for the $UO_2 - 7.99$ wt % Gd_2O_3 fuel.

Table 4-1. Cores Loaded During Experimental Program

Core	Core Description	No. of 2.46 wt % U-235 fuel pins	No. of 4.02 wt % U-235 fuel pins	No. of Gd fuel pins	No. of B ₄ C pins	No. of Ag-In-Cd pins	No. of void pins	No. of water holes	Moderator boron concentration, ppm
1	15x15, 0 Gd pin configuration	4808	0	0	0	0	0	153	1337.9 \pm 0.4
2	15x15, 0 Gd pin config., Ag-In-Cd in center assembly	4808	0	0	0	16	0	137	1250.0 \pm 1.0
3	15x15, 8 Gd pin config. checkerboard, 1/4 loading diagonals	4788	0	20	0	0	0	153	1239.3 \pm 0.7
4	15x15, 8 Gd pin config., checkerboard, 1/4 Gd loading in diagonals, Ag-In-Cd in center assembly	4788	0	20	0	16	0	137	1171.7 \pm 1.0
5	15x15, 12 Gd pin config., checkerboard, 1/4 Gd loading in diagonals	4780	0	28	0	0	0	153	1208.0 \pm 0.4
5A	15x15, 12 Gd pin config., checkerboard, 1/4 Gd loading diagonals	4776	0	32	0	0	0	153	1191.3 \pm 0.5
5B	15x15, 12 Gd pin config., checkerboard, 1/4 Gd loading in diagonals	4780	0	28	0	0	0	153	1207.1 \pm 1.0
6	15x15, 12 Gd pin config., checkerboard, 1/4 Gd loading in diagonals, Ag-In-Cd in center assembly	4780	0	28	0	16	0	137	1155.8 \pm 1.5
6A	15x15, 12 Gd pin config., checkerboard, 1/4 Gd loading in diagonals, Ag-In-Cd in center assembly	4776	0	32	0	16	0	137	1135.6 \pm 1.8
7	15x15, 12 Gd pin config., checkerboard, 1/4 Gd loading diagonals	4780	0	28 (Annular)	0	0	0	153	1208.8 \pm 0.5

4-15

Table 4-1. (Cont'd)

Core	Core Description	No. of 2.46 wt % U-235 fuel pins	No. of 4.02 wt % U-235 fuel pins	No. of Gd fuel pins	No. of B ₄ C pins	No. of Ag-In-Cd pins	No. of void pins	No. of water holes	Moderator boron concentration, ppm
8	15x15, 16 Gd pin config., checkerboard, 1/4 Gd loading in diagonals	4772	0	36	0	0	0	153	1170.7 \pm 0.5
9	15x15, 16 Gd pin config., checkerboard, 1/4 Gd loading in diagonals, Ag-In-Cd in center assembly	4772	0	36	0	16	0	137	1130.5 \pm 0.6
10	15x15, 16 Gd pin config., checkerboard, 1/4 Gd loading in diagonals, void pins in center assembly	4772	0	36	0	0	16	137	1177.1 \pm 0.6
11	Small, uniformly loaded core with approx. 3-in. diameter central, water-filled Resonance Integral Test Position	554	0	0	0	0	0	0	0.0
12	15x15, 0 Gd pin configuration	3920	888	0	0	0	0	153	1899.3 \pm 0.9
13	15x15, 0 Gd pin config., B ₄ C in center assembly	3920	888	0	16	0	0	137	1635.4 \pm 0.7
14	15x15, 12 Gd pin config., checkerboard, 1/4 Gd loading in diagonals	3920	860	28	0	0	0	153	1653.8 \pm 0.7
15	15x15, 12 Gd pin config., checkerboard, 1/4 Gd loading in diagonals, B ₄ C in center assembly	3920	860	28	16	0	0	137	1479.7 \pm 0.6
16	15x15, 16 Gd pin config., checkerboard, 1/4 Gd loading in diagonals	3920	852	36	0	0	0	153	1579.4 \pm 0.9
17	15x15, 16 Gd pin config., checkerboard, 1/4 Gd loading in diagonals, B ₄ C in center assembly	3920	852	36	16	0	0	137	1432.1 \pm 1.5

Table 4-1. (Cont'd)

Core	Core Description	No. of 2.46 wt % U-235 fuel pins	No. of 4.02 wt % U-235 fuel pins	No. of Gd fuel pins	No. of B ₄ C pins	No. of Ag-In-Cd pins	No. of void pins	No. of water pins	Moderator boron concentration, ppm
18	16x16, CE control config., 0 Gd pin config.	3676	944	0	0	0	0	180	1776.8 ±1.0
19	16x16, CE control config., 8 Gd pin config., checkerboard, 1/4 Gd loading in diagonals	3676	928	16	0	0	0	180	1628.3 ±0.8
20	16x16, CE control config., 16 Gd pin config., checkerboard, 1/4 Gd loading in diagonals	3676	912	32	0	0	0	180	1499.0 ±0.6

*In addition to the standard deviation shown, a systematic bias, which may be as large as 0.2% exists but cancels when differences are calculated.

Table 4-2. Measured Reactivity Worths of Gd Fuel Rods Using 2.46 wt % Enriched Fuel Region

<u>Core Description</u>	<u>Core</u>	<u>No. of Gd Fuel Rods</u>	<u>Moderator Boron Concentration, ppm</u>	<u>Moderator Boron Change, ppm</u>
15x15, 2.46 wt % fuel, 0 Gd pin configuration	1	0	1337.9 \pm 0.4	- - - - -
15x15 2.46 wt % fuel, 8 Gd pin config., checkerboard, 1/4 loading in diagonals	3	20	1239.3 \pm 0.7	98.6 \pm 0.8
15x15, 2.46 wt %, 12 Gd pin config., checkerboard, 1/4 Gd loading in diagonals	5	28	1208.0 \pm 0.4	129.9 \pm 0.6
15x15, 2.46 wt % fuel, alternate 12 Gd pin config., checkerboard, 1/4 Gd loading in diagonals	5A	32	1191.3 \pm 0.5	146.6 \pm 0.6
15x15, 2.46 wt % fuel, second alternate 12 Gd pin config., checkerboard, 1/4 Gd loading in diagonals	5B	28	1207.0 \pm 1.0	130.9 \pm 1.1
15x15, 2.46 wt % fuel, 12 Gd pin config., checkerboard, 1/4 Gd loading in diagonals with annular Gd fuel	7	28	1208.8 \pm 0.5	129.1 \pm 0.6
15x15, 2.46 wt % fuel, 16 Gd pin config., checkerboard, 1/4 Gd loading in diagonals	8	36	1170.7 \pm 0.5	167.2 \pm 0.6

Note: Auxiliary measurements show core 5B contains 0.6 \pm 0.3 ppm less moderator boron than does core 5 and that core 5 contains 0.7 \pm 0.3 ppm less moderator boron than does core 7.

Table 4-3. Measured Reactivity Worths of Ag-In-Cd and Void Pins Using 2.46 wt % Enriched Fuel Region

<u>Core Description</u>	<u>Cores Compared</u>	<u>Moderator Boron Concentration Difference, ppm</u>	<u>Moderator Boron Difference Due To</u>
15x15, 2.46 wt % fuel, 0 Gd pin configuration	1 & 2	-87.9 <u>+1.1</u>	16 water positions in center replaced by 16 Ag-In-Cd pins
15x15, 2.46 wt % fuel, 8 Gd pin configuration, checkerboard, 1/4 Gd loading in diagonals	3 & 4	-67.6 <u>+1.2</u>	"
15x15, 2.46 wt % fuel, 12 Gd pin configuration, checkerboard, 1/4 Gd loading in diagonals	5 & 6	-52.2 <u>+1.6</u>	"
15x15, 2.46 wt % fuel, alternate 12 Gd pin configuration, checkerboard, 1/4 Gd loading in diagonals	5A & 6A	-55.7 <u>+1.9</u>	"
15x15, 2.46 wt % fuel, 16 Gd pin configuration, checkerboard, 1/4 Gd loading in diagonals	8 & 9	-40.2 <u>+0.8</u>	"
15x15, 2.46 wt % fuel, 16 Gd pin configuration, checkerboard, 1/4 Gd loading in diagonals	8 & 10	+6.4 <u>+0.8</u>	16 water positions in center replaced by 16 void pins

4-19

Table 4-4. Measured Reactivity Worths of Gd Fuel Rods Using 2.46 wt % Enriched Fuel Region

15 x 15 Configurations

<u>Core</u>	<u>Core Description</u>	<u>No. of Gd Fuel Rods</u>	<u>Moderator Boron* Concentration, ppm</u>	<u>Moderator Boron Change, ppm</u>
12	15 x 15, 2.46 and 4.02 wt % fuel, 0 Gd pin configuration	0	1899.3 \pm 0.9	---
14	15 x 15, 2.46 and 4.02 wt % fuel, 12 Gd pin configuration, 1/4 Gd loading in diagonals	28	1653.8 \pm 0.7	245.5 \pm 1.1
16	15 x 15, 2.46 and 4.02 wt % fuel, 16 Gd pin configuration, checkerboard, 1/4 Gd loading in diagonals	36	1579.4 \pm 0.9	319.9 \pm 1.3

CE Control Configurations

<u>Core</u>	<u>Core Description</u>	<u>No. of Gd Fuel Rods</u>	<u>Moderator Boron* Concentration, ppm</u>	<u>Moderator Boron Change, ppm</u>
18	16 x 16 CE, 0 Gd pin configuration	0	1776.8 \pm 1.0	---
19	16 x 16 CE, 8 Gd pin configuration, checkerboard, 1/4 Gd loading in diagonals	16	1628.3 \pm 0.8	148.5 \pm 1.3
20	16 x 16 CE, 16 Gd pin configuration, checkerboard, 1/4 Gd loading in diagonals	32	1499.0 \pm 0.6	277.8 \pm 1.2

*In addition to the standard deviation shown, there is a systematic bias which may be as large as 0.2 percent. This bias cancels when differences are calculated.

Table 4-5. Measured Reactivity Worths of B₄C Rods Using 2.46/4.02 wt % Enriched Fuel Region

<u>Core Description</u>	<u>Cores Compared</u>	<u>Moderator Boron Concentration Difference, ppm</u>	<u>Moderator Boron Difference Due To</u>
15 x 15, 2.46 and 4.02 wt % fuel, 0 Gd pin configuration	12 & 13	-263.9 ±1.1	16 water-filled positions in center replaced by 16 B ₄ C rods
15 x 15, 2.46 and 4.02 wt % fuel, 12 Gd pin configuration, checkerboard, 1/4 Gd loading in diagonals	14 & 15	-174.1 ±0.9	"
15 x 15, 2.46 and 4.02 wt % fuel, 16 Gd pin configuration, checkerboard, 1/4 Gd loading in diagonals	16 & 17	-147.3 ±1.7	"

Table 4-6. Basic Fuel Rod Scan Data From Core 1

Fuel Rod Location	Run 1	Run 2	Run 3	Average ⁺	Fuel Rod Location	Run 1	Run 2	Run 3	Average ⁺
N1W1	1.000	1.007	1.016	1.008 \pm 0.005	N0W1	1.003	0.997	1.000	1.000 \pm 0.002
N1E0	1.002	1.006	1.010	1.006 \pm 0.002	S1E7	0.935	0.928	0.933	0.932 \pm 0.002
N1E1	1.005	0.998	1.006	1.003 \pm 0.003	S2E3	1.074	1.061	1.064	1.066 \pm 0.004
N0W1	0.995	1.007	0.998	1.000 \pm 0.004	S2E4	1.082	1.073	1.071	1.075 \pm 0.003
N0E1	0.997	0.997	0.997	0.997 \pm 0.000	S2E6	1.015	1.017	1.023	1.018 \pm 0.002
N0E2	1.001	0.989	1.000	0.997 \pm 0.004	S2E7	0.940	0.946	0.934	0.940 \pm 0.003
N0E3	0.969	0.978	0.971	0.973 \pm 0.003	S3E3	1.036	1.035	1.045	1.039 \pm 0.003
N0E4	0.972	0.964	0.966	0.967 \pm 0.002	S3E4	1.092	1.080	1.094	1.089 \pm 0.004
N0E5	0.984	0.979	0.986	0.983 \pm 0.002	S3E5	1.072	1.066	1.074	1.071 \pm 0.002
N0E6	0.952	0.950	0.956	0.953 \pm 0.002	S3E6	0.973	0.978	0.974	0.975 \pm 0.002
N0E7	0.930	0.935	0.930	0.932 \pm 0.002	S3E7	0.921	0.936	0.938	0.932 \pm 0.005
S1W1	0.998	1.006	0.993	0.999 \pm 0.004	S4E5	1.043	1.049	1.039	1.044 \pm 0.003
S1E0	1.013	1.016	1.004	1.011 \pm 0.004	S4E6	0.957	0.960	0.940	0.952 \pm 0.006
S1E1	1.011	1.004	1.010	1.008 \pm 0.004	S4E7	0.919	0.917	0.927	0.921 \pm 0.003
S1E2	1.057	1.052	1.048	1.052 \pm 0.003	S5E5	0.971	0.980	0.971	0.974 \pm 0.003
S1E3	0.996	1.002	0.996	0.998 \pm 0.002	S5E6	0.919	0.923	0.934	0.925 \pm 0.004
S1E4	0.995	0.997	0.992	0.995 \pm 0.001	S5E7	0.920	0.908	0.903	0.910 \pm 0.005
S1E5	1.044	1.041	1.043	1.043 \pm 0.001	S6E6	0.909	0.915	0.912	0.912 \pm 0.002
S1E6	0.985	0.984	0.985	0.985 \pm 0.000	S6E7	0.897	0.907	0.899	0.901 \pm 0.003
					S7E7	0.891	0.894	0.886	0.890 \pm 0.002

The average of locations N1E0, N0W1, N0E1, and S1E0, which are symmetrical locations, is 1.004 \pm 0.003.

The average of locations N1W1, N1E1, S1W1, and S1E1, which are symmetrical locations, is 1.005 \pm 0.002.

+ Uncertainty represents 1 standard deviation.

Table 4-7. Basic Fuel Rod Scan Data From Core 5

Fuel Rod Location	Run 1	Run 2	Run 3	Average ⁺	Fuel Rod Location	Run 1	Run 2	Run 3	Average ⁺	Fuel Rod Location	Run 1	Run 2	Run 3	Average ⁺
N1W1	1.009	0.999	1.007	1.005 ±0.003	N0W1	0.997	1.006	0.997	1.000 ±0.003	N0W1	1.000	1.005	0.995	1.000 ±0.003
N1E0	1.006	1.008	0.997	1.004 ±0.003	S1E7	1.089	1.093	1.080	1.087 ±0.004	S8E8	1.072	1.060	1.064	1.065 ±0.004
N1E1	0.998	0.990	0.977	0.988 ±0.006	S2E3	0.984	0.990	0.986	0.987 ±0.002	S9E9	1.015	1.017	1.019	1.017 ±0.001
N0W1	1.006	1.007	0.987	1.000 ±0.007	S2E4	1.085	1.078	1.093	1.085 ±0.004	S10E10*	0.194	0.194	0.193	0.194 ±0.000
N0E1	1.008	1.011	0.994	1.004 ±0.005	S2E6	1.154	1.161	1.152	1.156 ±0.003	S12E12*	0.185	0.184	0.184	0.184 ±0.000
N0E2	0.914	0.917	0.905	0.912 ±0.004	S2E7	1.085	1.101	1.107	1.098 ±0.007	S14E14	1.024	1.028	1.027	1.026 ±0.001
N0E3*	0.166	0.181	0.184	0.177 ±0.006	S3E3*	0.189	0.188	0.187	0.188 ±0.001	S16E16	1.016	1.018	1.010	1.015 ±0.002
N0E4	0.922	0.930	0.941	0.931 ±0.006	S3E4	1.044	1.053	1.046	1.048 ±0.003	S18E18	0.954	0.958	0.968	0.960 ±0.004
N0E5	1.028	1.027	1.047	1.034 ±0.007	S3E5	1.132	1.127	1.127	1.129 ±0.002	S20E20	0.798	0.791	0.804	0.798 ±0.004
N0E6	1.056	1.065	1.063	1.061 ±0.003	S3E6	1.089	1.082	1.086	1.086 ±0.002	S21E21	0.722	0.730	0.729	0.727 ±0.003
N0E7	1.059	1.069	1.083	1.070 ±0.007	S3E7	1.084	1.087	1.081	1.084 ±0.002	S22E22	0.642	0.640	0.637	0.640 ±0.001
S1W1	1.005	0.998	0.983	0.995 ±0.006	S4E5	1.056	1.036	1.046	1.046 ±0.006	S23E23	0.587	0.592	0.587	0.589 ±0.002
S1E0	1.012	1.011	0.999	1.007 ±0.004	S4E6	1.037	1.036	1.027	1.033 ±0.003	S24E24	0.525	0.525	0.528	0.526 ±0.001
S1E1	0.998	1.009	1.002	1.003 ±0.003	S4E7	1.068	1.072	1.063	1.068 ±0.003	S25E25	0.446	0.440	0.429	0.438 ±0.005
S1E2	1.010	1.018	1.021	1.016 ±0.003	S5E5*	0.195	0.196	0.193	0.195 ±0.001	S26E26	0.363	0.366	0.365	0.365 ±0.001
S1E3	0.924	0.946	0.920	0.930 ±0.008	S5E6	0.964	0.956	0.966	0.962 ±0.003	S27E27	0.292	0.290	0.298	0.293 ±0.002
S1E4	1.007	0.992	1.018	1.006 ±0.008	S5E7	1.061	1.048	1.046	1.052 ±0.005	S28E28	0.237	0.239	0.231	0.236 ±0.002
S1E5	1.129	1.108	1.131	1.123 ±0.007	S6E6	1.025	1.009	1.018	1.017 ±0.005	S29E29	0.191	0.193	0.194	0.193 ±0.001
S1E6	1.098	1.077	1.100	1.092 ±0.007	S6E7	1.050	1.063	1.062	1.058 ±0.004	S30E30	0.190	0.183	0.190	0.188 ±0.002
					S7E7	1.059	1.066	1.079	1.068 ±0.006					

The average of locations N1E0, N0W1, N0E1, and S1E0, which are symmetrical locations, is 1.004 ±0.002.
 The average of locations N1W1, N1E1, S1W1, and S1E1, which are symmetrical locations, is 0.998 ±0.004.

*UO₂-Gd₂O₃ fuel rod.

+Uncertainty represents 1 standard deviation.

Table 4-8. Basic Fuel Rod Scan Data from Core 12

Fuel Rod Location	Run 1	Run 2	Run 3	Average	Fuel Rod Location	Run 1	Run 2	Run 3	Average
NIW1	1.005	1.009	1.017	1.010 ± 0.004	NOW1	1.000	1.014	0.986	1.000 ± 0.008
NIEO	1.022	1.017	1.013	1.017 ± 0.003	S1E7	0.869	0.871	0.874	0.871 ± 0.001
NI E1	0.996	1.006	0.999	1.000 ± 0.003	S2E3	1.048	1.036	1.057	1.047 ± 0.006
NOW1	1.006	0.992	1.002	1.000 ± 0.004	S3E4	1.052	1.057	1.045	1.051 ± 0.003
NOE1	1.032	1.013	1.007	1.017 ± 0.008	S2E6	0.975	0.959	0.982	0.972 ± 0.007
NOE2	0.982	0.977	0.975	0.978 ± 0.002	S2E7	0.890	0.879	0.885	0.885 ± 0.003
NOE3	0.946	0.939	0.952	0.946 ± 0.004	S3E3	1.017	1.017	1.019	1.018 ± 0.001
NOE4	0.953	0.960	0.961	0.958 ± 0.003	S3E4	1.065	1.073	1.070	1.069 ± 0.002
NOE5	0.933	0.943	0.945	0.940 ± 0.004	S3E5	1.027	1.044	1.036	1.036 ± 0.005
NOE6	0.906	0.902	0.898	0.902 ± 0.002	S3E6	0.911	0.921	0.929	0.920 ± 0.005
NOE7	0.864	0.870	0.871	0.868 ± 0.002	S3E7	0.850	0.853	0.856	0.853 ± 0.002
SIW1	0.997	1.007	0.976	0.993 ± 0.009	S4E5	1.007	1.011	1.003	1.007 ± 0.002
S1EO	1.009	1.013	0.994	1.005 ± 0.006	S4E6	0.884	0.895	0.869	0.883 ± 0.008
S1E1	1.014	1.007	1.004	1.008 ± 0.003	S4E7	0.848	0.834	0.842	0.841 ± 0.004
S1E2	1.060	1.062	1.050	1.057 ± 0.004	S5E5	0.896	0.894	0.910	0.900 ± 0.005
S1E3	0.978	0.969	0.997	0.981 ± 0.008	S5E6	0.844	0.852	0.843	0.846 ± 0.003
S1E4	0.956	0.976	0.983	0.972 ± 0.008	S5E7	0.833	0.816	0.841	0.830 ± 0.007
S1E5	1.010	1.013	1.008	1.010 ± 0.001	S6E6	0.839	0.836	0.819	0.831 ± 0.006
S1E6	0.944	0.917	0.923	0.928 ± 0.008	S6E7	0.806	0.803	0.807	0.805 ± 0.001
					S7E7	0.793	0.790	0.798	0.794 ± 0.002

The average of locations N1EO, NOW1, and S1EO, which are symmetrical locations, is 1.010 ± 0.004
 The average of locations NIW1, N1E1, SIW1, and, S1E1, which are symmetrical locations, is 1.003 ± 0.004 .
 All fuel rods listed in this table are 4.02 wt % enriched UO₂.

Table 4-9. Basic Fuel Rod Scan Data from Core 14

Fuel Rod Location	Run 1	Run 2	Run 3	Average	Fuel Rod Location	Run 1	Run 2	Run 3	Average	Fuel Rod Location	Run 1	Run 2	Run 3	Average
N1W1	1.005	1.004	1.012	1.007 ±0.003	N0W1	0.997	1.013	0.990	1.000 ±0.007	N0W1	1.006	1.006	0.988	1.000 ±0.006
N1E0	1.025	1.009	1.000	1.011 ±0.007	S1E7	0.950	0.951	0.956	0.952 ±0.002	S8E8	0.850	0.849	0.849	0.849 ±0.000
N1E1	1.001	1.001	0.996	0.999 ±0.002	S2E3	0.989	1.001	0.990	0.993 ±0.004	S9E9	0.804	0.793	0.802	0.800 ±0.003
N0W1	0.996	1.011	0.993	1.000 ±0.006	S2E4	1.061	1.039	1.061	1.054 ±0.007	S10E10*	0.125	0.125	0.126	0.125 ±0.000
N0E1	1.013	1.034	1.002	1.016 ±0.009	S2E6	1.072	1.057	1.039	1.056 ±0.010	S12E12*	0.108	0.107	0.106	0.107 ±0.001
N0E2	0.925	0.910	0.921	0.919 ±0.004	S2E7	0.959	0.964	0.961	0.961 ±0.001	S14E14	0.608	0.619	0.615	0.614 ±0.003
N0E3*	0.149	0.153	0.155	0.152 ±0.002	S3E3*	0.155	0.155	0.152	0.154 ±0.001	S16E16**	0.423	0.425	0.423	0.424 ±0.001
N0E4	0.909	0.908	0.896	0.904 ±0.004	S3E4	1.024	1.042	1.030	1.032 ±0.005	S18E18**	0.354	0.360	0.355	0.356 ±0.002
N0E5	0.977	0.976	0.983	0.979 ±0.002	S3E5	1.068	1.064	1.066	1.066 ±0.001	S20E20**	0.275	0.269	0.277	0.274 ±0.002
N0E6	0.967	0.955	0.960	0.961 ±0.003	S3E6	0.991	0.976	0.977	0.981 ±0.005	S21E21**	0.247	0.247	0.248	0.247 ±0.000
N0E7	0.955	0.944	0.957	0.952 ±0.004	S3E7	0.943	0.940	0.932	0.938 ±0.003	S22E22**	0.213	0.212	0.218	0.214 ±0.002
S1W1	0.980	1.011	0.992	0.994 ±0.009	S4E5	0.990	1.007	1.004	1.000 ±0.005	S23E23**	0.180	0.183	0.181	0.181 ±0.001
S1E0	1.010	1.016	1.010	1.012 ±0.002	S4E6	0.935	0.928	0.944	0.936 ±0.005	S24E24**	0.157	0.158	0.157	0.157 ±0.000
S1E1	0.995	0.994	1.012	1.000 ±0.006	S4E7	0.917	0.931	0.938	0.929 ±0.006	S25E25**	0.131	0.129	0.132	0.131 ±0.001
S1E2	1.041	1.031	1.034	1.035 ±0.003	S5E5*	0.154	0.153	0.150	0.152 ±0.001	S26E26**	0.109	0.105	0.106	0.107 ±0.001
S1E3	0.930	0.918	0.931	0.926 ±0.004	S5E6	0.871	0.870	0.876	0.872 ±0.002	S27E27**	0.082	0.087	0.086	0.085 ±0.002
S1E4	0.960	0.984	0.984	0.976 ±0.008	S5E7	0.894	0.903	0.916	0.904 ±0.006	S28E28**	0.064	0.066	0.067	0.066 ±0.001
S1E5	1.070	1.067	1.079	1.072 ±0.004	S6E6	0.897	0.880	0.905	0.894 ±0.007	S29E29**	0.054	0.054	0.053	0.054 ±0.000
S1E6	1.008	1.007	1.014	1.010 ±0.002	S6E7	0.908	0.903	0.908	0.906 ±0.002	S30E30**	0.050	0.050	0.050	0.050 ±0.000
					S7E7	0.899	0.891	0.874	0.888 ±0.007					

The average of locations N1E0, N0W1, N0E1, and S1E0, which are symmetrical locations, is 1.010 ±0.003.
 The average of locations N1W1, N1E1, S1W1, and S1E1, which are symmetrical locations, is 1.000 ±0.003.

*UO₂-Gd₂O₃ fuel rod.

** 2.46 wt % enriched UO₂ fuel rod.

Unless otherwise indicated, fuel rods are 4.02 wt % enriched UO₂.

Table 4-10. Basic Fuel Rod Scan Data from Core 18

Fuel Rod Location	Run 1	Run 2	Run 3	Average	Fuel Rod Location	Run 1	Run 2	Run 3	Average
N2W2	0.881	0.888	0.897	0.889 ± 0.005	N1W2	1.002	0.998	1.000	1.000 ± 0.001
N2W1	0.998	0.989	0.989	0.992 ± 0.003	S2E7	0.801	0.787	0.758	0.782 ± 0.013
N2E1	1.005	0.995	0.994	0.998 ± 0.004	S2E8	0.760	0.749	0.752	0.754 ± 0.003
N2E2	0.898	0.882	0.890	0.890 ± 0.005	S3E3	0.867	0.887	0.889	0.881 ± 0.007
N1W2	1.004	0.984	1.012	1.000 ± 0.008	S3E4	1.021	1.025	0.998	1.015 ± 0.008
N1E2	0.986	0.994	1.007	0.996 ± 0.006	S3E5	1.003	0.988	0.995	0.995 ± 0.004
S1W2	0.982	1.009	0.994	0.995 ± 0.008	S3E6	0.857	0.858	0.870	0.862 ± 0.004
S1E2	0.997	1.002	0.989	0.996 ± 0.004	S3E7	0.793	0.795	0.785	0.791 ± 0.003
S1E3	0.844	0.857	0.862	0.854 ± 0.005	S3E8	0.760	0.759	0.782	0.767 ± 0.008
S1E4	0.819	0.830	0.822	0.824 ± 0.003	S4E6	0.981	0.978	0.976	0.978 ± 0.001
S1E5	0.810	0.808	0.807	0.808 ± 0.001	S4E7	0.811	0.809	0.795	0.805 ± 0.005
S1E6	0.804	0.803	0.771	0.793 ± 0.011	S4E8	0.765	0.754	0.773	0.764 ± 0.006
S1E7	0.767	0.785	0.781	0.778 ± 0.005	S5E6	0.955	0.977	0.970	0.967 ± 0.006
S1E8	0.753	0.746	0.758	0.752 ± 0.003	S5E7	0.795	0.805	0.805	0.802 ± 0.003
S2W2	0.888	0.895	0.894	0.892 ± 0.002	S5E8	0.747	0.758	0.750	0.752 ± 0.003
S2W1	1.007	0.987	0.991	0.995 ± 0.006	S6E6	0.819	0.813	0.837	0.823 ± 0.007
S2E1	0.990	0.997	0.995	0.994 ± 0.002	S6E7	0.781	0.749	0.763	0.764 ± 0.009

Table 4-10. (Cont'd)

<u>Fuel Rod Location</u>	<u>Run 1</u>	<u>Run 2</u>	<u>Run 3</u>	<u>Average</u>	<u>Fuel Rod Location</u>	<u>Run 1</u>	<u>Run 2</u>	<u>Run 3</u>	<u>Average</u>
S2E2	0.887	0.888	0.892	0.889 ± 0.002	S6E8	0.725	0.733	0.740	0.733 ± 0.004
S2E3	0.848	0.843	0.842	0.844 ± 0.002	S7E7	0.736	0.742	0.736	0.738 ± 0.002
S2E4	0.845	0.834	0.832	0.837 ± 0.004	S7E8	0.718	0.722	0.707	0.716 ± 0.004
S2E5	0.842	0.831	0.831	0.835 ± 0.004	S8E8	0.679	0.696	0.692	0.689 ± 0.005
S2E6	0.810	0.810	0.815	0.812 ± 0.002					

The average of locations N2W2, N2E2, S2W2, which are symmetrical locations, is 0.890 ± 0.002 .
 The average of symmetrical locations N2W1, S2E2, N2E1, N1E2, S1E2, S2E1, S2W1, S1W2, & N1W2 is 0.996 ± 0.002 .
 All fuel rods listed in this table are 4.02 wt % enriched UO_2 .

Table 4-11. Basic Fuel Rod Scan Data from Core 20

Fuel Rod Location	Run 1	Run 2	Run 3	Average	Fuel Rod Location	Run 1	Run 2	Run 3	Average	Fuel Rod Location	Run 1	Run 2	Run 3	Average
N1W2	0.996	1.000	1.004	1.000 ± 0.002	N1W2	1.002	0.991	1.007	1.000 ± 0.005	N1W2	0.999	1.005	0.996	1.000 ± 0.003
N2W2	0.868	0.862	0.883	0.871 ± 0.006	S2E7	0.752	0.765	0.766	0.761 ± 0.005	S9E9	0.701	0.699	0.700	0.700 ± 0.001
N2W1	1.011	0.984	0.995	0.997 ± 0.008	S2E8	0.772	0.761	0.766	0.766 ± 0.003	S10E10*	0.108	0.109	0.110	0.109 ± 0.001
N2E1	1.004	1.003	0.988	0.998 ± 0.005	S3E3*	0.133	0.133	0.134	0.133 ± 0.001	S11E11	0.684	0.680	0.687	0.684 ± 0.002
N2E2	0.856	0.878	0.857	0.864 ± 0.007	S3E4	0.964	0.966	0.973	0.968 ± 0.003	S14E14*	0.082	0.084	0.084	0.083 ± 0.001
N1E2	1.007	0.996	0.997	1.000 ± 0.004	S3E5	0.997	0.983	0.996	0.992 ± 0.005	S15E15	0.534	0.533	0.533	0.533 ± 0.001
S1W2	0.996	0.999	0.994	0.996 ± 0.001	S3E6	0.834	0.836	0.848	0.839 ± 0.004	S18E18**	0.338	0.345	0.345	0.343 ± 0.002
S1E2	0.998	0.996	1.007	1.000 ± 0.003	S3E7*	0.129	0.131	0.131	0.130 ± 0.001	S19E19**	0.307	0.308	0.309	0.308 ± 0.001
S1E3	0.843	0.838	0.856	0.846 ± 0.005	S3E8	0.747	0.744	0.746	0.746 ± 0.001	S22E22**	0.232	0.223	0.225	0.227 ± 0.003
S1E4	0.835	0.823	0.827	0.828 ± 0.004	S4E6	1.013	0.997	1.001	1.004 ± 0.005	S23E23**	0.188	0.181	0.181	0.183 ± 0.002
S1E5	0.810	0.830	0.809	0.816 ± 0.007	S4E7	0.765	0.773	0.741	0.760 ± 0.010	S24E24**	0.156	0.159	0.156	0.157 ± 0.001
S1E6	0.824	0.801	0.822	0.816 ± 0.007	S4E8	0.771	0.788	0.783	0.781 ± 0.005	S25E25**	0.134	0.134	0.131	0.133 ± 0.001
S1E7	0.800	0.801	0.785	0.795 ± 0.005	S5E6	1.002	0.997	1.005	1.001 ± 0.002	S26E26**	0.107	0.108	0.109	0.108 ± 0.001
S1E8	0.787	0.791	0.793	0.790 ± 0.002	S5E7	0.815	0.821	0.815	0.817 ± 0.002	S27E27**	0.085	0.085	0.087	0.086 ± 0.001
S2W2	0.869	0.868	0.865	0.867 ± 0.001	S5E8	0.785	0.782	0.777	0.781 ± 0.002	S28E28**	0.065	0.068	0.066	0.066 ± 0.001
S2W1	1.002	1.010	1.019	1.010 ± 0.005	S6E6	0.833	0.854	0.840	0.842 ± 0.006	S29E29**	0.054	0.054	0.056	0.055 ± 0.001
S2E1	0.983	0.990	0.997	0.990 ± 0.004	S6E7	0.756	0.755	0.744	0.752 ± 0.004	S30E30**	0.052	0.054	0.053	0.053 ± 0.001
S2E2	0.874	0.876	0.857	0.869 ± 0.006	S6E8	0.768	0.760	0.768	0.765 ± 0.003					
S2E3	0.790	0.798	0.784	0.791 ± 0.004	S7E7*	0.124	0.125	0.125	0.125 ± 0.001					
S2E4	0.832	0.811	0.840	0.828 ± 0.009	S7E8	0.704	0.704	0.704	0.704 ± 0.000					
S2E5	0.842	0.844	0.836	0.841 ± 0.002	S8E8	0.727	0.727	0.729	0.728 ± 0.001					
S2E6	0.797	0.821	0.808	0.809 ± 0.007										

Average of locations N2W2, N2E2, S2W2, and S2E2, which are symmetrical locations, is 0.868 ± 0.001 .

Average of symmetrical locations N2W1, N2E1, N1E2, S1E2, S2E1, S2W1, S1W2, and N1W2 is 0.999 ± 0.002 .

** 2.46% enriched UO₂ fuel rod.

* UO₂-Gd₂O₃ fuel rod.

Unless otherwise indicated, fuel rods are 4.02 wt % enriched UO₂.

Table 4-12. Core 1 Normalized* Midplane Power Distribution Through Center Assembly

East →

South ↓

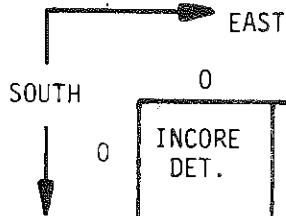
	0	1	2	3	4	5	6	7
0	INCORE DET.	1.018	1.011	0.987	0.981	0.997	0.966	0.945
1	1.018	1.019	1.067	1.012	1.009	1.058	0.999	0.945
2	1.011	1.067	WATER	1.081	1.090	WATER	1.032	0.953
3	0.987	1.012	1.081	1.054	1.104	1.086	0.989	0.945
4	0.981	1.009	1.090	1.104	WATER	1.059	0.965	0.934
5	0.997	1.058	WATER	1.086	1.059	0.988	0.938	0.923
6	0.966	0.999	1.032	0.989	0.965	0.938	0.925	0.914
7	0.945	0.945	0.953	0.945	0.934	0.923	0.914	0.903

X.XXX

2.46 wt % U-235 in UO₂.
Measured relative rod power.

*Average power per fuel rod is unity within the central 15x15 assembly.

Table 4-13. Core 5 Normalized* Midplane Power Distribution Through Center Assembly



	0	1	2	3	4	5	6	7
0	INCORE DET.	1.005	0.913	GD 0.170 FUEL	0.932	1.036	1.063	1.072
1	1.005	0.999	1.017	0.931	1.007	1.125	1.094	1.089
2	0.913	1.017	WATER	0.988	1.087	WATER	1.158	1.100
3	GD 0.170 FUEL	0.931	0.988	GD 0.181 FUEL	1.050	1.131	1.088	1.086
4	0.932	1.007	1.087	1.050	WATER	1.048	1.035	1.070
5	1.036	1.125	WATER	1.131	1.048	GD 0.187 FUEL	0.963	1.054
6	1.063	1.094	1.158	1.088	1.035	0.963	1.018	1.060
7	1.072	1.089	1.100	1.086	1.070	1.054	1.060	1.070

X.XXX 2.46 wt % U-235 in UO₂.
Measured relative rod power.

GD
X.XXX
FUEL 1.944 wt % U-235/4.0 wt % Gd₂O₃ in UO₂-10.11 gm/cc
Measured relative rod power.

*Average power per fuel rod is unity within the central 15x15 assembly.

Table 4-14. Core 5 Normalized* Midplane Power Distribution
Along Core Diagonal

<u>Fuel Pin Position</u>	<u>Relative Power</u>	<u>Fuel Pin Position</u>	<u>Relative Power</u>
S1E1	0.999	S16E16	1.016
S2E2	WATER	S17E17	WATER
S3E3*	0.181	S18E18	0.961
S4E4	WATER	S19E19	WATER
S5E5*	0.187	S20E20	0.799
S6E6	1.018	S21E21	0.728
S7E7	1.070	S22E22	0.641
S8E8	1.067	S23E23	0.590
S9E9	1.018	S24E24	0.527
S10E10*	0.187	S25E25	0.439
S11E11	WATER	S26E26	0.366
S12E12*	0.177	S27E27	0.293
S13E13	WATER	S28E28	0.236
S14E14	1.028	S29E29	0.193
S15E15	WATER	S30E30	0.188

⁺Normalized to central assembly, which is normalized to one.

*Location of $UO_2-Gd_2O_3$ fuel rod.

Unless otherwise indicated, fuel rods are 2.46 wt % enriched UO_2 .

S = South
E = East

Table 4-15. Core 12 Normalized* Midplane Power Distribution Through Center Assembly

EAST →

↓ SOUTH

	0	1	2	3	4	5	6	7
0	INCORE DET.	1.075	1.041	1.006	1.019	1.000	0.960	0.923
1	1.075	1.067	1.125	1.044	1.034	1.075	0.987	0.927
2	1.041	1.125	WATER	1.114	1.118	WATER	1.034	0.942
3	1.006	1.044	1.114	1.083	1.137	1.102	0.979	0.908
4	1.019	1.034	1.118	1.137	WATER	1.071	0.939	0.895
5	1.000	1.075	WATER	1.102	1.071	0.958	0.900	0.883
6	0.960	0.987	1.034	0.979	0.939	0.900	0.884	0.856
7	0.923	0.927	0.942	0.908	0.895	0.883	0.856	0.845

X.XXX

4.02 wt % U-235 in UO₂.
Measured relative rod power.

*Average fuel rod power in center assembly is 1.0.

Table 4-16. Core 14 Normalized* Midplane Power Distribution Through Center Assembly

	0	1	2	3	4	5	6	7
0	INCORE DET.	1.091	0.992	Gd 0.162 Fuel	0.976	1.057	1.038	1.028
1	1.091	1.080	1.118	1.000	1.054	1.158	1.091	1.028
2	0.992	1.118	WATER	1.072	1.138	WATER	1.140	1.038
3	Gd 0.162 Fuel	1.000	1.072	Gd 0.164 Fuel	1.114	1.151	1.059	1.013
4	0.976	1.054	1.138	1.114	WATER	1.080	1.011	1.003
5	1.057	1.158	WATER	1.151	1.080	Gd 0.162 Fuel	0.942	0.976
6	1.038	1.091	1.140	1.059	1.011	0.942	0.965	0.978
7	1.028	1.028	1.038	1.013	1.003	0.976	0.978	0.959

X.XXX

4.02 wt % U-235 in UO₂.
Measured relative rod power.

GD
X.XXX
FUEL

1.944 wt % U-235/4.0 wt % Gd₂O₃ in UO₂.
Measured relative rod power.

*Average fuel rod power in center assembly is 1.0.

Table 4-17. Core 14 Normalized[†] Midplane Power Distribution Along Core Diagonal

<u>Fuel Pin Position</u>	<u>Relative Power</u>	<u>Fuel Pin Position</u>	<u>Relative Power</u>
S1E1	1.080	S16E16**	0.470
S2E2	WATER	S17E17	WATER
S3E3*	0.164	S18E18**	0.394
S4E4	WATER	S19E19	WATER
S5E5*	0.162	S20E20**	0.303
S6E6	0.965	S21E21**	0.273
S7E7	0.959	S22E22**	0.238
S8E8	0.917	S23E23**	0.201
S9E9	0.864	S24E24**	0.174
S10E10*	0.133	S25E25**	0.145
S11E11	WATER	S26E26**	0.119
S12E12*	0.113	S27E27**	0.094
S13E13	WATER	S28E28**	0.073
S14E14	0.663	S29E29**	0.059
S15E15	WATER	S30E30**	0.055

[†]Normalized to central assembly, which is normalized to one.

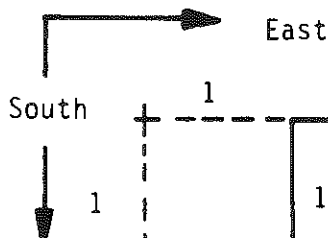
*Location of UO₂-Gd₂O₃ fuel rod.

**Location of 2.46 wt % enriched UO₂ fuel rod.

Unless otherwise indicated, fuel rods are 4.02 wt % enriched UO₂.

S = South
E = East

Table 4-18. Core 18 Normalized* Midplane Power Distribution
Through Center Assembly



	1	2	3	4	5	6	7	8
1		1.205	1.033	0.997	0.977	0.959	0.941	0.909
2	1.205	1.076	1.021	1.012	1.010	0.982	0.946	0.912
3	1.033	1.021	1.065	1.228	1.203	1.043	0.957	0.928
4	0.997	1.012	1.228	WATER REGION		1.183	0.974	0.924
5	0.977	1.010	1.203			1.170	0.970	0.909
6	0.959	0.982	1.043	1.183	1.170	0.995	0.924	0.886
7	0.941	0.946	0.957	0.974	0.970	0.924	0.893	0.866
8	0.909	0.912	0.928	0.924	0.909	0.886	0.866	0.833

X.XXX

4.02 wt % U-235 in UO₂.
Measured relative rod power.

*Average fuel rod power in center assembly is 1.0.

Table 4-19. Core 20 Normalized* Midplane Power Distribution Through Center Assembly

	1	2	3	4	5	6	7	8
1		1.277	1.082	1.059	1.043	1.043	1.017	1.010
2	1.277	1.110	1.011	1.059	1.075	1.034	0.973	0.979
3	1.082	1.011	Gd 0.168 Fuel	1.238	1.268	1.073	Gd 0.164 Fuel	0.954
4	1.059	1.059	1.238	WATER REGION		1.284	0.972	0.999
5	1.043	1.075	1.268			1.280	1.045	0.999
6	1.043	1.034	1.073	1.284	1.280	1.077	0.962	0.978
7	1.017	0.973	Gd 0.164 Fuel	0.972	1.045	0.962	Gd 0.158 Fuel	0.900
8	1.010	0.979	0.954	0.999	0.999	0.978	0.900	0.931

X.XXX 4.02 wt % U-235 in UO₂
Measured relative rod power.

Gd
X.XXX
Fuel 1.944 wt % U-235/4.0 wt % Gd₂O₃ in UO₂
Measured relative rod power.

*Average fuel rod power in center assembly is 1.0.

Table 4-20. Core 20 Normalized[†] Midplane Power Distribution
Along Core Diagonal

<u>Fuel Pin Position</u>	<u>Relative Power</u>	<u>Fuel Pin Position</u>	<u>Relative Power</u>
S2E2	1.110	S19E19**	0.404
S3E3*	0.168	S22E22**	0.298
S6E6	1.077	S23E23**	0.240
S7E7*	0.158	S24E24**	0.206
S8E8	0.931	S25E25**	0.174
S9E9	0.895	S26E26**	0.142
S10E10*	0.137	S27E27**	0.113
S11E11	0.875	S28E28**	0.087
S14E14*	0.105	S29E29**	0.072
S15E15	0.682	S30E30**	0.069
S18E18**	0.450		

[†]Normalized to central assembly, which is normalized to one.

*Location of $UO_2-Gd_2O_3$ fuel rod.

**Location of 2.46 wt % enriched UO_2 fuel rod.

Unless otherwise indicated, fuel rods are 4.02 wt % enriched UO_2 .

S = South
E = East

Table 4-21. Comparison of Incore Detector Response

<u>Cores Compared</u>	<u>Location of Std. Fuel Rod</u>	<u>Ratio of Detector Signal from Core Containing Gadolinia to that from Core Containing None</u>	
		<u>Ratio when the Power Generation in the Std. Fuel Rods of the Two Cores Is Identical</u>	<u>Ratio when the Power Generation in the Center Assembly of the Two Cores Is Identical</u>
1 & 5	NOW1	1.015 \pm 0.005	1.002 \pm 0.006
12 & 14	NOW1	0.998 \pm 0.006	1.012 \pm 0.007
18 & 20	N1W2	0.988 \pm 0.006	1.047 \pm 0.007

Table 4-22. Measured Fission Distribution Through $UO_2-Gd_2O_3$ Fuel Pellet

<u>Radius at Which Sample was Taken, in.</u>	<u>Relative Fissions per Unit Uranium Mass</u>	<u>Point-to-Average Fission Ratio</u>
0.0035	1.15	0.865
0.0245	1.15	0.865
0.0525	1.18	0.887
0.1005	1.17	0.880
0.1025	1.21	0.910
0.1035	1.19	0.895
0.1235	1.205	0.906
0.1525	1.265	0.951
0.1535	1.27	0.955
0.1605	1.31	0.985
0.200 (Surface)	2.57	1.932
0.200 (Surface)	2.25	1.692
0.200 (Surface)	2.39	1.797
Entire Pellet #1	1.31	
Entire Pellet #2	1.35	

Table 4-23. Measured Fission Distribution Through 2.46 wt % Enriched UO₂ Fuel Pellet

<u>Radius at Which Sample was Taken, inches</u>	<u>Relative Fissions Per Unit Uranium Mass</u>	<u>Point-to-Average Fission Ratio</u>
0.006	3.85	0.944
0.027	3.71	0.909
0.061	3.78	0.926
0.071	3.65	0.895
0.095	3.84	0.941
0.103	3.80	0.931
0.106	4.04	0.990
0.122	3.93	0.963
0.125	4.00	0.980
0.144	3.96	0.971
0.146	3.93	0.963
0.200 (Surface)	4.49	1.100
0.200 (Surface)	4.50	1.103
Entire Pellet	4.08	

Table 4-24. Dimensions of Pellets for Resonance Integral Measurements

Pellet type	OD, in.	ID, in.	Length, in.	Void fraction	UO ₂ mass, g	$\sqrt{S/M}^*$
Solid UO ₂	0.3681	0	0.4925	0	8.951	0.6407
	0.3682	0	0.5004	0	9.077	0.6414
	0.3685	0	0.5018	0	9.120	0.6411
	0.3688	0	0.4994	0	9.039	0.6426
				0.000 avg		0.6415 avg
Annular UO ₂	0.3684	0.084	0.5019	0.052	8.718	0.6556
	0.3686	0.084	0.4945	0.052	8.559	0.6570
	0.3683	0.085	0.4932	0.053	8.547	0.6563
				0.052 avg		0.6563 avg
Annular UO ₂	0.3686	0.116	0.4856	0.099	7.988	0.6739
	0.3689	0.116	0.4931	0.099	8.105	0.6745
	0.3686	0.117	0.4845	0.101	7.955	0.6745
				0.100 avg		0.6743 avg
Annular UO ₂	0.3688	0.145	0.4942	0.155	7.678	0.6936
	0.3688	0.143	0.5032	0.150	7.829	0.6931
	0.3682	0.144	0.4869	0.153	7.541	0.6942
				0.153 avg		0.6936 avg
Annular UO ₂ -Gd ₂ O ₃	0.3687	0.122	0.5084	0.109	7.362	0.7184
	0.3687	0.124	0.5116	0.113	7.353	0.7211
	0.3686	0.119	0.5177	0.104	7.532	0.7166
				0.109 avg		0.7187 avg
Solid UO ₂ -Gd ₂ O ₃	0.368	0	0.410	0	6.662	0.677
	0.368	0	0.401	0	6.554	0.676
	0.368	0	0.401	0	6.560	0.675
				0.000 avg		0.676 avg

*Units of (cm²/g)^{1/2}; S=outer surface area of pellet, m=UO₂ mass.

Table 4-25. Resonance Integral Data Reduction

Pellet* type	Relative corrected U-238 absorption in pellet, counts	UO ₂ mass in pellet, g	Relative core power during activation, counts	Relative ** resonance integral
Solid UO ₂	739868	8.951	35162	2.351
	775198	9.077	35687	2.393
	778409	9.120	35721	2.389
	758135	9.039	35530	<u>2.361</u>
				2.3735 ±0.0103 avg
Annular UO ₂	763053	8.718	35664	2.454
	737465	8.559	35330	2.439
	729475	8.547	35665	<u>2.393</u>
				2.4287 ±0.0184 avg
Annular UO ₂	719253	7.988	35552	2.533
	715633	8.105	35544	2.484
	700116	7.955	35547	<u>2.476</u>
				2.4977 ±0.0178 avg
Annular UO ₂	736475	7.678	37648	2.548
	703568	7.829	35458	2.534
	677473	7.541	35574	<u>2.525</u>
				2.5357 ±0.0067 avg
Annular UO ₂ -Gd ₂ O ₃	632431	7.362	35288	2.434
	649337	7.353	35632	2.478
	652015	7.532	35372	<u>2.447</u>
				2.4530 ±0.0131 avg
Solid UO ₂ -Gd ₂ O ₃	558117	6.662	35762	2.343
	547665	6.554	35702	2.341
	539895	6.560	35574	<u>2.314</u>
				2.3327 ±0.0094 avg

*0.214 wt % U-235 and, where applicable, 0.214 wt % U-235/7.99 wt % Gd₂O₃.

Table 4-26. Results of the Resonance Integral Measurements

Pellet Type	$\sqrt{S/M}^*$	Relative RI	Normalized RI**
UO ₂ Solid	0.6407	2.351	21.21637
	0.6414	2.393	21.59539
	0.6411	2.389	21.55929
	0.6426	2.361	21.30661
	$\sqrt{S/M} = 0.64145 \pm 0.00041$		R I = 21.41942 ± 0.09331
UO ₂ Void=5.2%	0.6556	2.454	22.14588
	0.6570	2.439	22.01051
	0.6563	2.393	21.59539
	$\sqrt{S/M} = 0.65630 \pm 0.00040$		R I = 21.91726 ± 0.16561
UO ₂ Void=10.0%	0.6739	2.533	22.85881
	0.6745	2.484	22.41661
	0.6745	2.476	22.34442
	$\sqrt{S/M} = 0.67430 \pm 0.00020$		R I = 22.53995 ± 0.16079
UO ₂ Void=15.3%	0.6936	2.548	22.99417
	0.6931	2.534	22.86783
	0.6942	2.525	22.78661
	$\sqrt{S/M} = 0.69363 \pm 0.00032$		R I = 22.88287 ± 0.6039
UO ₂ -Gd ₂ O ₃ void=10.9%	0.7184	2.444	22.05293
	0.7211	2.488	22.45181
	0.7166	2.457	22.17115
	$\sqrt{S/M} = 0.71870 \pm 0.00131$		R I = 22.22530 ± 0.11829
UO ₂ -Gd ₂ O ₃ Solid	0.6775	2.352	21.22900
	0.6755	2.350	21.21095
	0.6752	2.323	20.96639
	$\sqrt{S/M} = 0.67607 \pm 0.00072$		R I = 21.13545 ± 0.08469

*Units of (cm²/g)^{1/2}; S=outer surface area of pellet, M=UO₂ mass.

**A normalization factor of 1.004 has been applied to the UO₂-Gd₂O₃ pellet data to correct for the small thermal flux inside the cadmium capsule during the UO₂ pellet irradiation (factor not applied in Table 4-25).

***A normalization factor of 9.0244 was used to match the Hellstrand value 4.60 + 26.3 $\sqrt{S/M}$ for the solid UO₂ pellet type.

Table 4-27. Parameters of Overlapping U-238 and Cd Resonances

Isotope	E_0, eV	Γ, meV	$g\Gamma_n, \text{meV}$	$\Gamma_\gamma, \text{meV}$	$\sigma_{\gamma_0}, \text{b}$	I, b
U-238	66.15 ± 0.15	48	26	22	9870	11.25
Cd-112	66.77 ± 0.09	92*	7	85	2795	6.05
U-238	102.47 ± 0.09	96	70	26	5069	7.46
Cd-111	102.93 ± 0.09	101**	0.77	100***	195	0.30
U-238	208.46 ± 0.25	75	53	22	2611	1.47
Cd-111	208.57 ± 0.17	100**	0.26	100***	33	0.02

*Assumes $J = \frac{1}{2}$.

**Assumes $J=1$.

*** Γ_γ estimated from neighboring values.

Table 4-28. Estimate of Cadmium Shadowing Effect

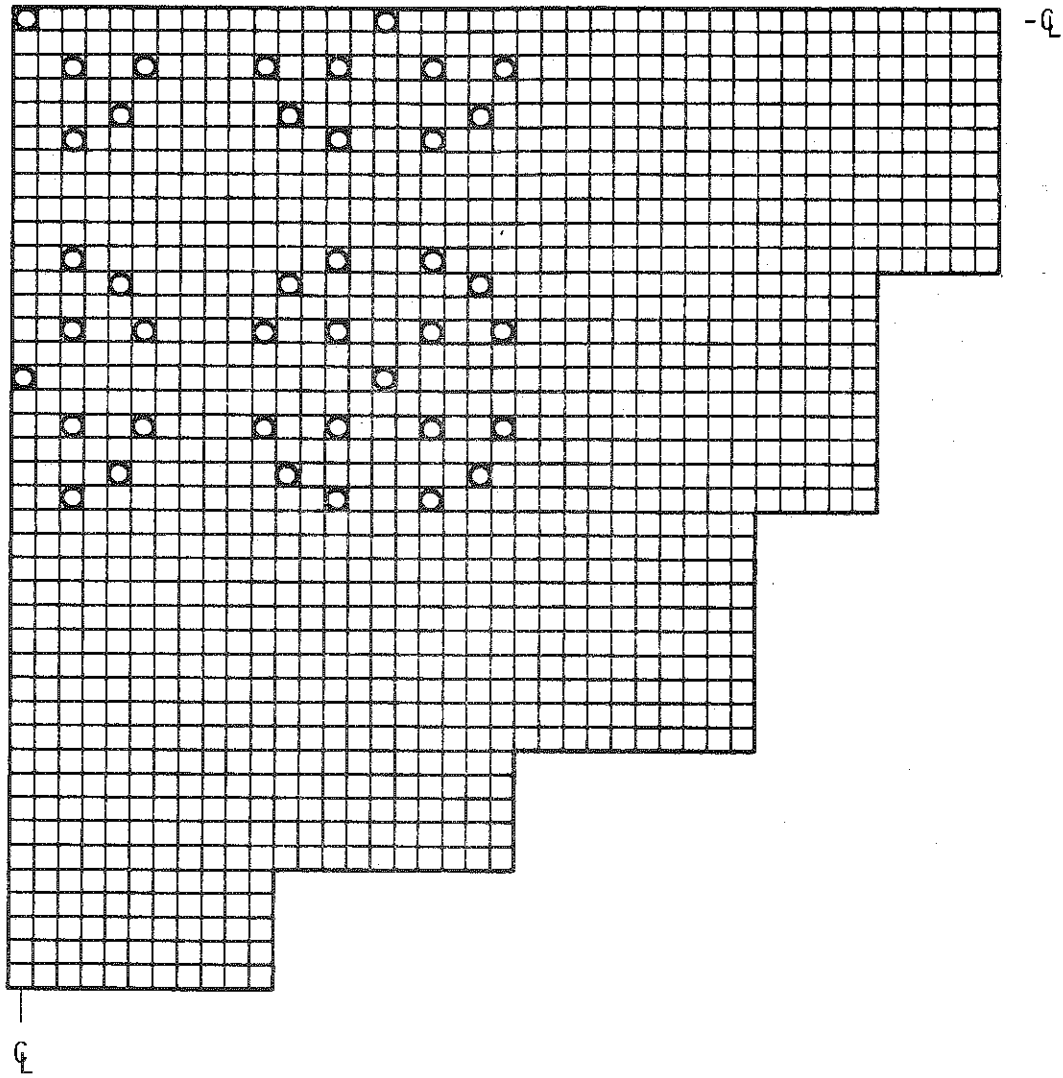
ANISN Group	Energy Bounds, eV	E_0 for Shadowed U-238 Res.	Fraction* of Total Absorption Lying in This Group	Fraction** of Group Absorption Due to Res. at E_0	Shadowing*** Factor	Net Reduction in Resonance Capture
22	$\frac{275.36}{167.02}$	208.46	$\frac{4.461}{112.745} \approx 4\%$	20%	30%	0.24%
23	$\frac{167.02}{101.30}$	102.47	$\frac{7.146}{112.745} \approx 6\%$	40%	20%	0.48%
24	$\frac{101.30}{61.44}$	66.15	$\frac{6.722}{112.745} \approx 6\%$	50%	10%	0.30%
						1.02% Total

*From spectrum correction calculations.

**Estimated from resonance parameters in BNL-325.¹³

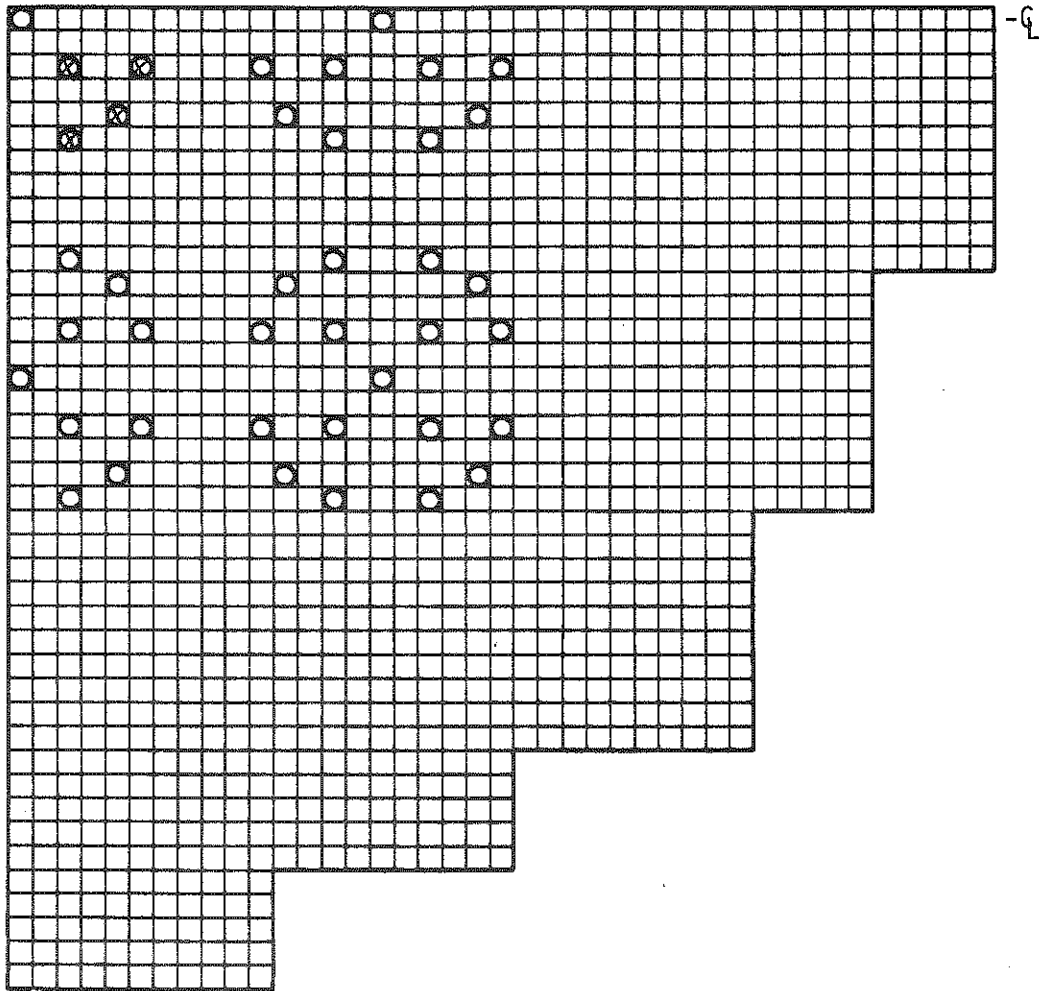
***Estimated from separation of U^{238} and Cd E_0 values with consideration of Cd isotopic abundance.

Figure 4-1. Core 1 Loading Diagram



-  VACANT WATER-FILLED POSITION
-  2.46 wt % U-235 ENRICHED FUEL

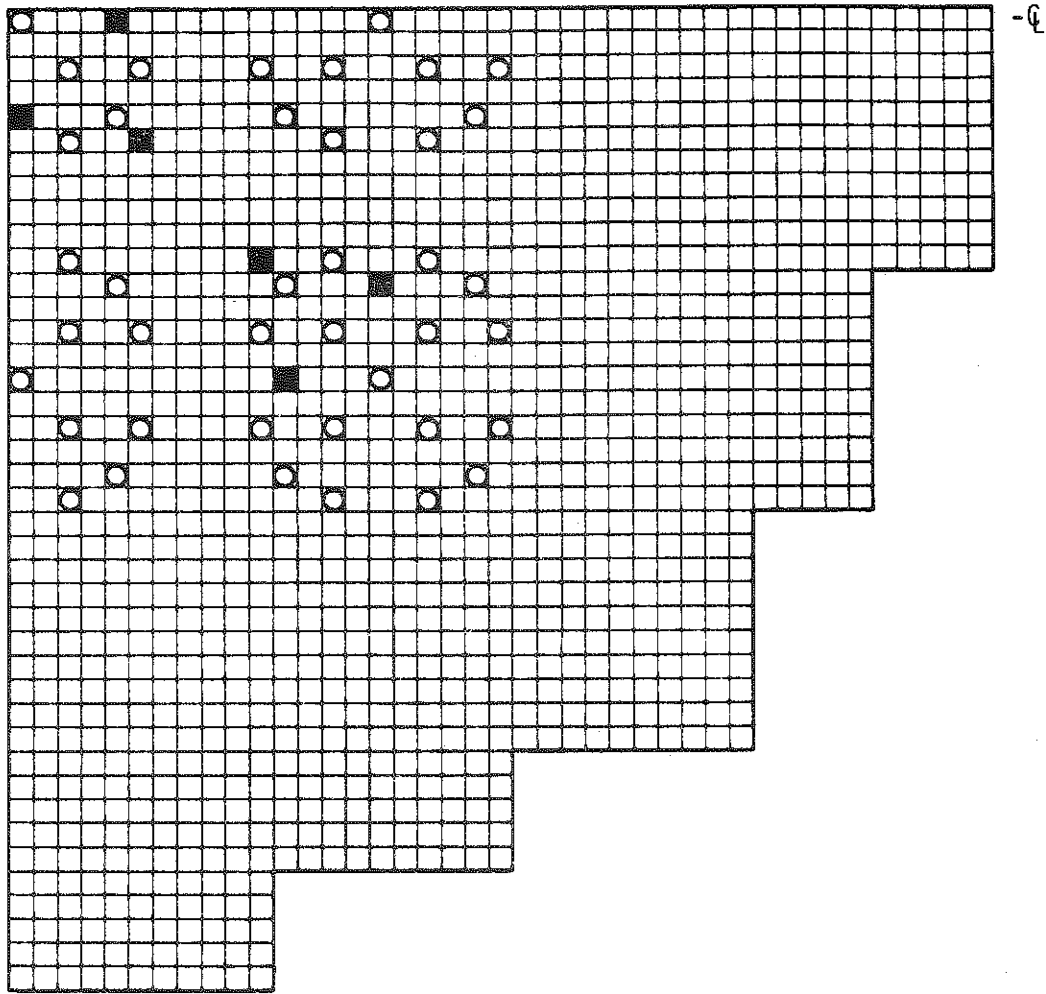
Figure 4-2. Core 2 Loading Diagram



1
2

-  VACANT WATER-FILLED POSITION
-  2.46 wt % U-235 ENRICHED FUEL
-  Ag-In-Cd ROD POSITION

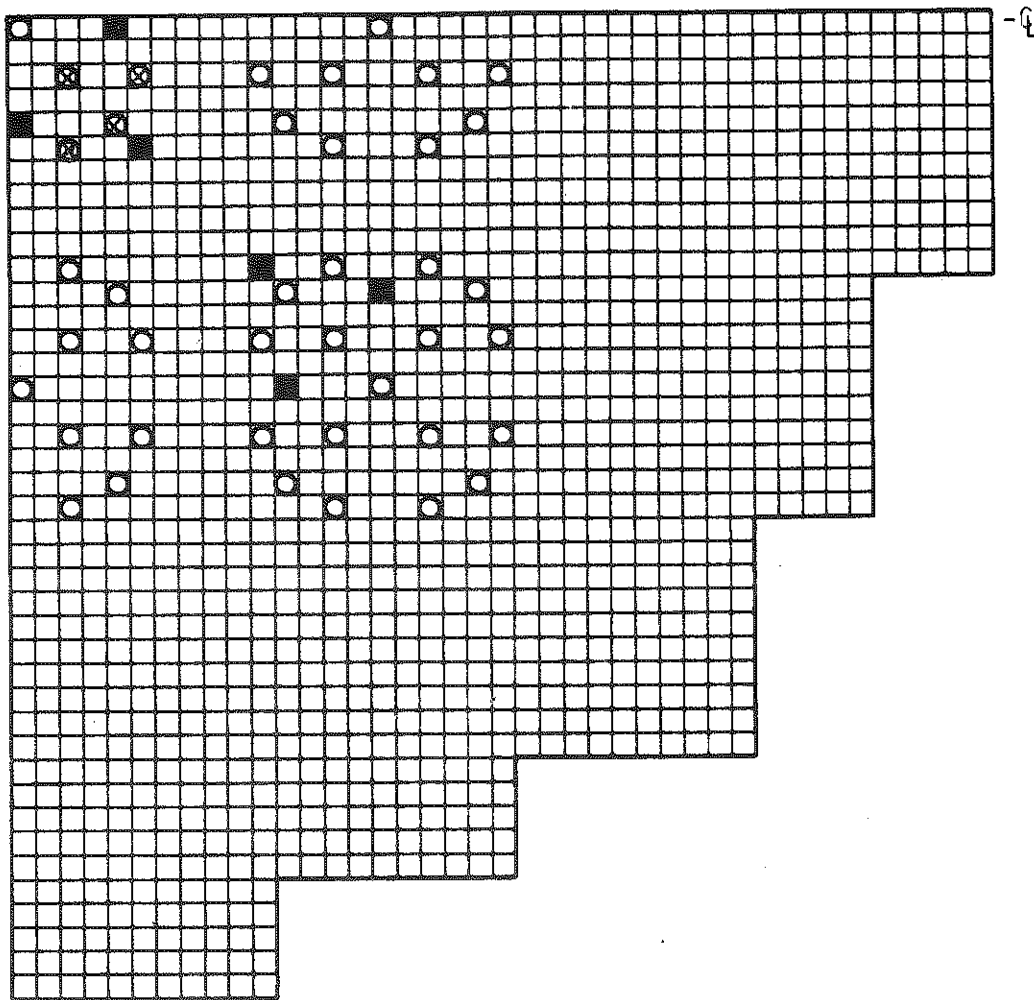
Figure 4-3. Core 3 Loading Diagram



1
2

-  VACANT WATER-FILLED POSITION
-  2.46 wt % U-235 ENRICHED FUEL
-  4.00 wt % Gd_2O_3 /1.94 wt % U-235 ENRICHED FUEL

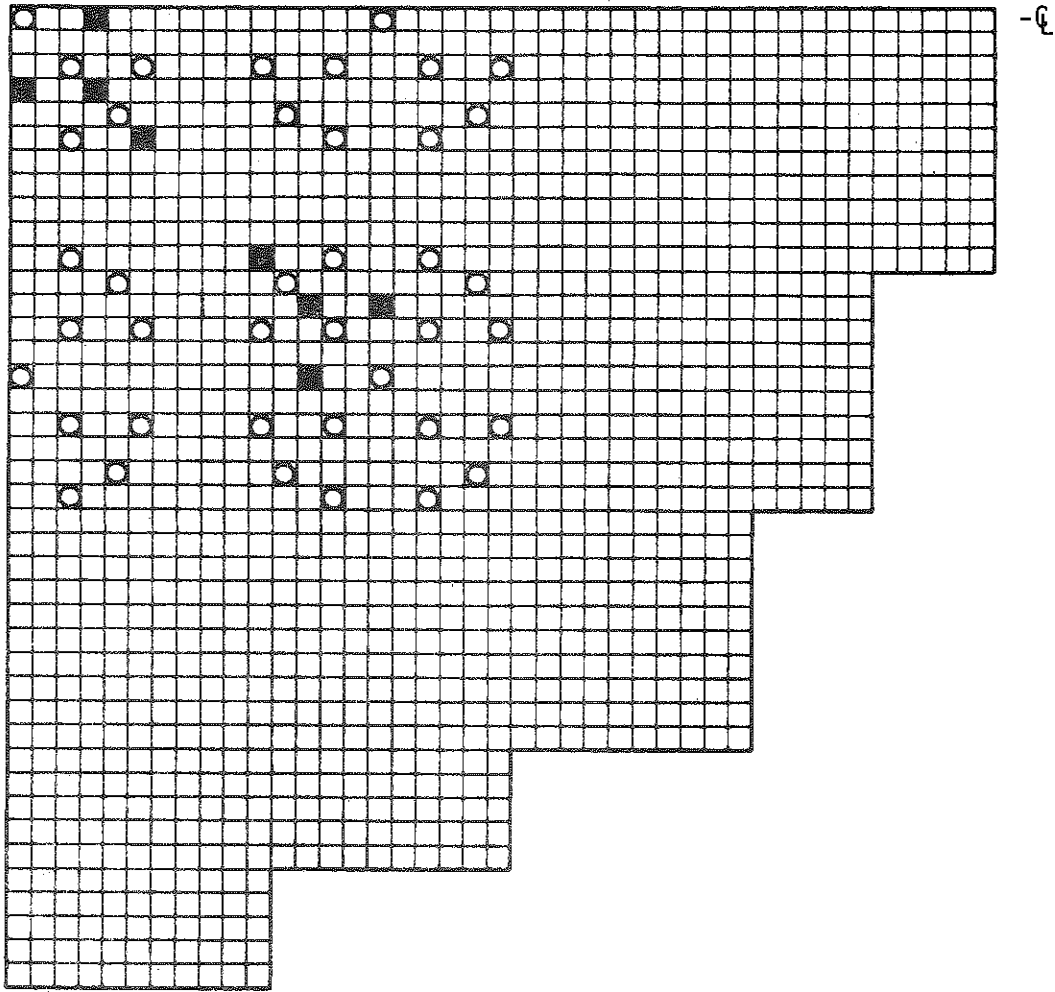
Figure 4-4. Core 4 Loading Diagram



1
Q

-  VACANT WATER-FILLED POSITION
-  2.46 wt % U-235 ENRICHED FUEL
-  4.00 wt % Gd₂O₃/1.94 wt % U-235 ENRICHED FUEL
-  Ag-In-Cd ROD POSITION

Figure 4-5. Core 5 Loading Diagram



Q



VACANT WATER-FILLED POSITION

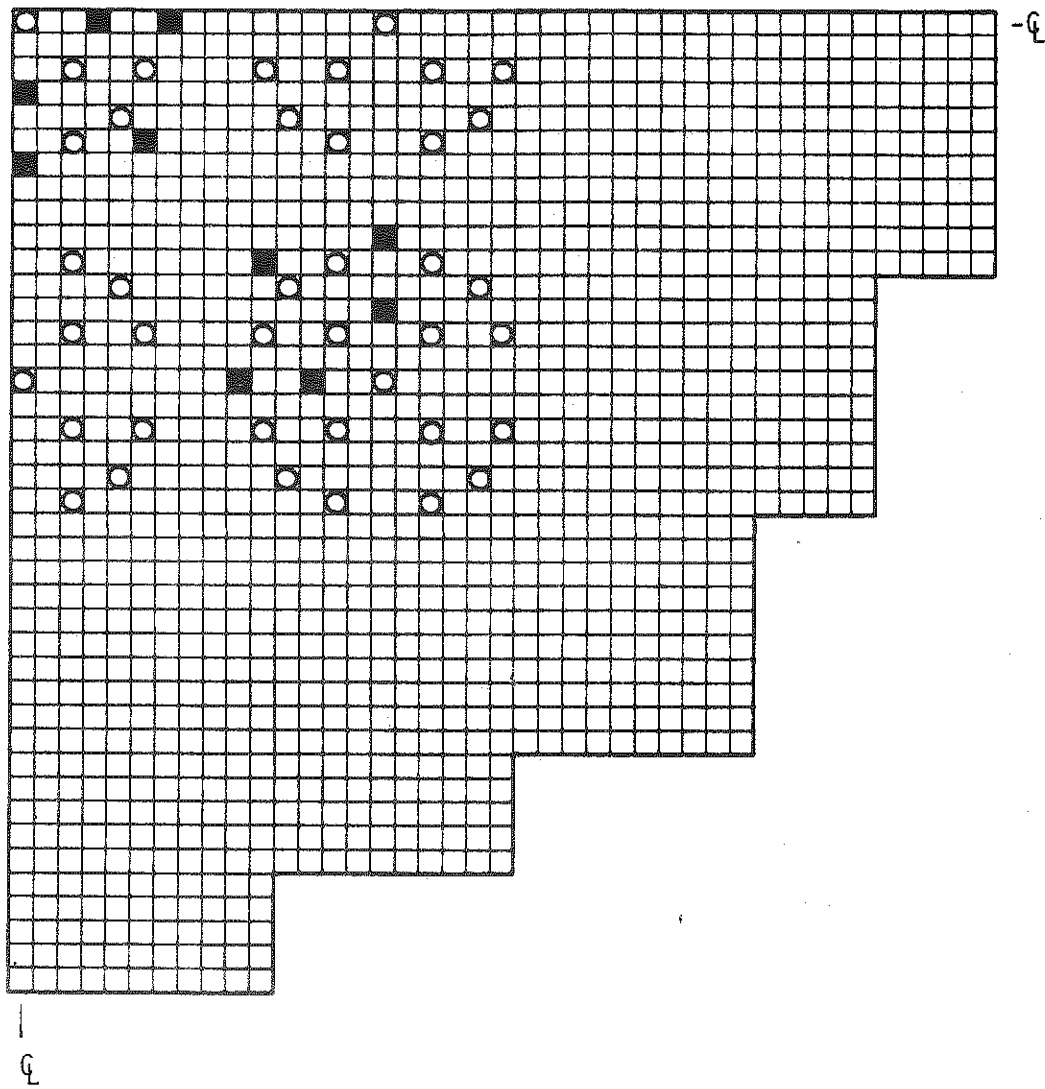


2.46 wt % U-235 ENRICHED FUEL



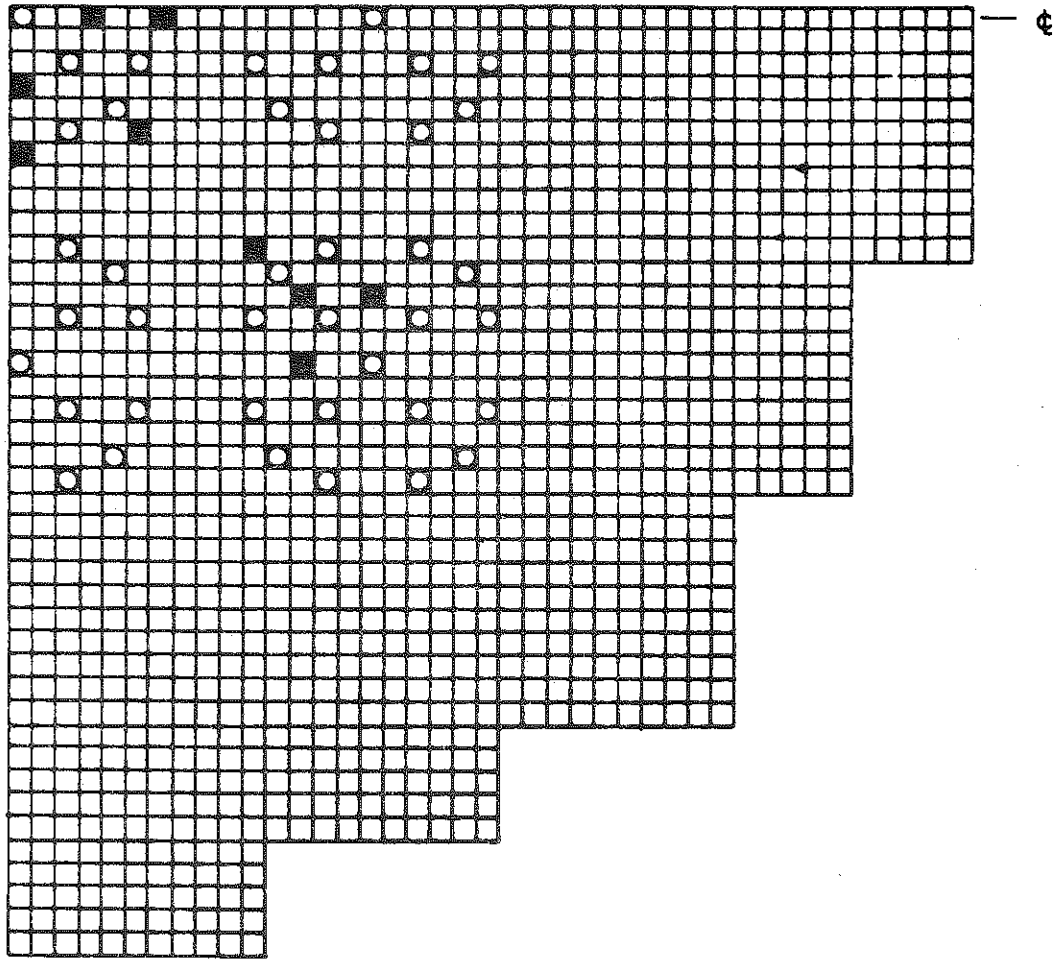
4.00 wt % Gd_2O_3 /1.94 wt % U-235 ENRICHED FUEL

Figure 4-6. Core 5-A Loading Diagram



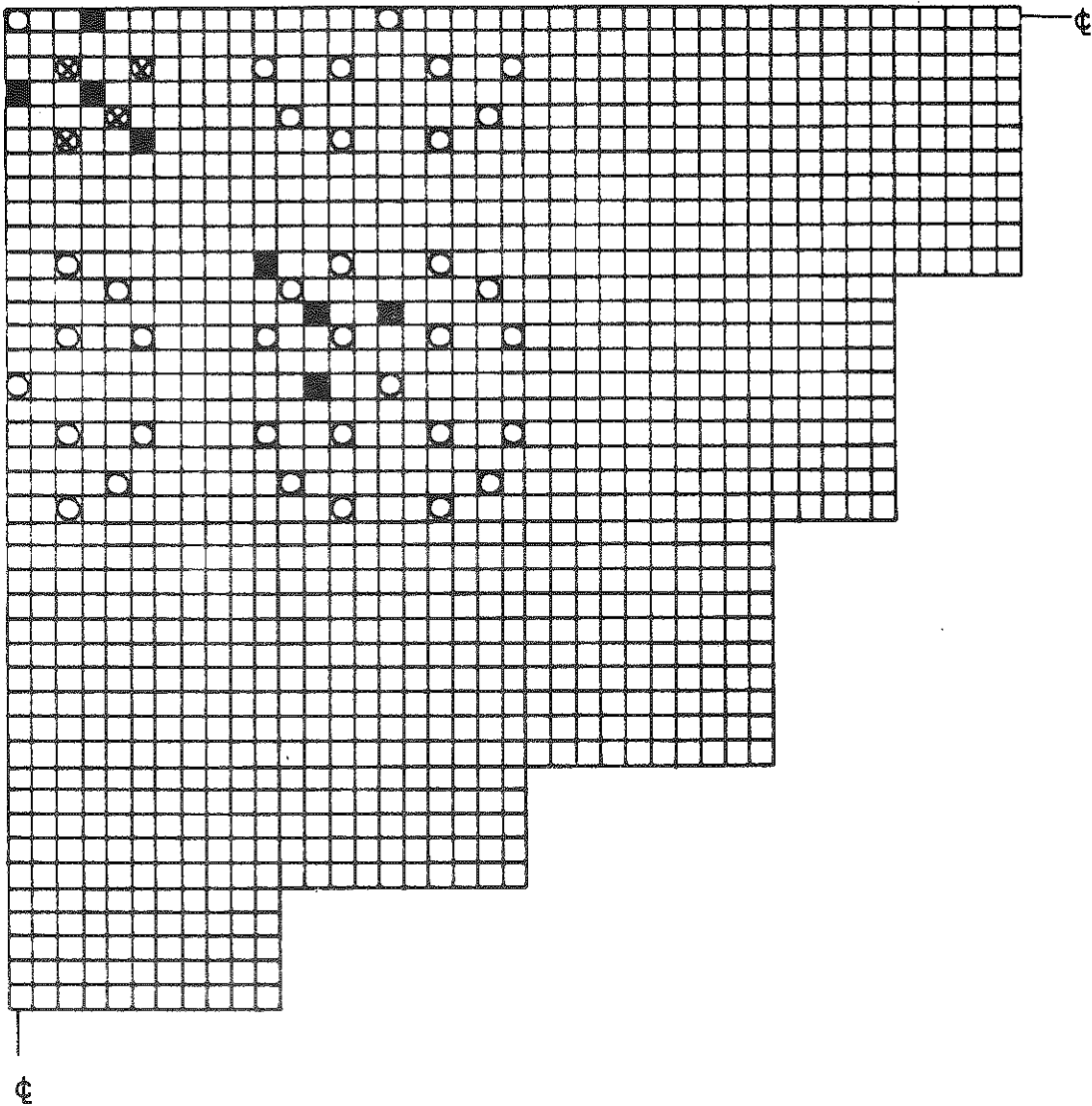
-  VACANT WATER-FILLED POSITION
-  2.46 wt % U-235 ENRICHED FUEL
-  4.00 wt % Gd₂O₃/1.94 wt % U-235 ENRICHED FUEL

Figure 4-7. Core 5-B Loading Diagram



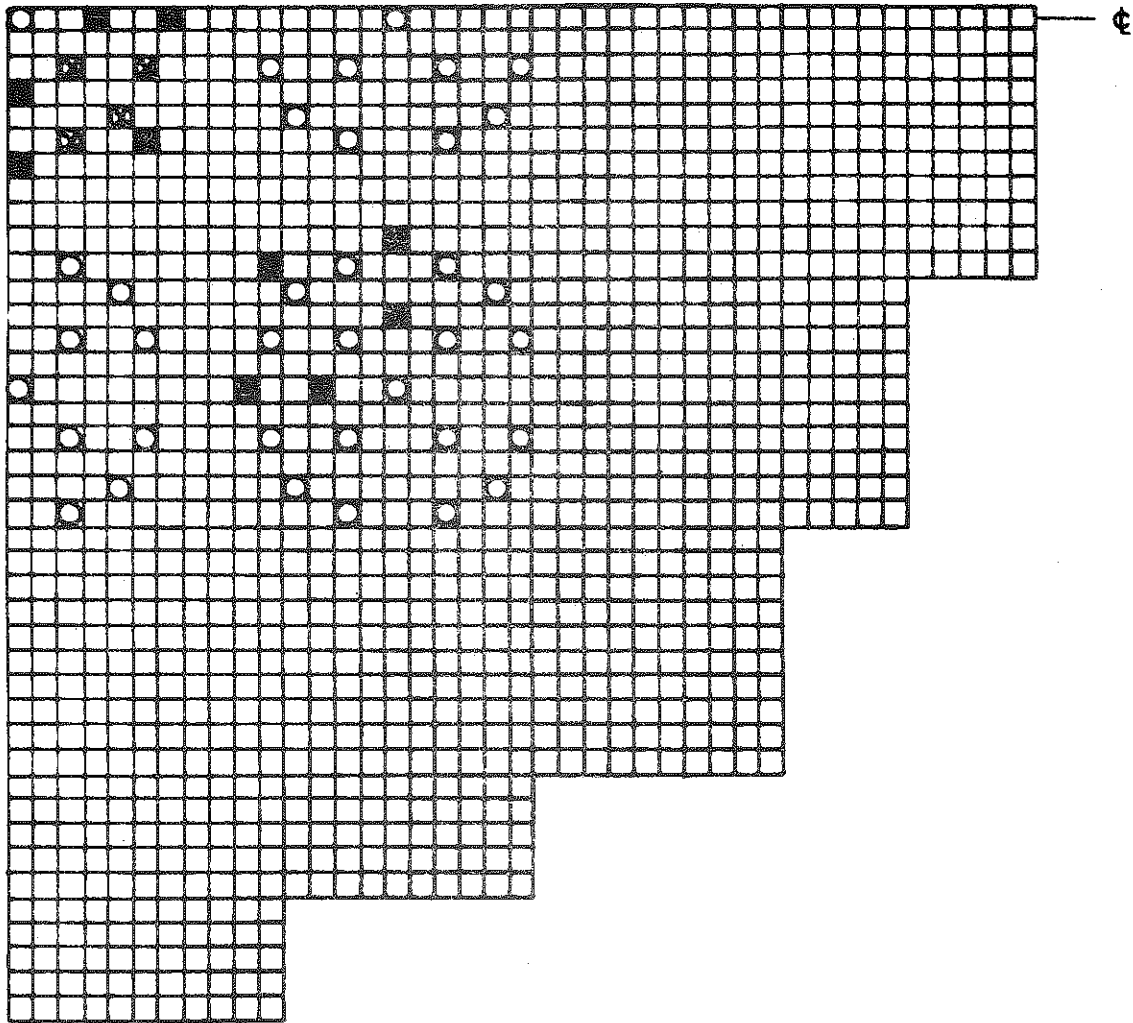
-  VACANT WATER-FILLED POSITION
-  2.46 wt % U-235 ENRICHED FUEL
-  4.00 wt % Gd₂O₃/1.94 wt % U-235 ENRICHED FUEL

Figure 4-8. Core 6 Loading Diagram



-  VACANT WATER-FILLED POSITION
-  2.46 wt % U-235 ENRICHED FUEL
-  4.00 wt % Gd_2O_3 /1.94 wt % U-235 ENRICHED FUEL
-  Ag-In-Cd ROD POSITION

Figure 4-9. Core 6-A Loading Diagram



⊕



VACANT WATER-FILLED POSITION



2.46 wt % U-235 Enriched Fuel

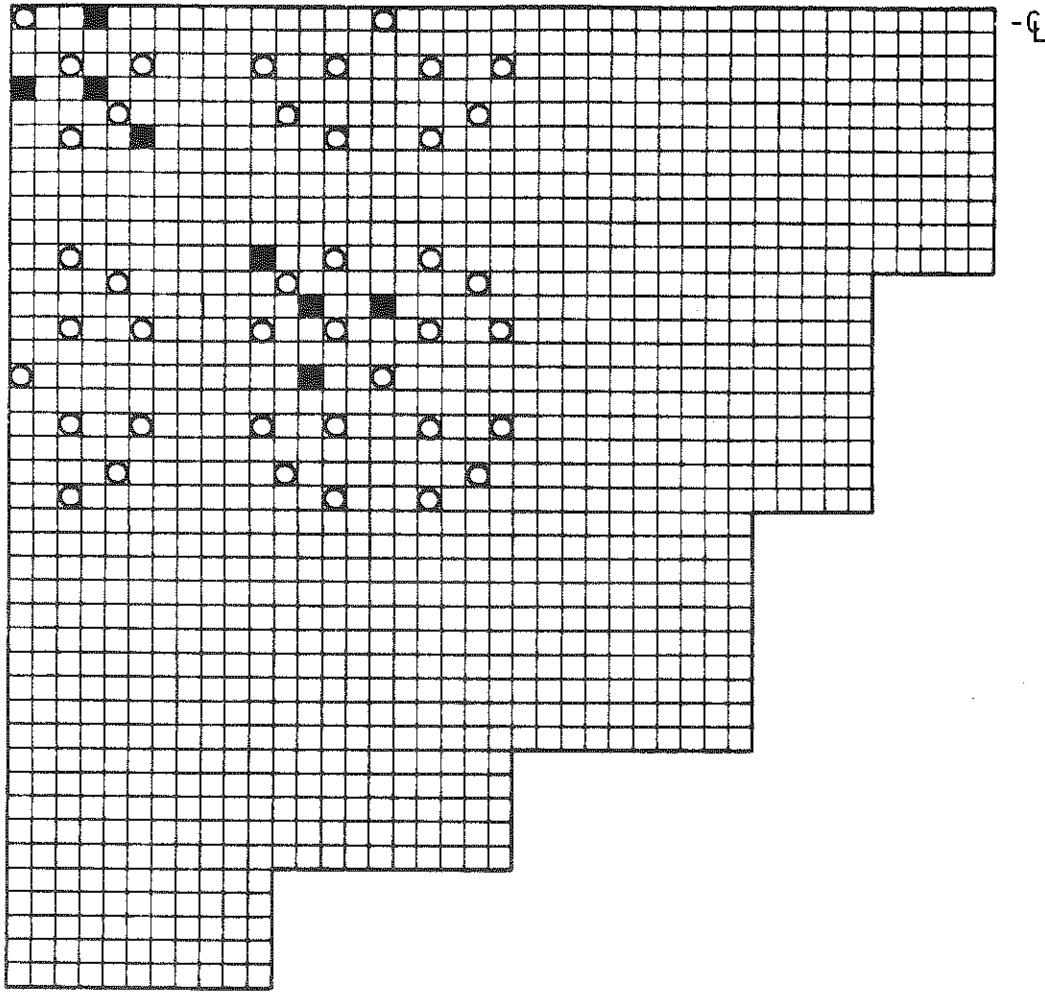


4.00 wt % Gd_2O_3 /1.94 wt % U-235 Enriched Fuel



Ag-In-Cd ROD POSITION

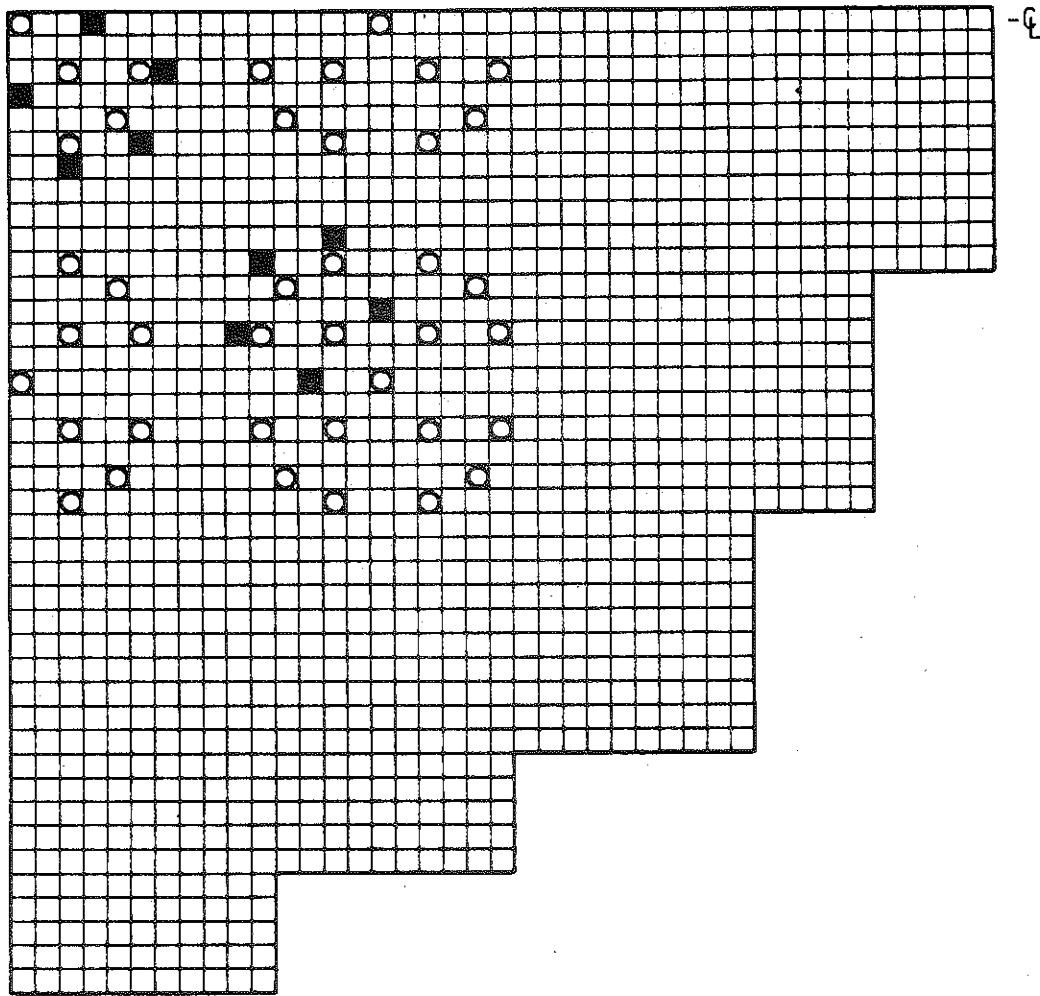
Figure 4-10. Core 7 Loading Diagram



1
2

-  VACANT WATER-FILLED POSITION
-  2.46 wt % U-235 ENRICHED FUEL
-  4.00 wt % Gd₂O₃/1.94 wt % U-235 ENRICHED FUEL ANNULAR

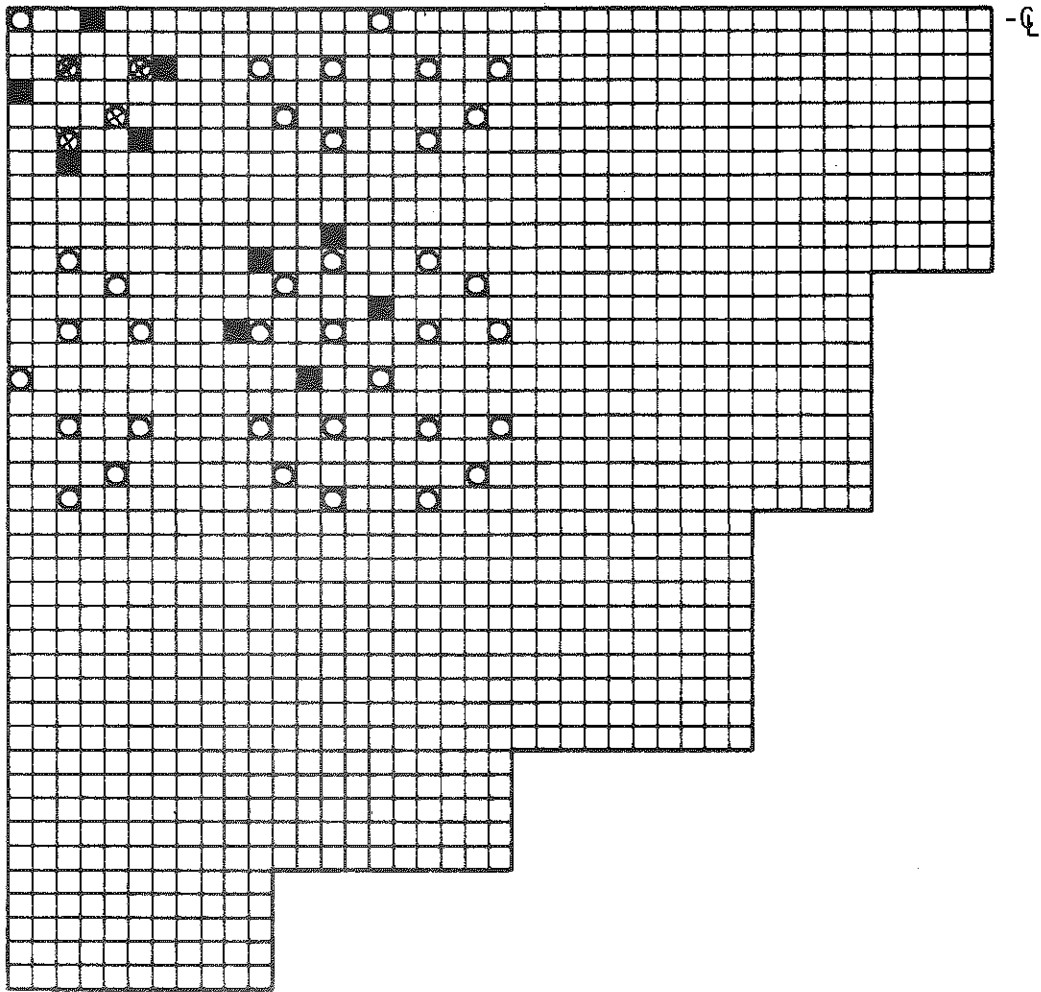
Figure 4-11. Core 8 Loading Diagram



1
Q

-  VACANT WATER-FILLED POSITION
-  2.46 wt % U-235 ENRICHED FUEL
-  4.00 wt % Gd₂O₃/1.94 wt % U-235 ENRICHED FUEL

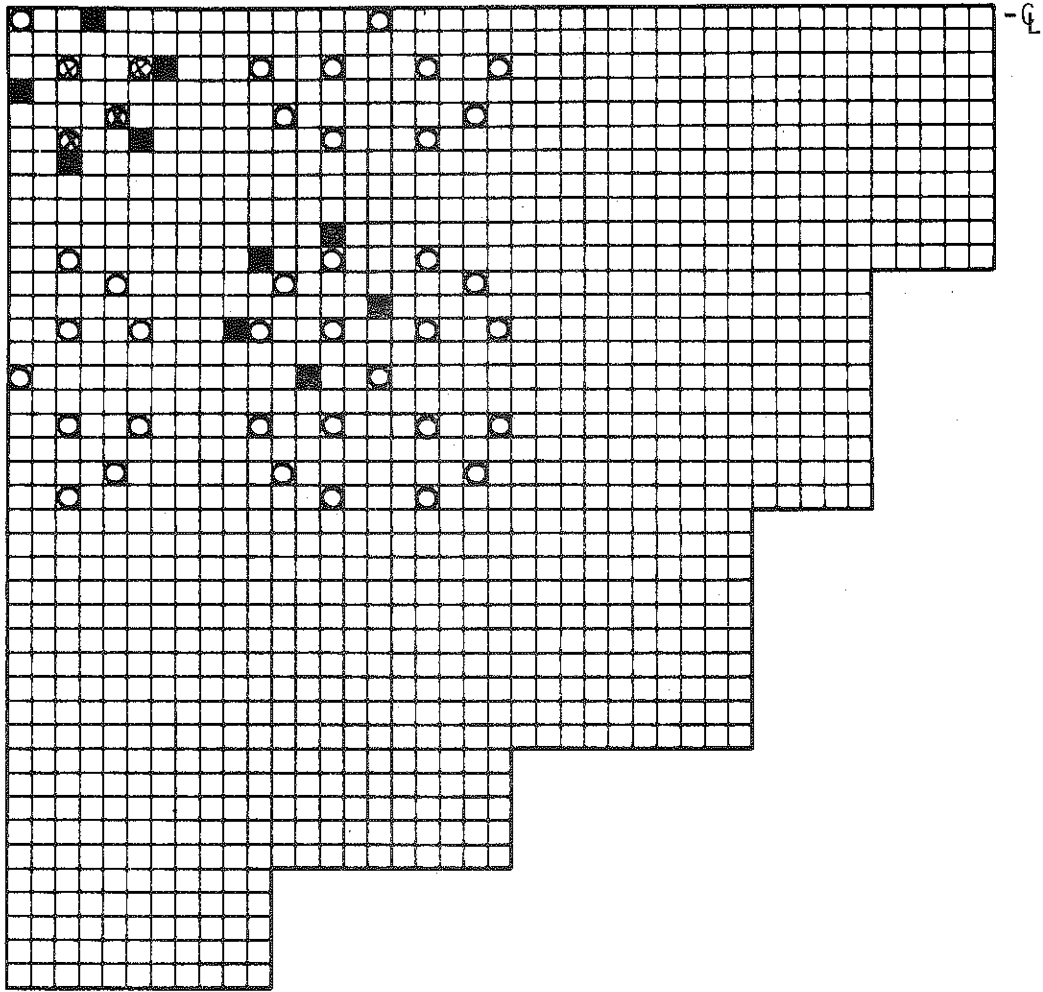
Figure 4-12. Core 9 Loading Diagram



I
G

-  VACANT WATER-FILLED POSITION
-  2.46 wt % U-235 ENRICHED FUEL
-  4.00 wt % Gd_2O_3 /1.94 wt % U-235 ENRICHED FUEL
-  Ag-In-Cd ROD POSITION

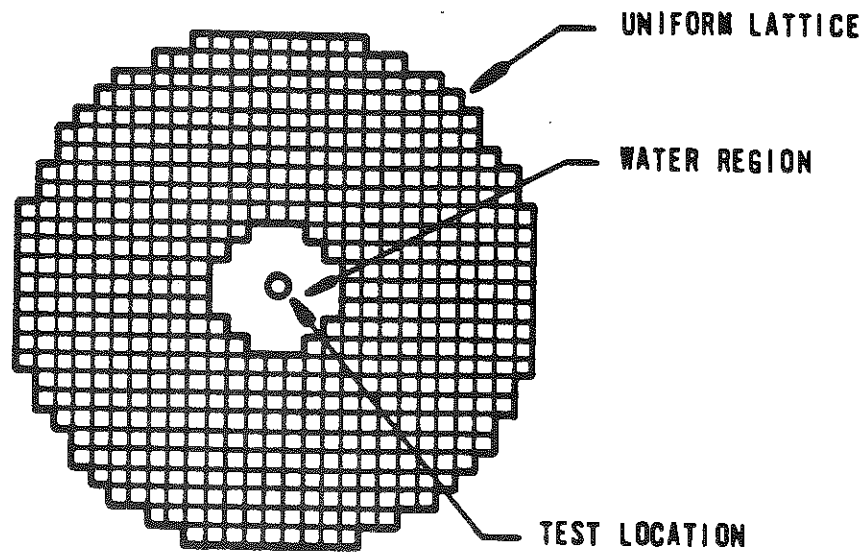
Figure 4-13. Core 10 Loading Diagram



Q
Q

-  VACANT WATER-FILLED POSITION
-  2.46 wt % U-235 ENRICHED FUEL
-  4.00 wt % Gd_2O_3 /1.94 wt % U-235 ENRICHED FUEL
-  VOID ROD LOCATION

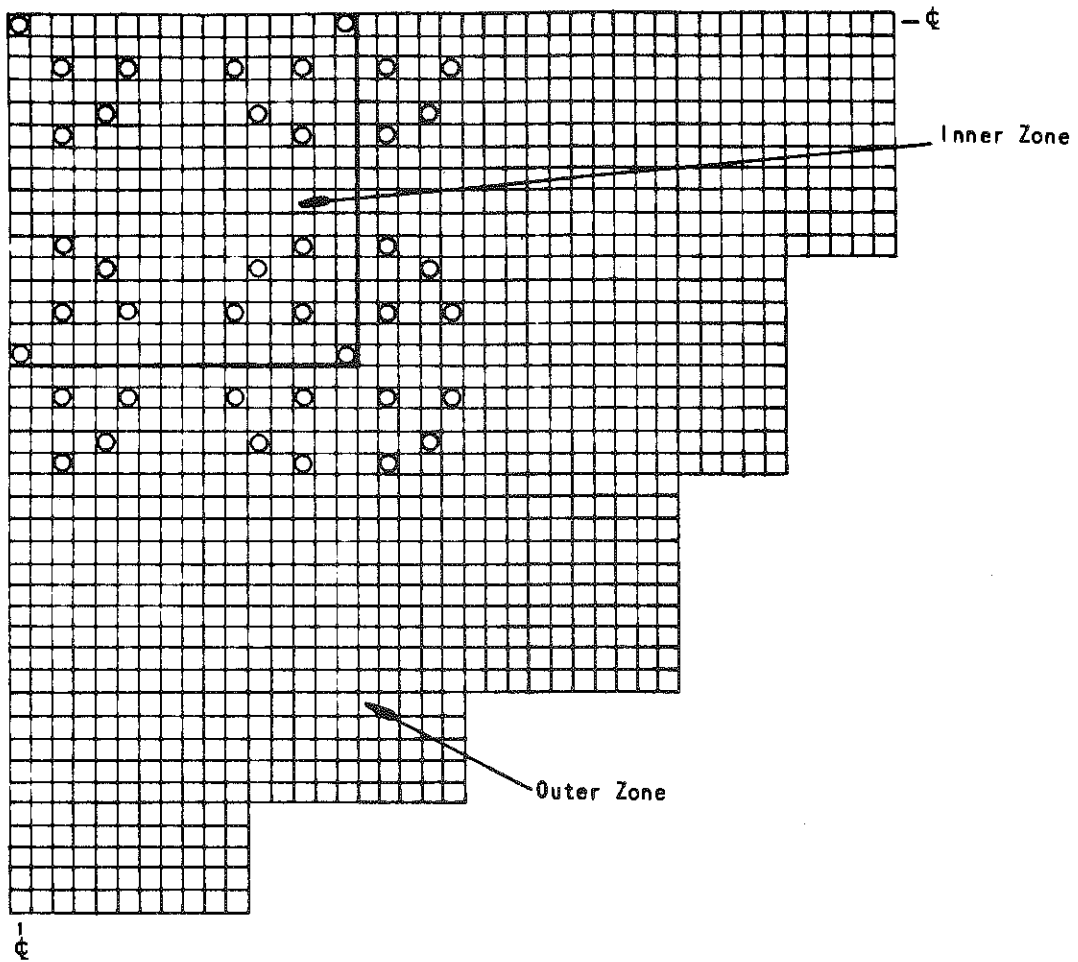
Figure 4-14. Core 11, U-238 Resonance Integral Measurements Core Configuration



554 FUEL RODS, 2.46 wt % U-235
37 FUEL RODS OMITTED FROM CENTER

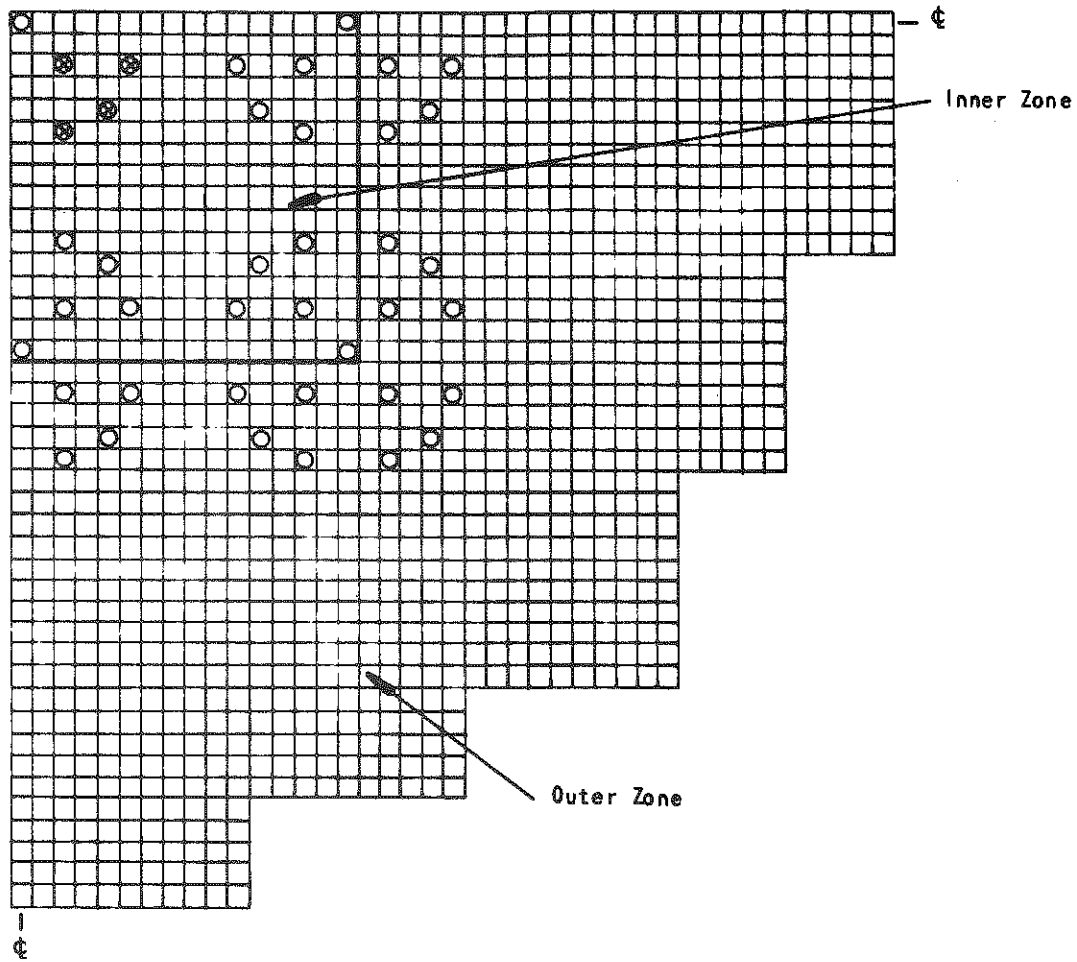
0.625-INCH OD x 0.065-INCH WALL
TUBE IN CENTER SEALED ON
BOTTOM TO EXCLUDE WATER

Figure 4-15. Core 12 Loading Diagram



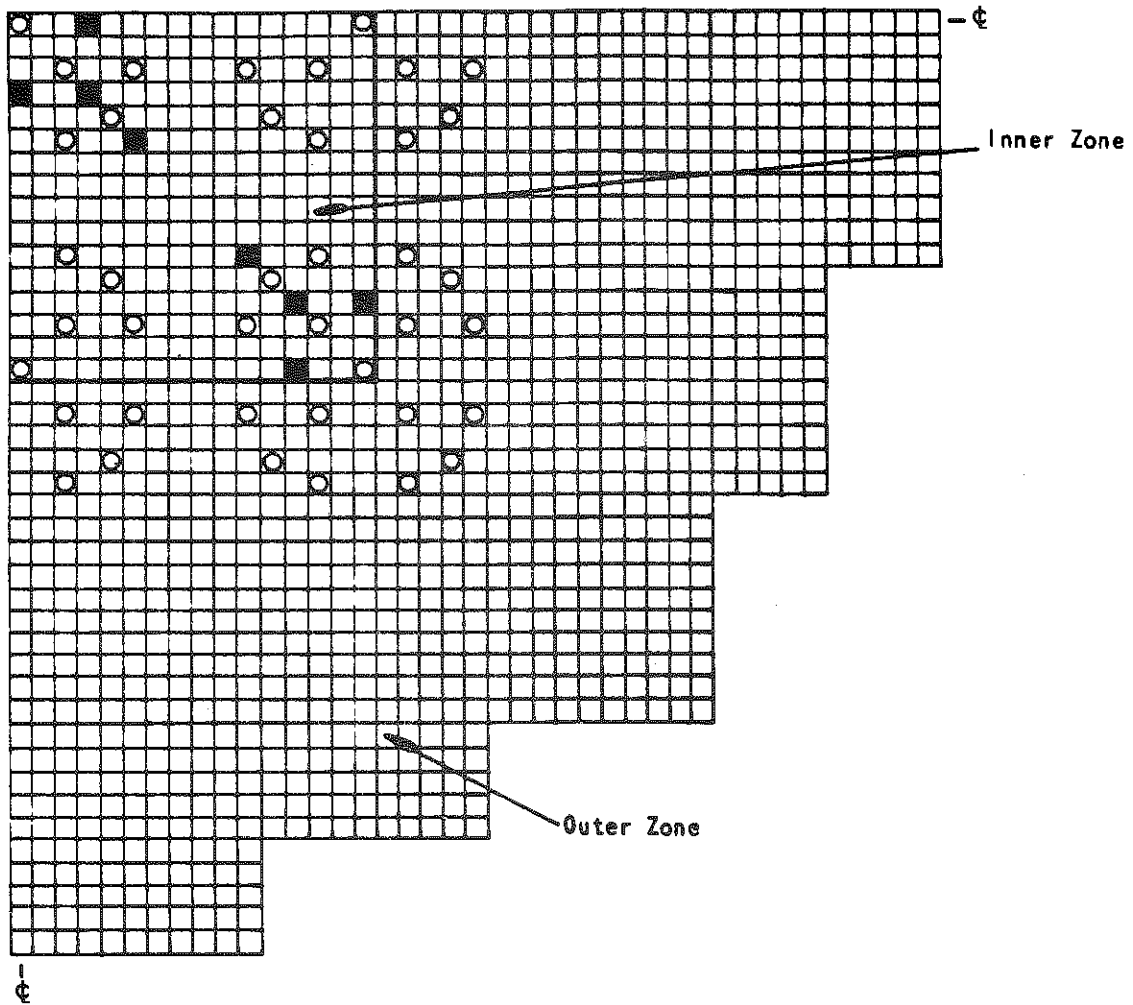
- VACANT WATER-FILLED POSITION
- 2.46 wt % U-235 ENRICHED FUEL: OUTER ZONE
- 4.02 wt % U-235 ENRICHED FUEL: INNER ZONE

Figure 4-16. Core 13 Loading Diagram



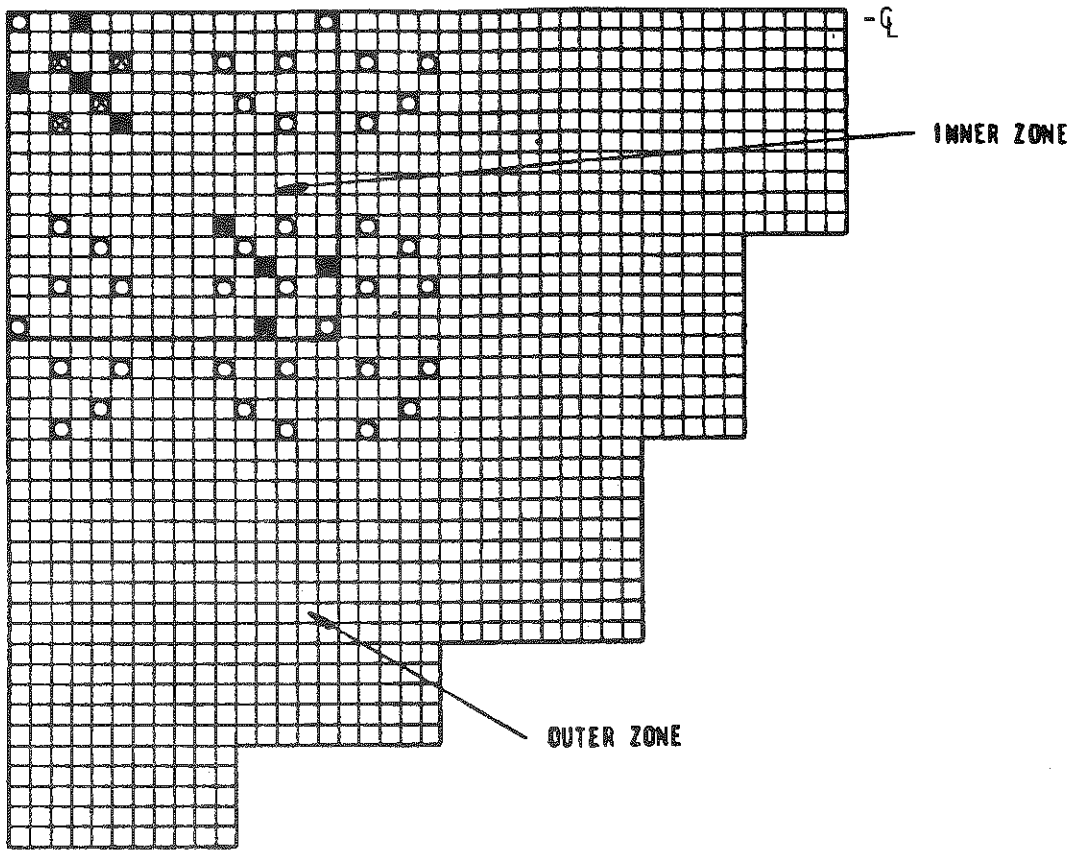
- VACANT WATER-FILLED POSITION
- 2.46 wt % U-235 ENRICHED FUEL: OUTER ZONE
- ◻ 4.02 wt % U-235 ENRICHED FUEL: INNER ZONE
- ⊗ B₄C ROD POSITION

Figure 4-17. Core 14 Loading Diagram



- ◻ (with a circle inside) VACANT WATER-FILLED POSITION
- ◻ (with a circle inside) 2.46 wt % U-235 ENRICHED FUEL: OUTER ZONE
- ◻ (with a circle inside) 4.02 wt % U-235 ENRICHED FUEL: INNER ZONE
- ◼ (with a circle inside) 4.00 wt % Gd₂O₃/1.94 wt % U-235 ENRICHED FUEL

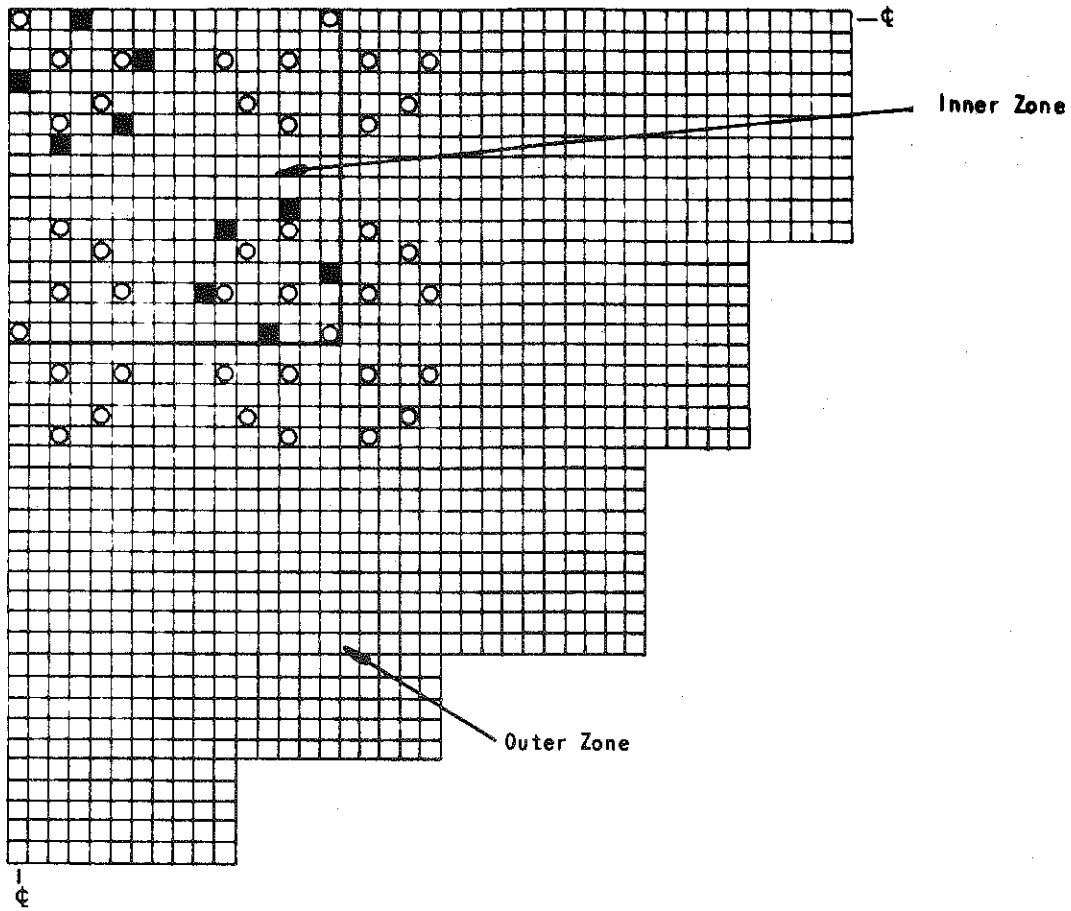
Figure 4-18. Core 15 Loading Diagram



I
Q

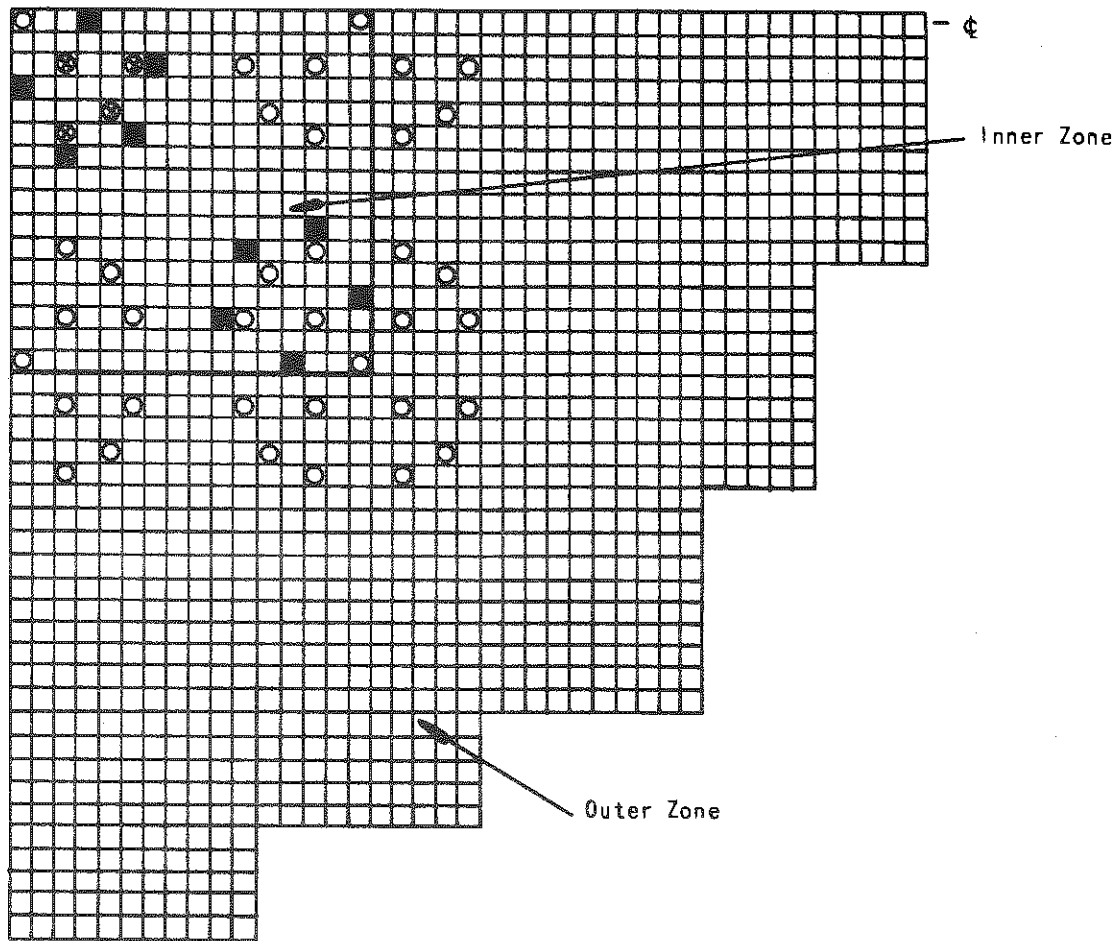
-  VACANT WATER-FILLED POSITION
-  2.46 wt % U-235 ENRICHED FUEL: OUTER ZONE
-  4.02 wt % U-235 ENRICHED FUEL: INNER ZONE
-  4.00 wt % Gd₂O₃/1.94 wt % U-235 ENRICHED FUEL
-  CONTROL (B₄C) ROD

Figure 4-19. Core 16 Loading Diagram



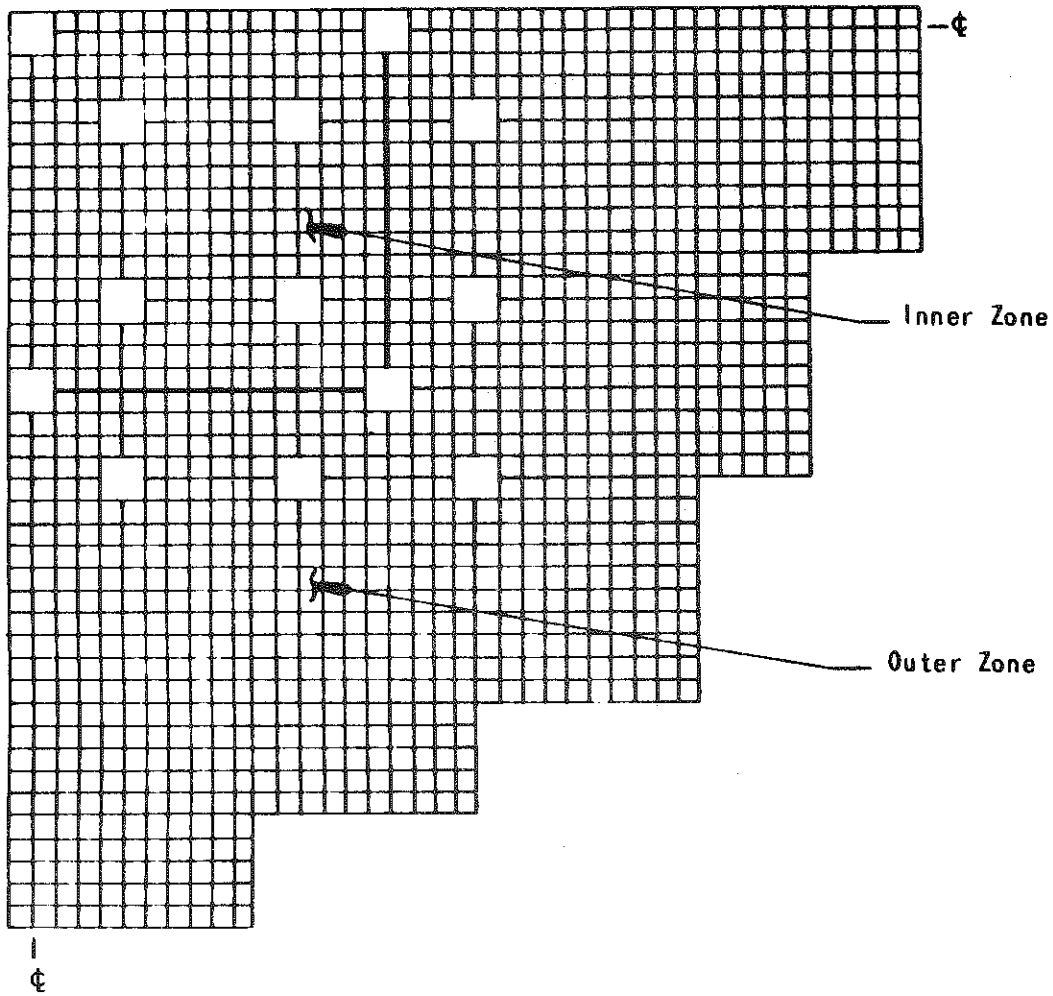
- ☐ VACANT WATER-FILLED POSITION
- ☐ 2.46 wt % U-235 ENRICHED FUEL: OUTER ZONE
- ☐ 4.02 wt % U-235 ENRICHED FUEL: INNER ZONE
- 4.00 wt % Gd_2O_3 /1.94 wt % U-235 ENRICHED FUEL

Figure 4-20. Core 17 Loading Diagram



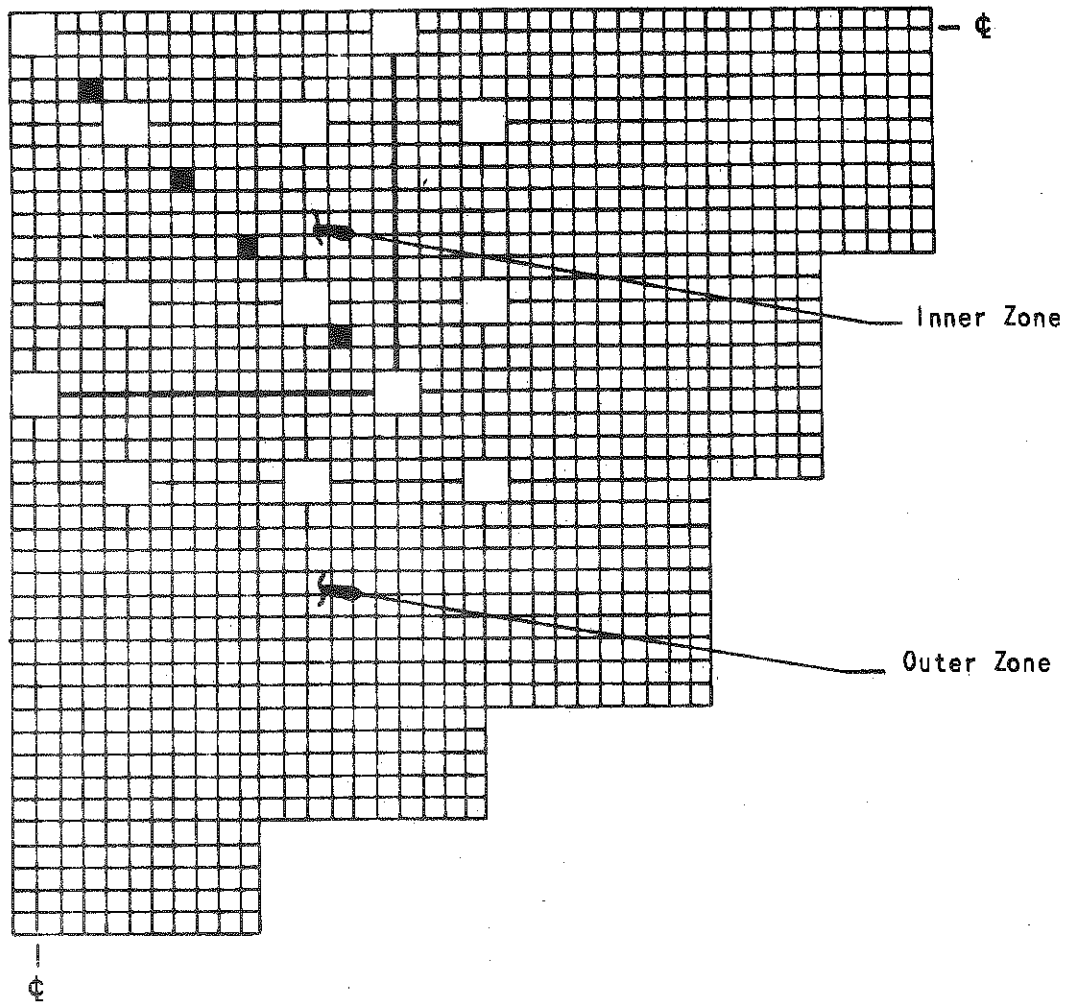
- ☐ VACANT WATER-FILLED POSITION
- ☐ 2.46 wt % U-235 ENRICHED FUEL: OUTER ZONE
- ☐ 4.02 wt % U-235 ENRICHED FUEL: INNER ZONE
- 4.00 wt % Gd₂O₃/1.94 wt % U-235 ENRICHED FUEL
- ⊗ B₄C ROD POSITION

Figure 4-21. Core 18 Loading Diagram



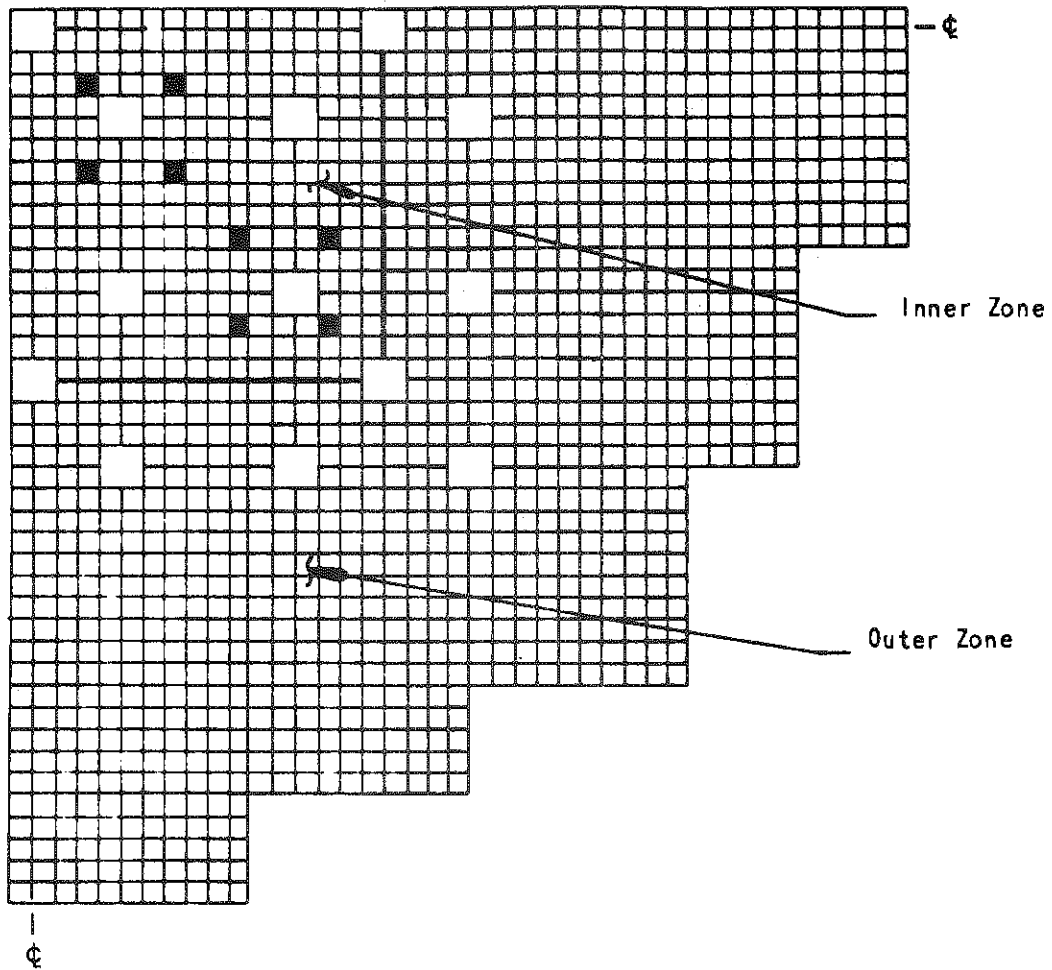
- VACANT WATER-FILLED POSITION
- 2.46 wt % U-235 ENRICHED FUEL: OUTER ZONE
- 4.02 wt % U-235 ENRICHED FUEL: INNER ZONE

Figure 4-22. Core 19 Loading Diagram



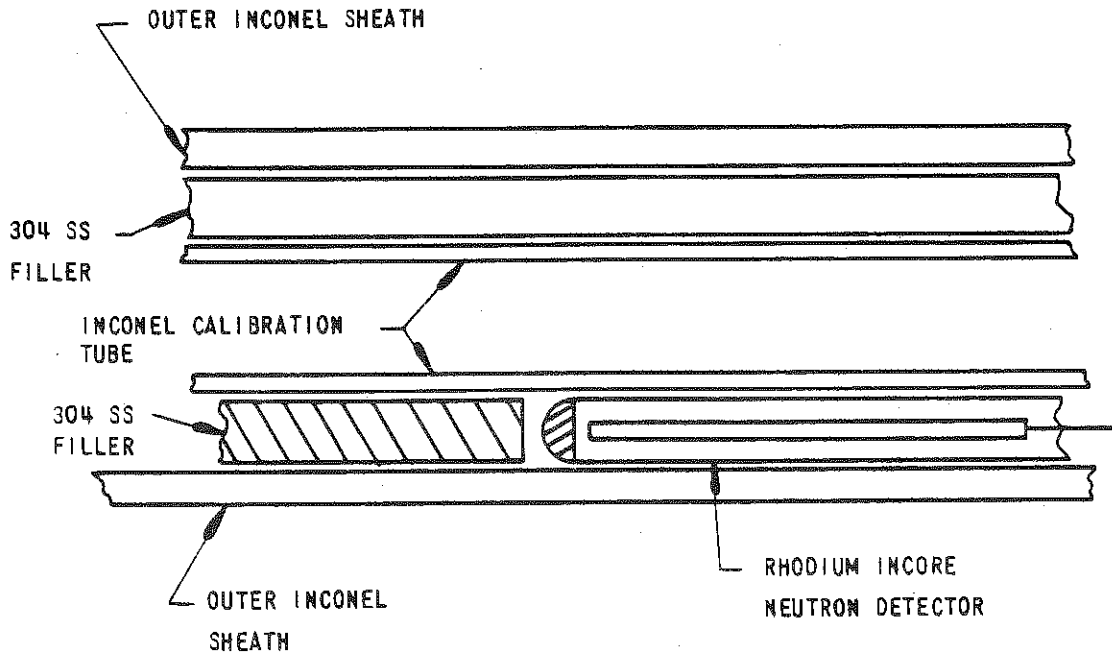
- VACANT WATER-FILLED POSITION
- 2.46 wt % U-235 ENRICHED FUEL: OUTER ZONE
- 4.02 wt % U-235 ENRICHED FUEL: INNER ZONE
- 4.00 wt % Gd_2O_3 /1.94 wt % U-235 ENRICHED FUEL

Figure 4-23. Core 20 Loading Diagram

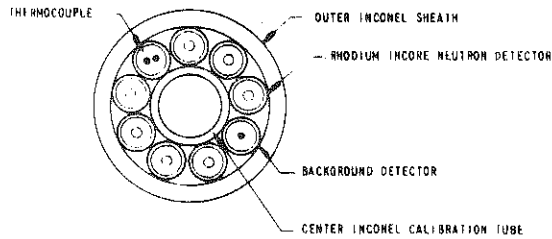


- VACANT WATER-FILLED POSITION
- 2.46 wt % U-235 ENRICHED FUEL: OUTER ZONE
- 4.02 wt % U-235 ENRICHED FUEL: INNER ZONE
- 4.00 wt % Gd_2O_3 /1.94 wt % U-235 ENRICHED FUEL

Figure 4-24. Incore Detector Assembly



Cross Section

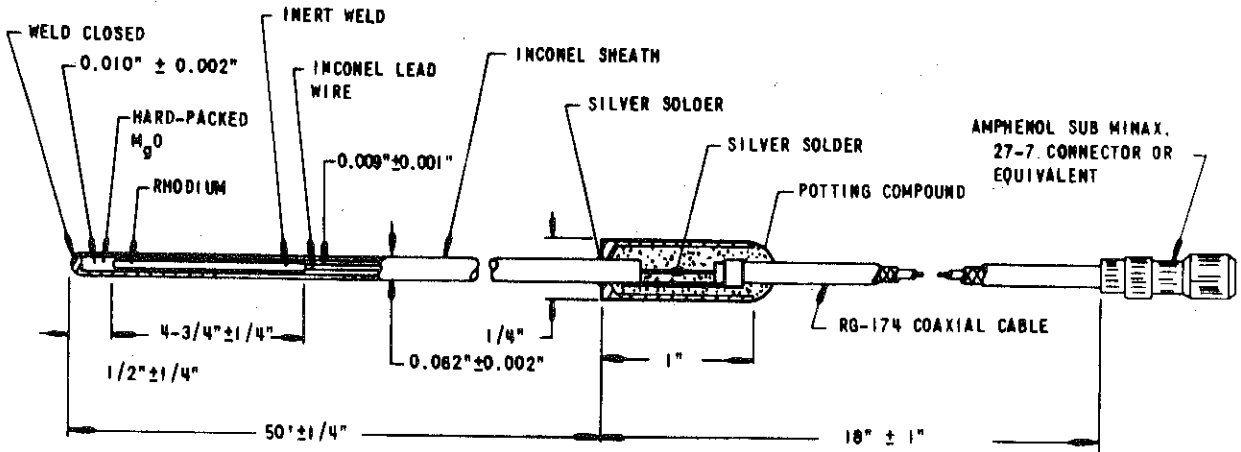


DETECTOR LOCATION, CM FROM TOP OF BASE PLATE

DISTANCE, CM *	DETECTOR *
0.0	TOP OF BASE PLATE
11.20	1
33.27	2
54.94	3
77.17	4
99.01	5
120.35	6
143.61	7

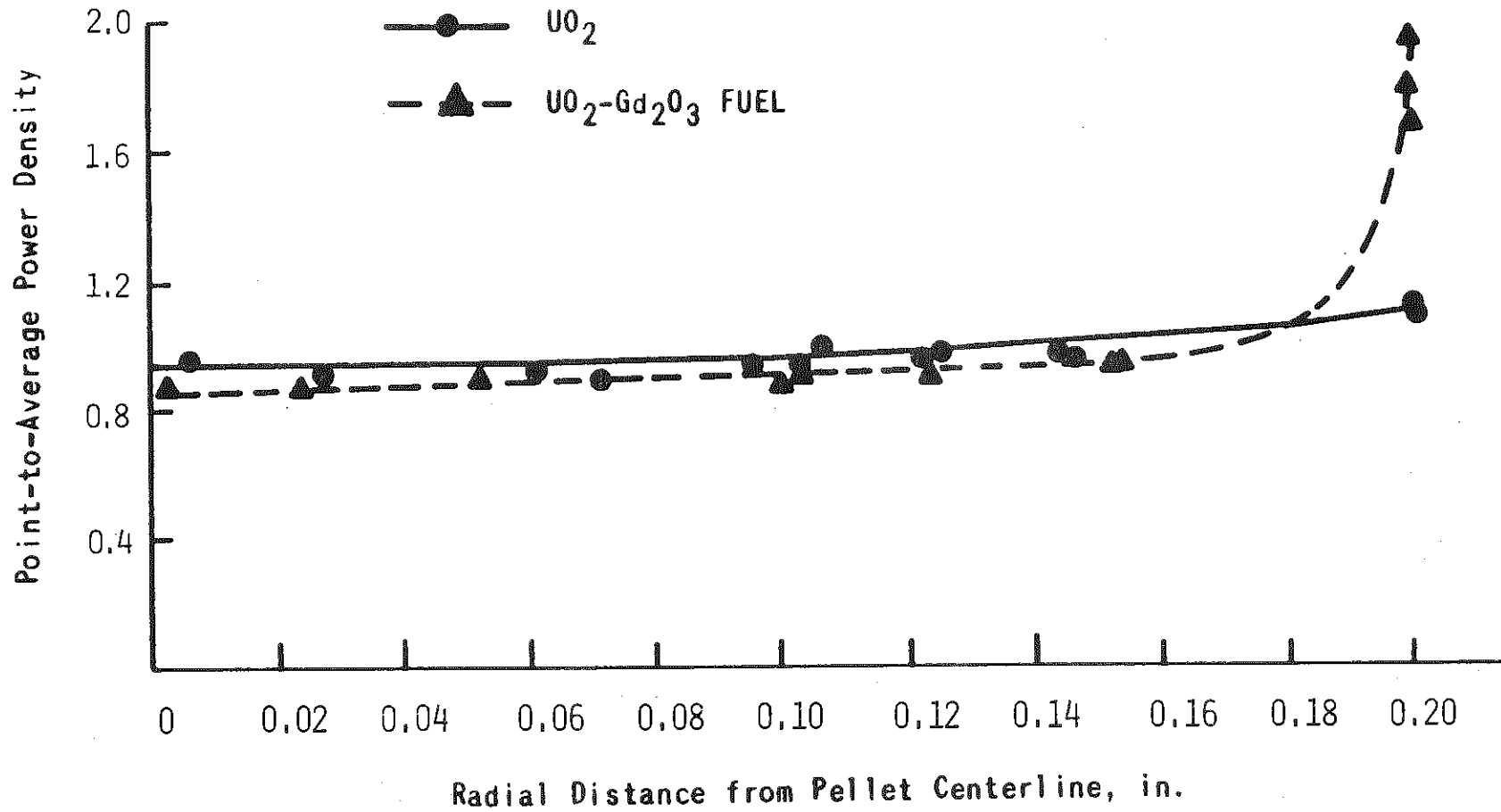
*DISTANCE TO THE CENTER OF THE EMITTER WHICH IS ITSELF 13-14 CM LONG

Figure 4-25. All-Solid Incore Neutron Detector



NOTE: FOR BACKGROUND DETECTOR, EXTEND INCONEL LEAD WIRE TO OCCUPY REGION SHOWN HERE FOR RHODIUM

Figure 4-26. Radial Power Distribution Through Fuel Pellet



NOTE: AREA UNDER CURVE EQUALS 1.0

Figure 4-27. Comparison of Solid and Annular Fuel U-238 Resonance Integral

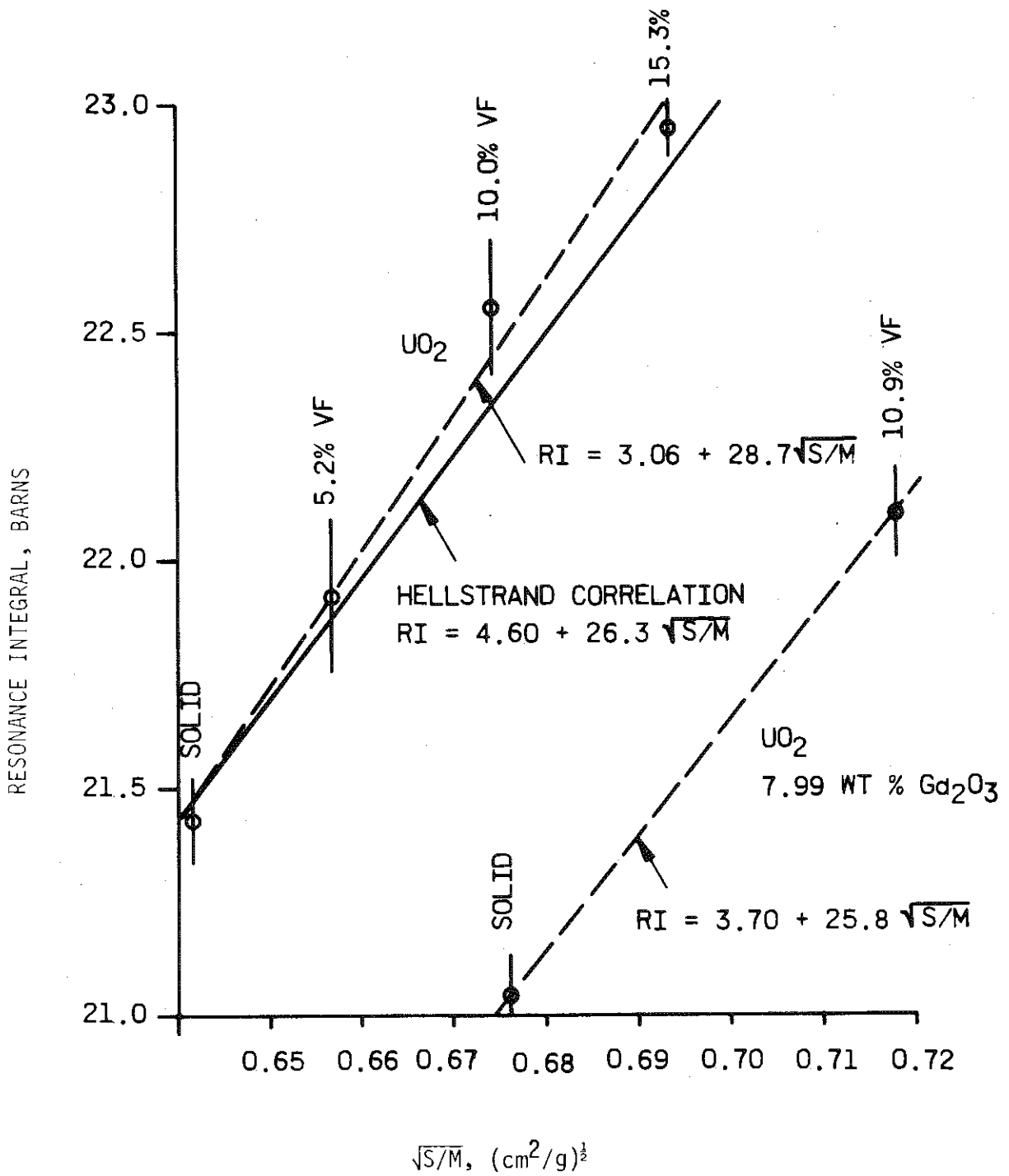


Figure 4-28. Neutron Spectrum in the Test Position

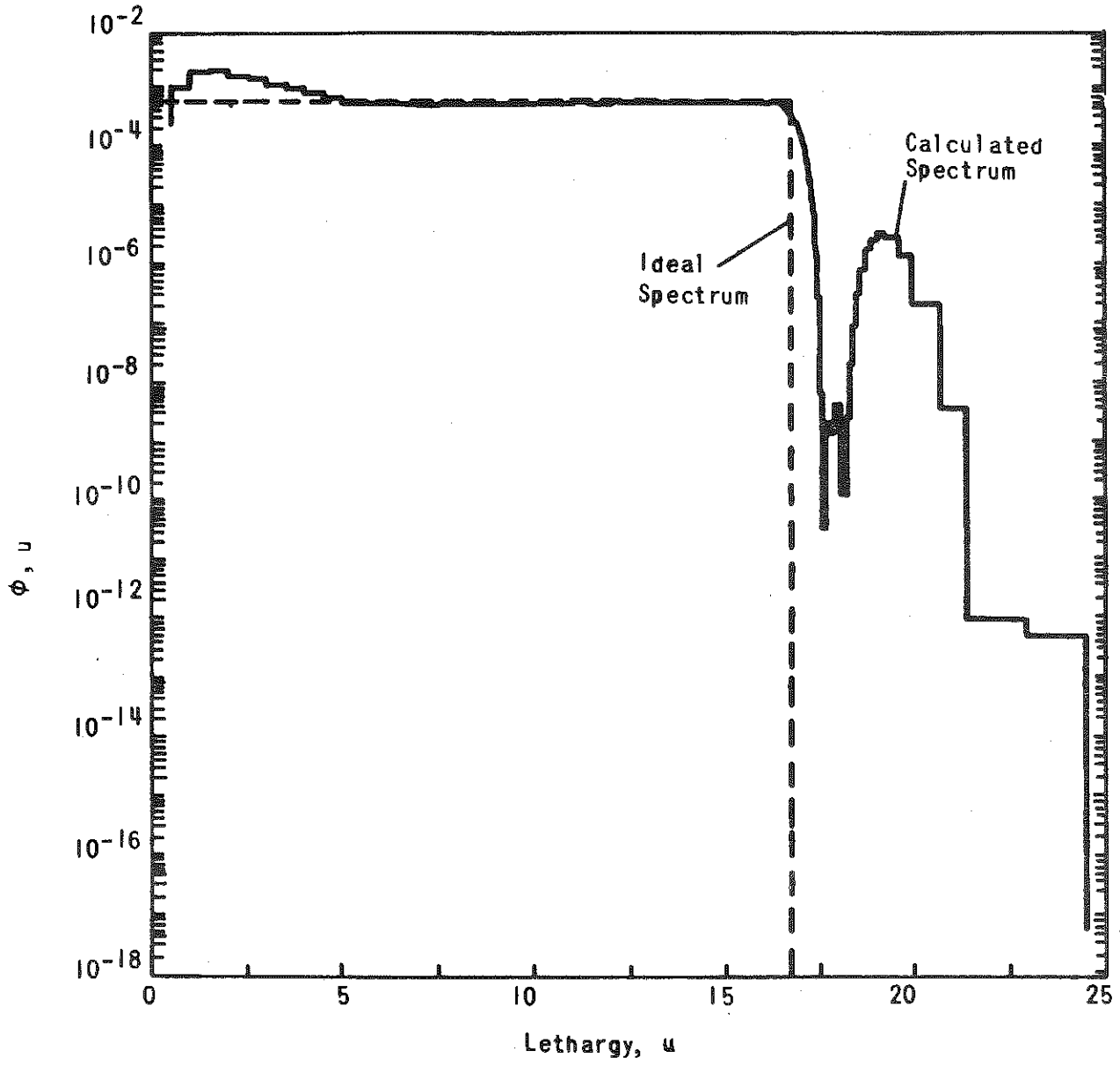


Figure 4-29. Comparison of U-238 and Cd Resonance Structures

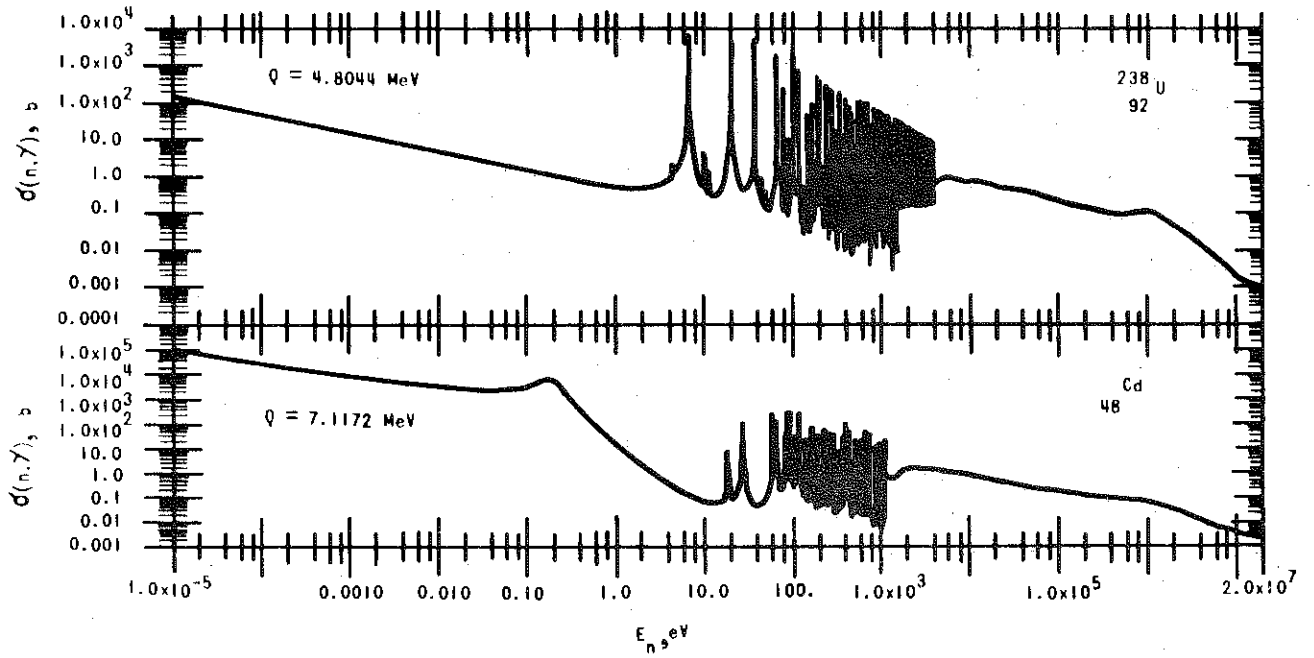


Figure 4-30. Schematic of Actual and Ideal Sample Configurations

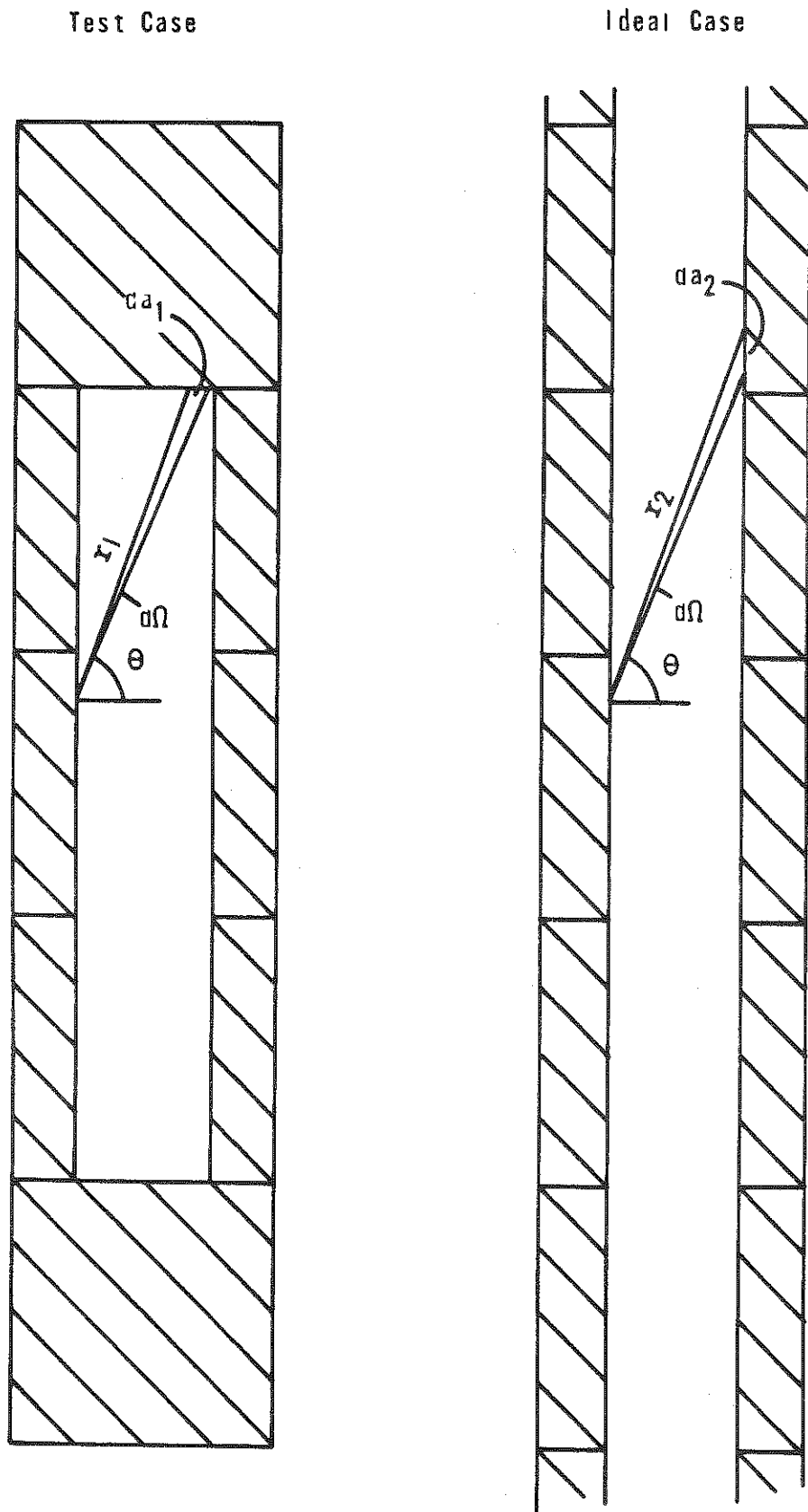


Figure 4-31. Emergent Flux Cones from a Uniform Isotropic Source Region

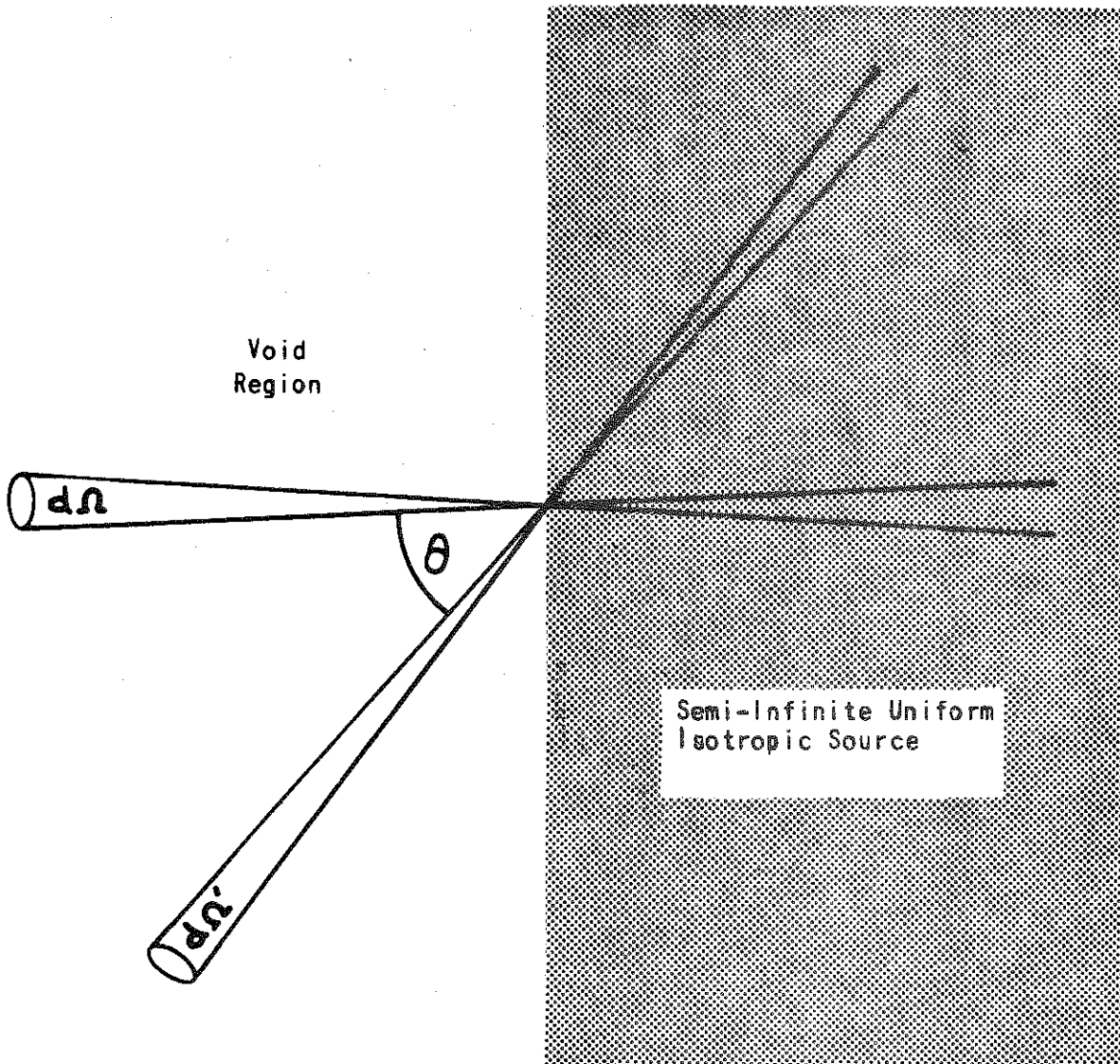
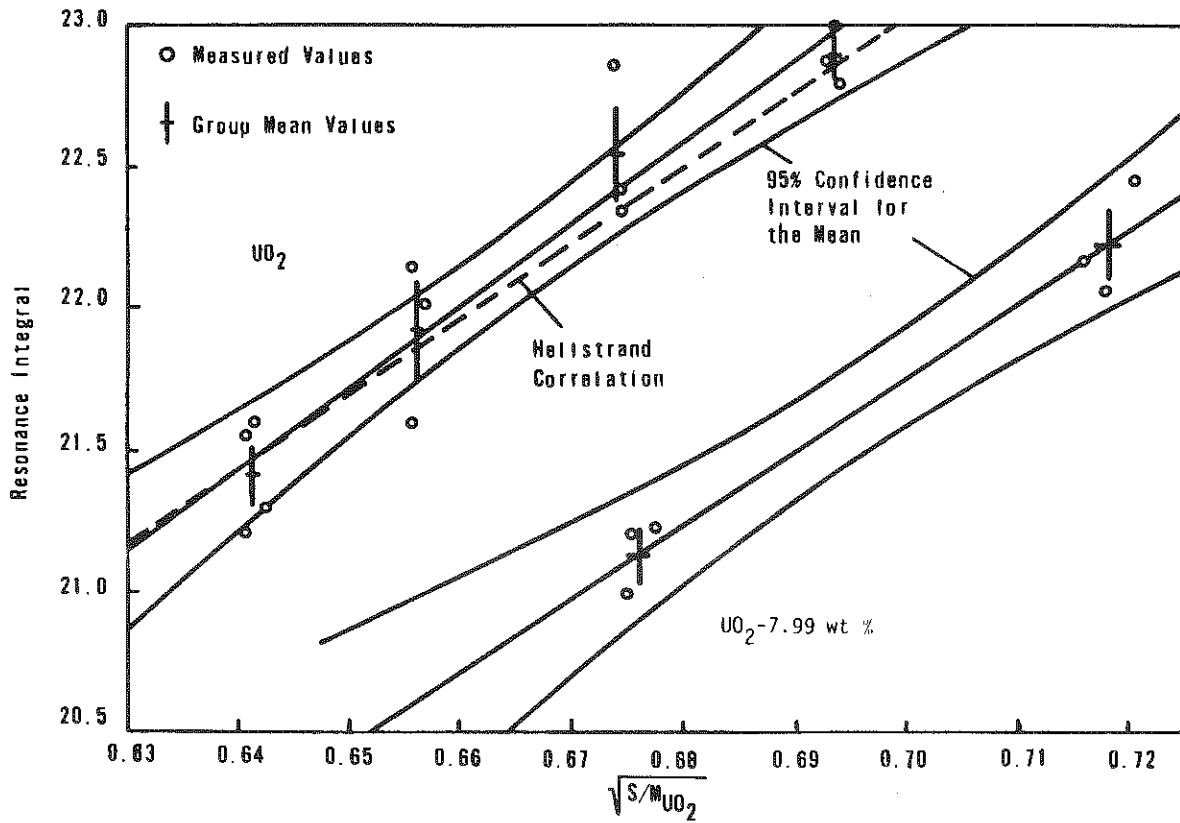


Figure 4-32. Linear Regression Results with all Points Equally Weighted



5. NUCLEAR MODEL DEVELOPMENT AND VERIFICATION

5.1. Introduction

The addition of Gd_2O_3 to UO_2 makes the computation of the isotopic depletion and reactivity of the fuel more complex. Gadolinium, a black absorber, creates an extremely large flux gradient within a fuel pellet. In addition, the gadolinium produces an "onion peeling" effect by depleting from the periphery of the fuel pellet to the center. Finally, modeling the homogenous UO_2 - Gd_2O_3 system, as opposed to the separate fuel/boron burnable absorber systems, creates the complexity of coupling the UO_2 and Gd_2O_3 depletion effects within the fuel cell.

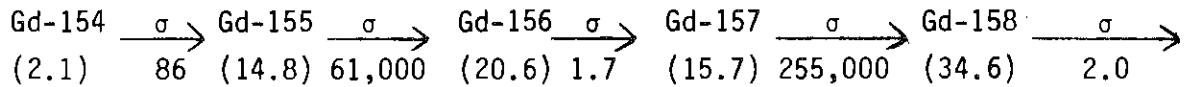
The development of a UO_2 - Gd_2O_3 nuclear depletion model is described in the following four sections:

- Implementing gadolinium depletion chains (section 5.2)
- Generating few-group cross sections (section 5.3)
- Developing an adjustment factor to account for higher-order effects (section 5.4)
- Developing thermal-group flux factors (section 5.5)

5.2. Gadolinium Depletion Chains

Natural gadolinium consists of seven isotopes with widely varying natural percentage abundances and 2200 m/s neutron capture cross sections (see Table 5-1). The extremely large thermal cross sections of Gd-155 and Gd-157 complicate the calculation of isotopic depletion and reactivity because the neutron flux in the UO_2 - Gd_2O_3 pellet is strongly space- and energy-dependent. Initially, Gd-157 shields all other isotopes in the pellet; thus, it is consumed first and followed by Gd-155 and U-235 depletion (see Figure 5-1 for U-235 concentration versus pellet radius and burnup). Eventually, Gd-155 and Gd-157 production and depletion reach equilibrium leaving only the residual gadolinium effect.

In modeling gadolinium depletion, Gd-152 and Gd-160 can be neglected because of their small abundances and cross sections. Their residual absorption effects are included in the Gd-158 contribution to yield a simplified five-isotope depletion chain represented by:



The PEEL¹⁶ code, a one-dimensional, integral transport code, computes the spatial dependence of the neutron spectrum and isotopic depletion. The epithermal spectrum and fast group constants are computed with the NULIF¹² code. An example of the gadolinium worth versus burnup using the simplified chain is given in Figure 5-2. The five-isotope gadolinium chain is estimated to provide burnup-dependent gadolinium worths within 0.5% of the complete chain.

5.3. Neutron Cross Section Data for Gadolinium

The process and computer codes used to establish the few-group cross sections for gadolinium are illustrated in Figure 5-3 and fully explained in references 11, 12, and 16 through 23. Calculations to generate few-group cross sections for UO₂-Gd₂O₃ fuel are performed with the NULIF-PEEL multigroup, integral-transport codes.^{12,16} Equal-volume mesh spacing within the pellet is used to provide more accurate representation of the energy and space dependencies. In one-dimensional, cylindrical geometry, 15 mesh points are used within the pellet; one in the clad, four in an annular, coolant region, and five in an annular, outer buffer region consisting of the homogenized, eight-neighboring fuel cells in a 3x3 fuel rod array. This model is similar to that described by Mosteller for the EPRI-CELL code.²⁴

5.4. Developing an Adjustment Factor for Higher-Order Effects

A calculation of a unit cell containing a UO₂-Gd₂O₃ was performed using the ANISN code to develop an adjustment factor to account for higher-order effects. Since the ANISN model allows for a P₁ scattering term and PEEL allows only P₀ scattering, adjustment factors (G-factors) were developed by

taking ratios of the ANISN two-group constants to the two-group constants from the corresponding PEEL calculation. Also included in the ratio is the effect created by ANISN's 111 group structure (80 thermal, 31 epithermal) versus PEEL's 41 group structure (40 thermal, 1 epithermal). The G-factors generated as described above increased the magnitude of the PEEL-generated cross sections. These G-factors, when applied by PDQ07²³ to the interpolated PEEL constants, effectively approximate ANISN constants.

5.5. Thermal Flux Factors

Core fuel cycle design studies are performed with the PDQ07 diffusion theory depletion code. Since diffusion theory does not accurately predict the flux depression in the strongly absorbing $UO_2-Gd_2O_3$ fuel with a one mesh per fuel rod geometry, a flux factor must be applied to correlate the reaction rates in the discrete PDQ07 array with those of integral transport (NULIF-PEEL) calculations. The flux factor, computed by an iterative method at selected burnups during the depletion cycle, is applied to the thermal absorption and fission cross sections input to PDQ07.

Using the flux factor results in a difference of less than 0.03% in total cell k_{∞} between NULIF-PEEL and PDQ07. This simple method of forcing agreement between reaction rates, which is similar to that of Mosteller, provides excellent agreement between NULIF-PEEL and PDQ07.²⁴

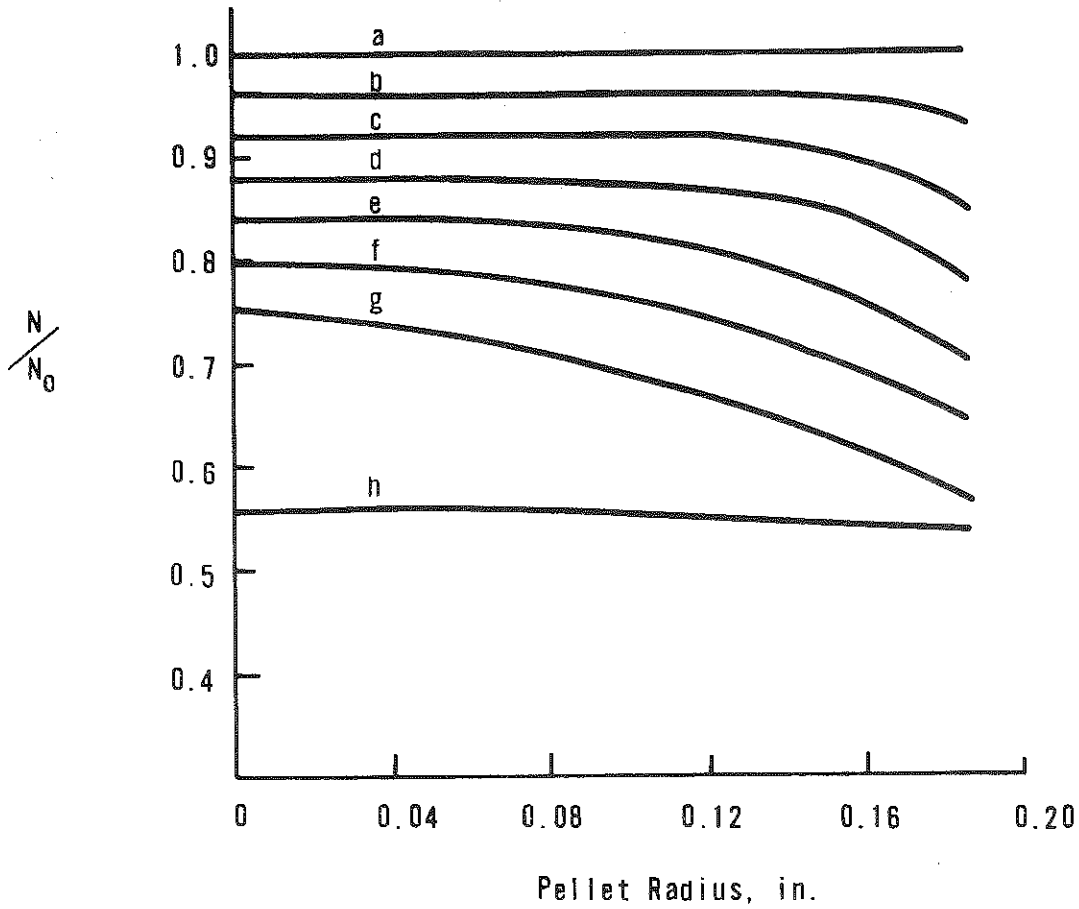
Using PDQ07 for fuel cycle analysis requires that cross sections for isotopes in the fuel be fit as a function of burnup, fuel temperature, coolant specific volume and other core operating parameters. Considerably more fit points are required for $UO_2-Gd_2O_3$ fuel than for UO_2 because of the rapid variation of cross sections during gadolinium burnout. Examples of this effect are illustrated in Figures 5-4 and 5-5. Also, the accuracy of depletion equations for $UO_2-Gd_2O_3$ is strongly dependent on the size of the depletion step. Using NULIF-PEEL, depletion calculations were made with time step intervals of 1, 2, 4, and 8 effective full-power days (EFPDs) (EFPD = 33.52 MWd/mtU). The percentage differences of the computed values of k_{∞} and gadolinium worth, respectively, as a function of total cell burnup are shown in Figures 5-6 and

5-7. A one-day time step is certainly adequate for fuel cycle design, and a larger time step may be adequate when correlations with a larger time step increment are incorporated.

Table 5-1. Characteristics of Natural Gadolinium

<u>Isotope</u>	<u>Natural Abundance, %</u>	<u>Neutron Capture Cross Section, 2200 m/s</u>
Gd-152	0.2	14
Gd-154	2.1	86
Gd-155	14.8	61,000
Gd-156	20.6	1.7
Gd-157	15.7	255,000
Gd-158	24.8	2.0
Gd-160	21.8	0.77

Figure 5-1. U-235 Concentration Vs Pellet Radius and Burnup



INITIAL CONCENTRATIONS

U-235, wt % 2.0
 N_0 (U-235), ATOMS/CC 4.076×10^{20}
 Gd₂O₃, wt % 8.0

BURNUP MWd/mtU

a = 0 WITH Gd₂O₃
 b = 959 WITH Gd₂O₃
 c = 2206 WITH Gd₂O₃
 d = 3762 WITH Gd₂O₃
 e = 5653 WITH Gd₂O₃
 f = 7846 WITH Gd₂O₃
 g = 10348 WITH Gd₂O₃
 h = 10214 WITHOUT Gd₂O₃

Figure 5-2. Gadolinium Worth Vs Burnup

3 x 3 FUEL PIN CELL ARRAY

INNER CELL:

2.0 wt % U235 in U

4.0 and 8.0 wt % Gd₂O₃ in UO₂-Gd₂O₃

OUTER CELLS:

3.5 wt % U235 in U

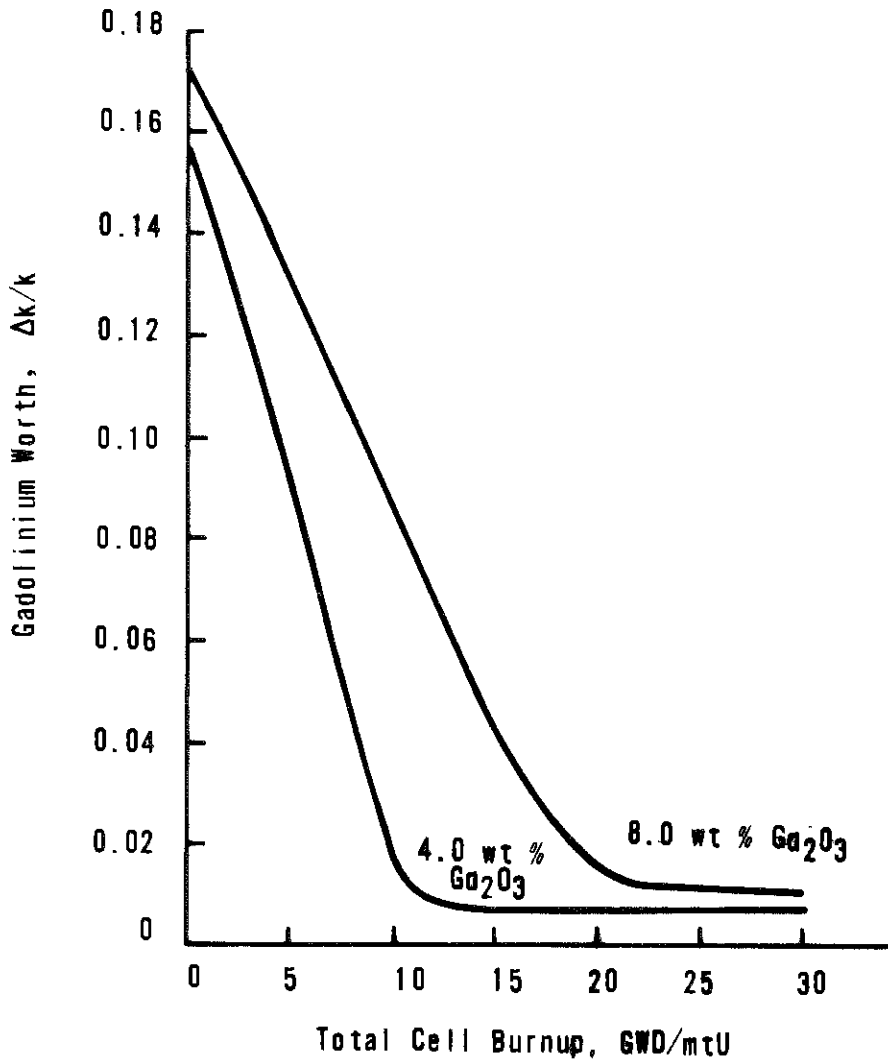


Figure 5-3. Gadolinium Multigroup Nuclear Library Generation

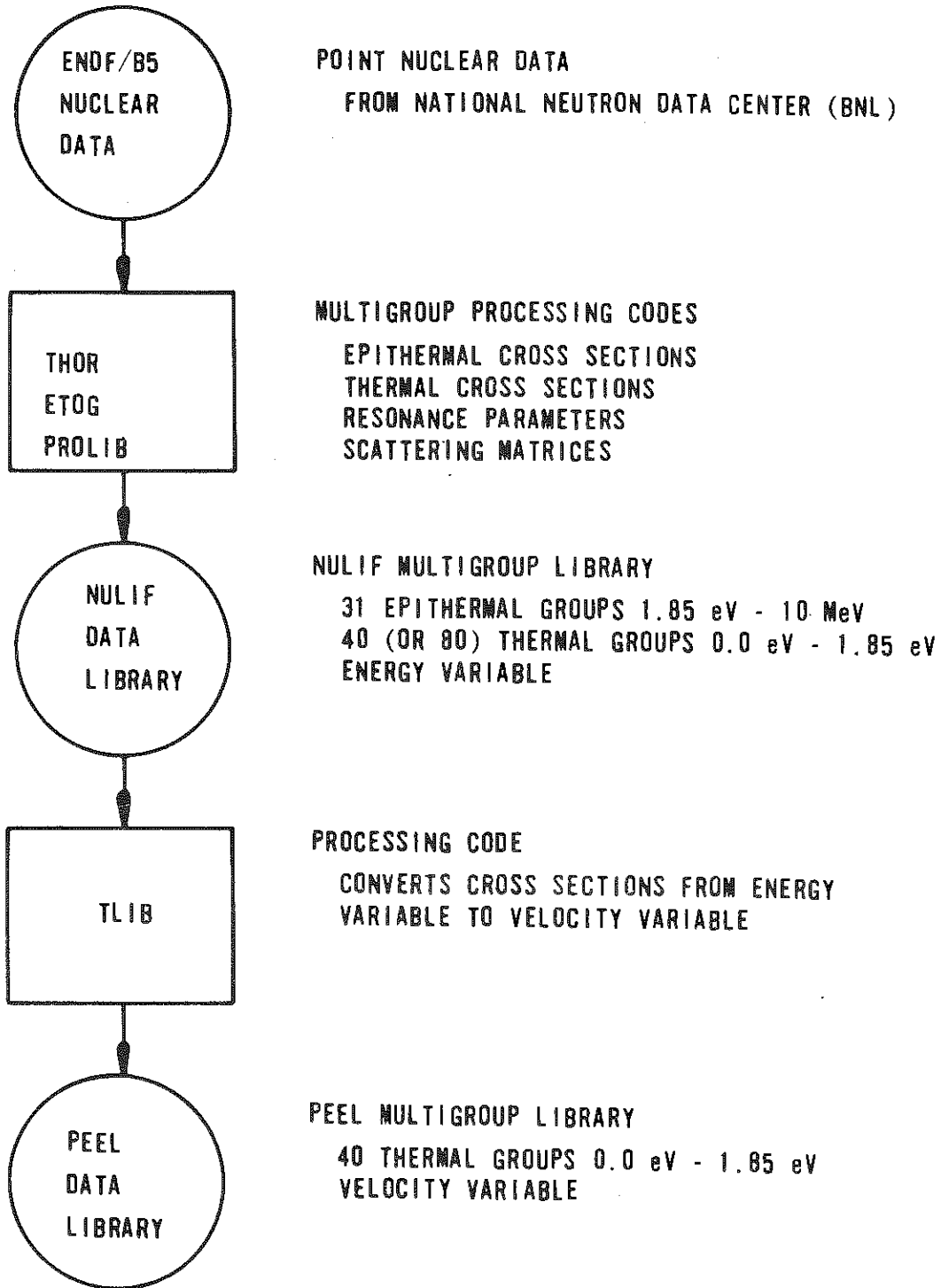
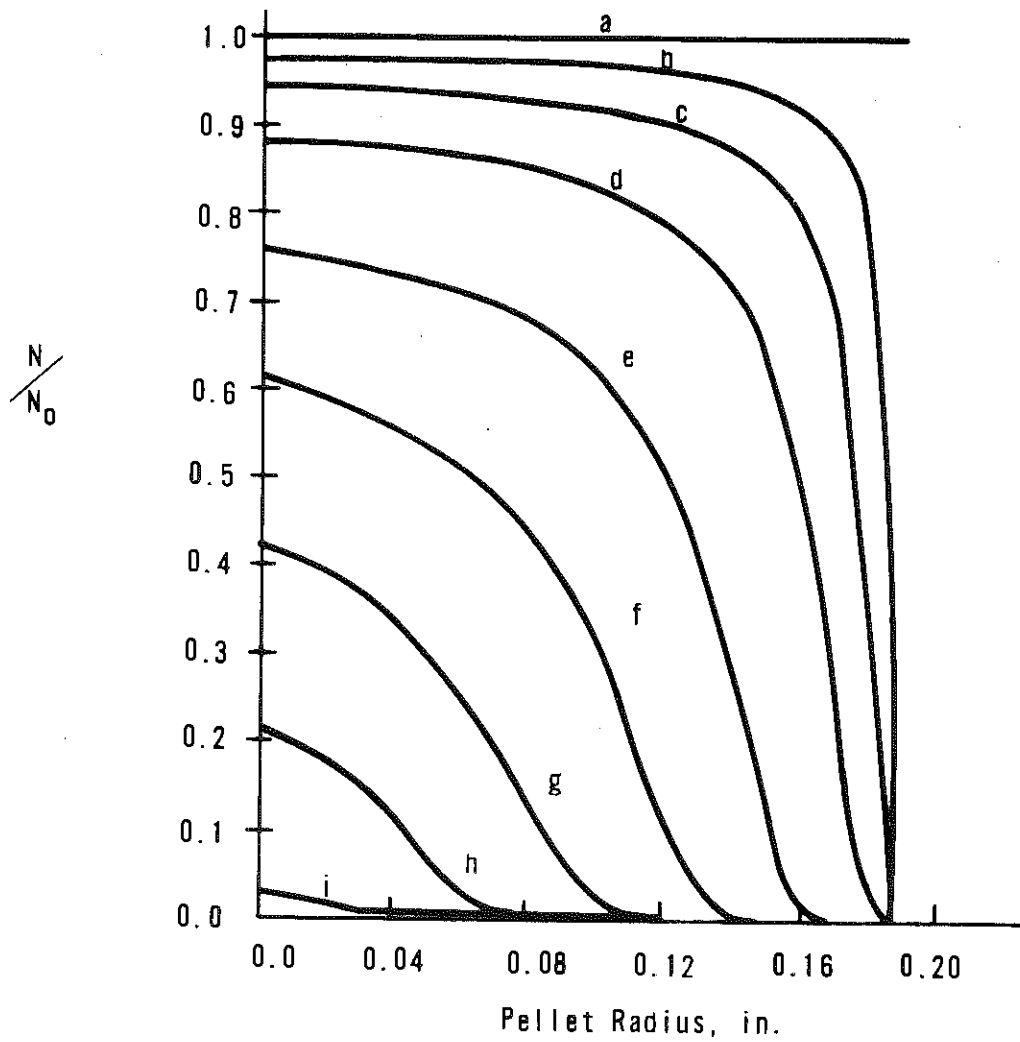
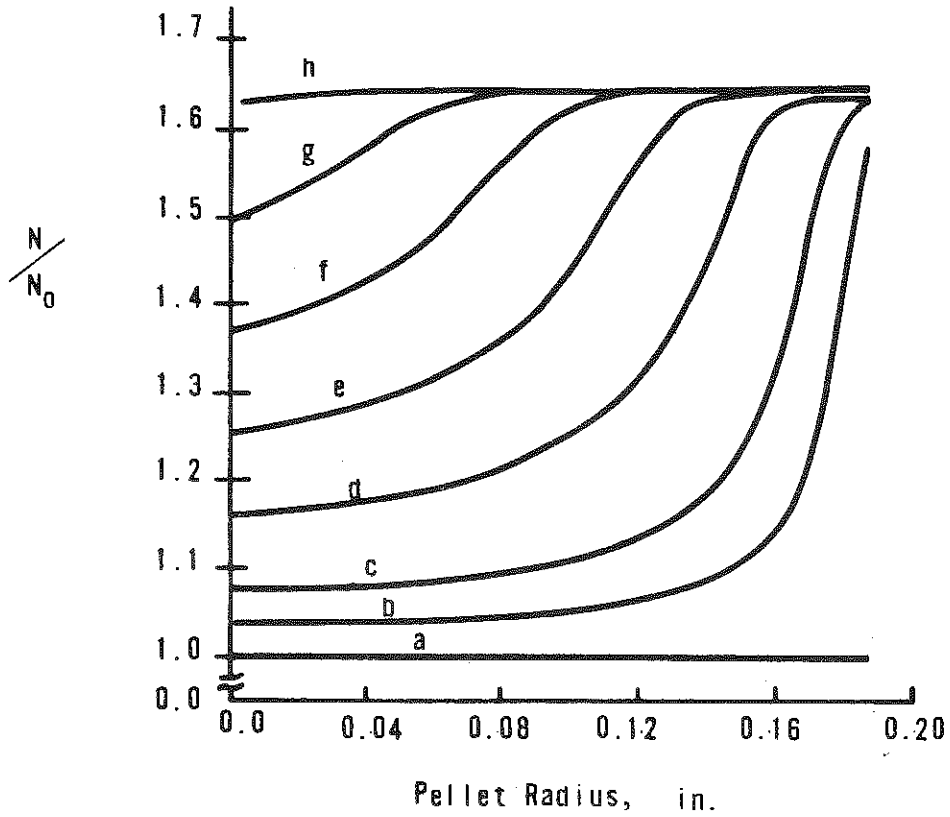


Figure 5-4. Gd-157 Concentration Vs Pellet Radius and Burnup



INITIAL CONCENTRATIONS		BURNUP, MWd/mtU
U-235, wt %	2.0	a = 0
Gd ₂ O ₃ , wt %	8.0	b = 172
N ₀ (Gd-157) ATOMS/CC	4.095 x 10 ²⁰	c = 451
		d = 969
		e = 2206
		f = 3762
		g = 5653
		h = 7846
		i = 10348

Figure 5-5. Gd-158 Concentration Vs Pellet Radius and Burnup



INITIAL CONCENTRATIONS		BURNUP, MWd/mtU
U-235, wt %	2.0	a = 0
Gd ₂ O ₃ , wt %	8.0	b = 451
N ₀ (Gd-158), ATOMS/CC	0.409 x 10 ²⁰	c = 969
		d = 2206
		e = 3762
		f = 5653
		g = 7846
		h = 10348

Figure 5-6. Difference in k_{∞} Vs Time Step Size and Burnup

A-1 DAY STEP
B-2 DAY STEP
C-4 DAY STEP
D-8 DAY STEP

FUEL COMPOSITION, 1.8 wt% U-235

3.0 wt% Gd_2O_3

1 DAY = 33.52 MWd/mtU

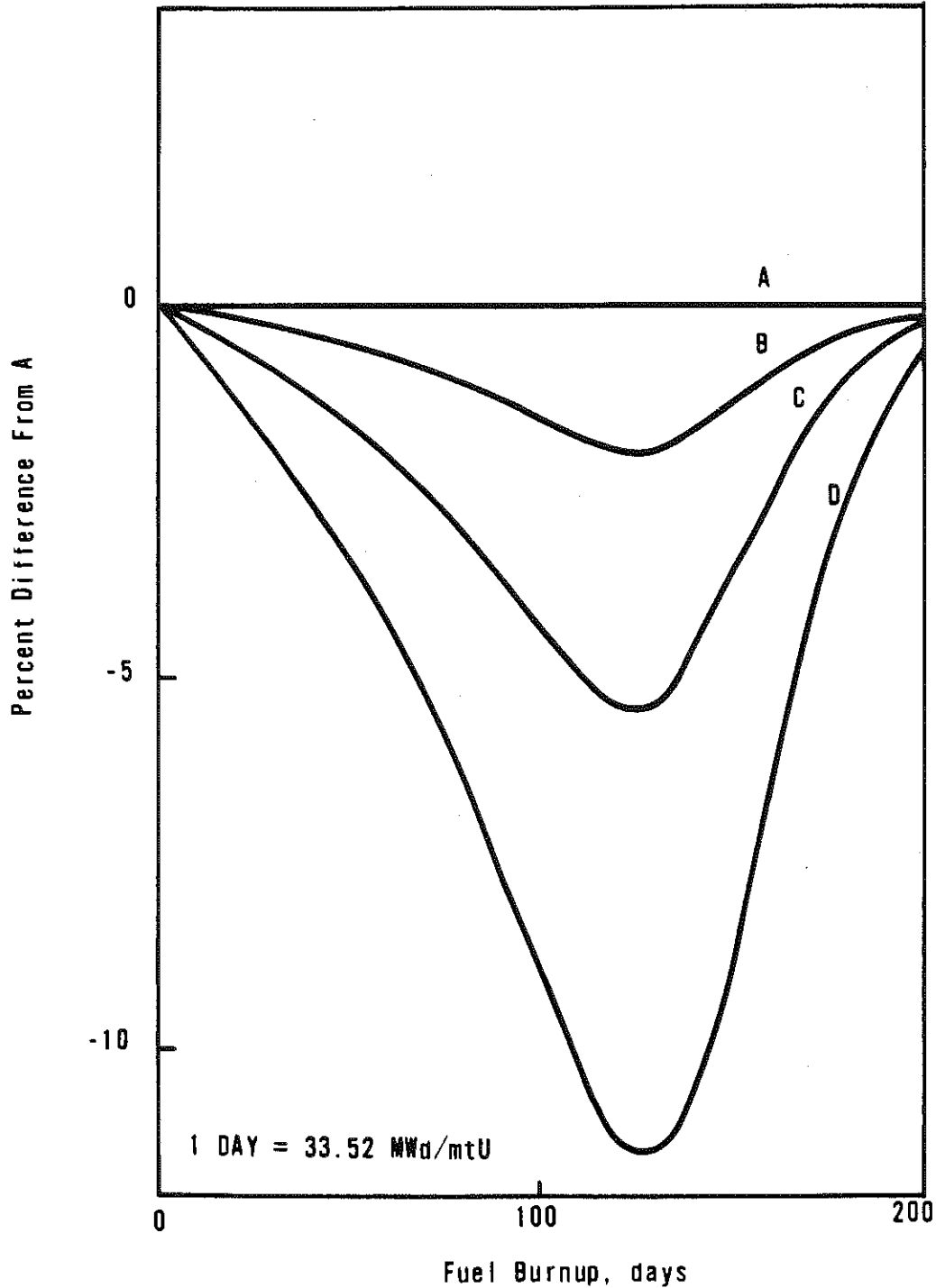


Figure 5-7. Difference in Gadolinium Worth Vs Time Step Size and Burnup

A-1 DAY STEP

B-2 DAY STEP

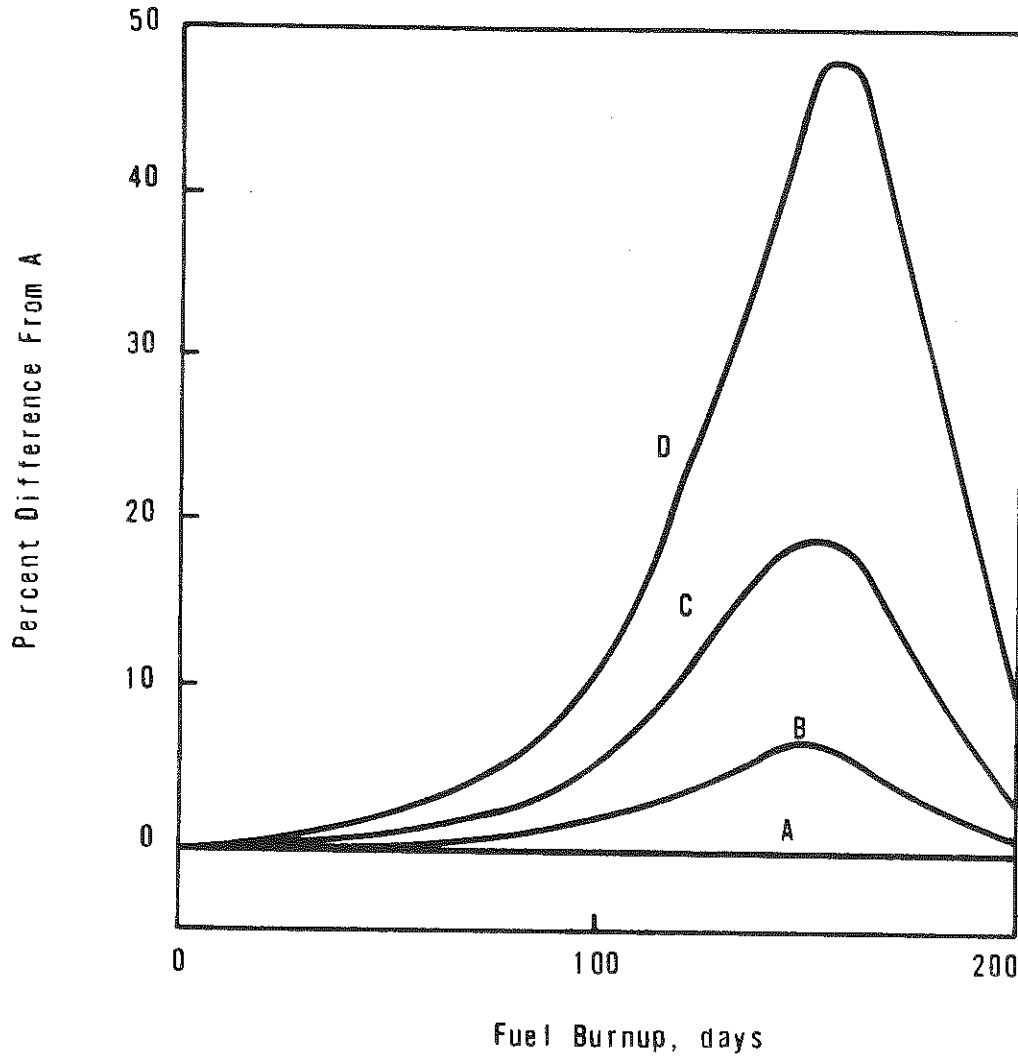
C-4 DAY STEP

D-8 DAY STEP

1 DAY = 33.52 MWd/mtU

FUEL COMPOSITION, 1.8 wt % U-235

3.0 wt % Gd₂O₃



6. COMPARISON OF MEASURED AND CALCULATED RESULTS

6.1. Introduction

Comparisons of measured values with calculated results for reactivity worths and fuel rod average radial powers were performed for core configurations simulating a 15x15 assembly lattice. Detailed radial power profiles across fuel pellets were compared, also. The measurements are, in part, those discussed in section 4. The modeling techniques and model used in the comparisons were described in section 5. Section 6.2 presents the reactivity worth comparisons, and section 6.3 gives the radial power comparisons. The conclusions from the comparisons of the measured and calculated results are given in section 6.4.

6.2. Measured and Calculated Reactivity Worths Comparison

Reactivity worths were compared for UO_2 - Gd_2O_3 , control (Ag-In-Cd or B_4C), and void rods. For these comparisons, the reference cores are designated cores 1 and 12, which have only UO_2 and water holes in the 15x15 lattice. The soluble boron concentration for the calculation was matched to that measured for the reference core configuration to establish a critical eigenvalue for the calculational model. The remaining calculations are performed by varying the soluble boron concentration until the reference critical eigenvalue is obtained. Using this method, a direct comparison can be made between the measured and calculated soluble boron concentrations for the various core configurations.

Measured and calculated soluble boron concentrations were compared for cores 1 through 10 and cores 12 through 17 (described in section 4). The results of these comparisons are given in Tables 6-1 and 6-2.

Figure 6-1 shows the measured and calculated gadolinium worths without either Ag-In-Cd or B_4C control rods present. For those configurations having the 2.46 wt % enriched UO_2 fuel (cores 1 through 10), gadolinium worths without control rods present were predicted within 1.35%, or 2 ppm boron, the

measurement uncertainty for individual data points. The average deviation between measured and predicted $UO_2-Gd_2O_3$ fuel rod worths is -0.28% with a range from -1.3 to +0.9% for the individual cores.

For those cores having an inner zone of 4.02 wt % enriched UO_2 fuel and an outer zone of 2.46 wt % enriched fuel, the predicted gadolinium worths without control rods were within 4.5%, or 11 ppm boron, of those measured. Similar differences were observed in the measurements with control rods present in the mixed enrichment core, suggesting that a bias of about 8.5 ppm boron exists between the measured and calculated results. This bias may be attributed to many factors such as the properties of the UO_2 fuel (sintered pellets versus swaged powder) and uncertainties in the measured (reference) boron of Core 12.

Measured and predicted control rod worths are compared in Figure 6-2. The Ag-In-Cd and B_4C control rod worths are predicted within an average deviation of 0.09% and range from +7.7 to -6.1%. These variations are not considered surprising since the control rods and the gadolinium bearing rods must compete for the thermal neutrons. The combined worths of the $UO_2-Gd_2O_3$ fuel rods and Ag-In-Cd control rods are predicted within an average deviation of -1.48% and range from -3.4 to -0.9%. In four of the five measured cases, the predicted total worths fall within the measurement uncertainty. The combined worths of the $UO_2-Gd_2O_3$ rods and B_4C control rods are predicted within an average deviation of 1.7%. As observed in the mixed enrichment cores without control rods present, the mixed core with control rods shows about an 8.5 ppm boron bias in predicted values relative to measured values.

6.3. Measured and Calculated Radial Power Comparisons

Calculated relative RPDs for the fuel pellets and fuel rods were compared with the measured data reported in section 4. Fuel pellet relative radial power profiles for UO_2 and $UO_2-Gd_2O_3$ pellets were calculated and compared to measurements. Fuel rod relative radial powers for the center assembly for core configurations 1, 5, 12, and 14 and fuel rod relative radial powers along the diagonal of core configurations 5 and 14 were calculated and compared to measurements. The relative radial power for the fuel pellets were produced

using the PEEL code, and the fuel rod (core) power distributions were predicted with the PDQ07 model.

RPDs were calculated for core configurations having 2.46 wt % enriched UO_2 fuel rods (cores 1 and 5) and a combination of 4.02 and 2.46 wt % enriched UO_2 fuel rods (cores 12 and 14). The $UO_2-Gd_2O_3$ fuel rods were modeled as 1.944 wt % enriched UO_2 with 4.0 wt % Gd_2O_3 . The geometric arrangement of the fuel rods and the water holes represented a 3x3 arrangement of fuel assemblies in the central region of a reactor. In this arrangement, the center "assembly" is the primary region of interest because it would closely simulate an assembly in a full-core loading environment. An incore detector string as described in section 4 was modeled, also.

The calculated relative radial power profiles for the UO_2 and $UO_2-Gd_2O_3$ fuel pellets compare excellently with the measured values. Figures 6-3 and 6-4, respectively, show the results of these comparisons. In the comparison for the UO_2 fuel pellet, its relatively flat power profile is accurately predicted by the PEEL model having 15 mesh points across the pellet. In contrast to this flat radial power profile for the fuel pellet, the radial power profile for the $UO_2-Gd_2O_3$ pellet increased markedly at the pellet surface because of the neutron absorption and self-shielding characteristics of the gadolinia. As shown in the figure, the PEEL model accurately predicts these characteristics.

For the relative radial fuel rod profiles, the average root mean square (RMS) (in ΔRPD) of the RPDs in the central assembly of cores 1, 5, 12, and 14 is 0.018 with a maximum RMS of 0.022 and a minimum of 0.013. The RMS values for these four cores are similar in magnitude to values obtained from previous comparisons for poisoned and non-poisoned experiments.²⁵ The average deviation between measured and predicted RPDs for $UO_2-Gd_2O_3$ rods in the central assembly of cores 5 and 14 is 0.012 ΔRPD with a maximum and minimum deviation of 0.019 and 0.006 ΔRPD , respectively. The agreement between measured and calculated values is excellent considering that the measured uncertainty associated with the type of measurement is $\pm 0.01 \Delta RPD$.²⁵

The UO_2 rods surrounding the $UO_2-Gd_2O_3$ rods, in general, have a higher deviation than the average deviation of the assembly. This trend is expected since diffusion theory has inherent difficulty calculating interface effects between neighbors having very dissimilar materials such as UO_2 next to $UO_2-Gd_2O_3$ fuel rods. This trend, however, is amplified because the standard mesh size used in design calculations (one mesh interval per cell) was used for this benchmark, also. The higher-than-average deviation in the UO_2 rods surrounding the $UO_2-Gd_2O_3$ rods has no impact on reactor operating and safety calculations since the important parameter is the radial local value of the assembly (ratio of maximum power rod to assembly average power). As seen from Tables 6-3 through 6-8, the radial local value is predicted within the nuclear uncertainty for design calculations.²⁵ The locations of the fuel rod having the peak measured relative radial power are correctly predicted for cores 1, 5, and 12. For core 14, the rods having the measured and predicted peak power are on the opposite sides of a water hole. Close examination of the measured and predicted power distribution in the center assembly of core 14, especially the maximum power location and its neighboring locations, indicates that the measured peak power might be in error. Examining deviations in the locations neighboring the maximum measured power location, then correlating these deviations with predictions would give a "measured" relative power for the identified peak pin location of 1.126 maximum. Thus, the "true" measured peak location would be in the same location as the predicted peak location.

As seen in Figures 6-5 and 6-6, the differences in the relative radial powers for fuel rods along the core diagonal of core 5 (only 2.46 wt % enriched fuel) and core 14 (4.02 wt % enriched fuel - inner zone and 2.46 wt % enriched fuel - outer zone) compare favorably with results from the central assembly in terms of RMS ΔRPD . Specifically, for core 5, the RMS ΔRPD along the diagonal was 0.015 compared to 0.022 for the central core 5 assembly. For core 14, the RMS ΔRPD s for the diagonal and the central assembly were 0.023 and 0.022, respectively. Examining percent deviation between measured and predicted relative radial power for the fuel rods along the diagonal of cores 5 and 14 revealed an average deviation of 5.6% for $UO_2-Gd_2O_3$ rod locations compared to a 3% deviation for the UO_2 rod locations. This trend is expected because the

relative powers of the $UO_2-Gd_2O_3$ rods are small (~ 0.17), which in turn causes these deviations to be misleadingly larger than for the UO_2 rods with relative powers around 1.0.

The percent deviations for the UO_2 rods in the outer zone of core 14 have a 14% deviation. Even though the relative powers of these rods are smaller than typical for UO_2 rods, a comparable outer zone taken from core 5 showed deviations similar to the inner zones of cores 5 and 14, i.e., a deviation of about 3%. This 11% bias suggests that, in performing the measurements for core 14, both the inner and outer zone should have contained a "master" rod for normalizing measured activity rates.

6.4. Conclusions

The comparisons of measured and calculated data have verified that the modeling techniques and models used to predict the nuclear (nondepletion) characteristics of $UO_2-Gd_2O_3$ fuel and a core containing $UO_2-Gd_2O_3$ fuel are accurate. The two-group, diffusion theory methodology used in core design can accurately predict $UO_2-Gd_2O_3$ effects provided appropriate adjustments are made to the cross-section inputs. These adjustments should at least account for the differences between reaction rates predicted by detailed geometry, transport theory versus those predicted by coarse-mesh, diffusion theory, and include higher-order effects (P_1 versus P_0 scattering approximations) as well as the effect of a multi-epithermal group structure (31 versus 1). These results provide added assurance that the methods and model described herein can be used to design and analyze gadolinia-loaded PWR assemblies without affecting existing nuclear uncertainties.

Table 6-1. Measured and Calculated Worths of Absorber Rods in Various Configurations

Core No.	No. Gd Rods Core/Ctr. FA	Control Rods in Ctr. FA	Moderator Boron Concentration, ppm		Δppm Boron Due to Absorber Rods		% Deviation
			Meas. ±1σ**	Calc*	Meas. ±1σ	Calc.	
-----Cores With 2.46 wt % Enriched UO ₂ Fuel-----							
1	0/0	None	1337.9 ±0.4	1338.0	--	--	--
3	20/8	"	1239.3 ±0.7	1240.7	98.6 ±0.8	97.3	-1.3
5	28/12	"	1208.0 ±0.4	1206.9	129.9 ±0.6	131.1	0.9
5A	32/12	"	1191.3 ±0.5	1192.6	146.6 ±0.6	145.4	-0.8
5B	28/12	"	1207.0 ±1.0	1207.7	130.9 ±1.1	130.3	-0.5
7	28/12 [†]	"	1208.8 ±0.5	1207.9	129.1 ±0.6	130.1	0.8
8	36/16	"	1170.7 ±0.5	1172.2	167.2 ±0.6	165.8	-0.8
2	0/0	(Ag-In-Cd Al Clad)	1250.0 ±1.0	1246.1	87.9 ±1.0	91.9	-4.5
4	20/8	"	1171.7 ±1.0	1177.2	166.2 ±1.1	160.8	-3.4
6	28/12	"	1155.8 ±1.5	1157.5	182.1 ±1.6	180.5	-0.9
6A	32/12	"	1135.6 ±1.8	1139.0	202.3 ±1.8	199.0	-1.6
9	36/16	"	1130.5 ±0.6	1131.8	207.4 ±0.7	206.0	-0.6
10	36/16	Void	1177.1 ±0.6	1178.7	160.8 ±0.7	159.3	-0.9
-----Cores With 4.02/2.46 wt % Enriched Inter/Outer Zone UO ₂ Fuel-----							
12	0/0	None	1899.3 ±0.9	1899.0	--	--	--
14	28/12	"	1653.8 ±0.7	1642.5	245.5 ±1.1	256.5	4.5
16	36/16	"	1579.4 ±0.9	1571.4	319.9 ±1.3	327.6	2.4
13	0/0	(B ₄ C Al ⁴ C ₁ Clad)	1635.4 ±0.7	1617.0	263.9 ±1.1	282.0	6.7
15	28/12	"	1479.7 ±0.6	1463.3	419.6 ±1.1	425.7	1.5
17	36/16	"	1432.1 ±1.5	1412.8	467.2 ±1.7	476.2	1.9

† - Annular Gd rods used instead of solid rods.

* - Calculated by boron iteration for a constant eigenvalue.

** - A ±1σ deviation applies to the series of measurements used to determine the average soluble boron concentration; individual measurements have a ±2 ppm uncertainty.

Table 6-2. Measured and Calculated Worth of 16 Control Rods in Various Gd Configurations

Core No.'s	No. Gd Rods Core/Ctr FA	Control Rods in Ctr. FA	Δppm Boron Due to Control Rods		% Deviation
			Meas. ±1σ	Calc.	
-----Cores With 2.46 wt % Enriched UO ₂ Fuel-----					
1-2	0/0	Ag-In-Cd	87.9 ±1.1	91.1	3.6
3-4	20/8	"	67.6 ±1.2	63.5	-6.1
5-6	28/12	"	52.2 ±1.6	49.4	-5.4
5A-6A	32/12	"	55.7 ±1.9	53.6	-3.8
8-9	36/16	"	40.2 ±0.8	40.4	0.5
8-10	36/16	Void	-6.4 ±0.8	-6.5	1.6
-----Cores With 4.02/2.46 wt % Enriched Inner/Outer Zone UO ₂ Fuel-----					
12-13	0/0	B ₄ C	263.9 ±1.1	282.0	6.9
14-15	28/12	"	174.1 ±0.9	179.2	2.9
16-17	36/16	"	147.3 ±1.7	158.6	7.7

See footnotes on Table 6-1.

Table 6-3. Comparison of Normalized* Relative Power Densities for Center Assembly, Core 1 – without $UO_2-Gd_2O_3$

INCORE DET	1.025	1.013	1.002	0.997	0.992	0.970	0.945
	1.018	1.011	0.987	0.981	0.997	0.966	0.945
	0.007	0.002	0.015	0.016	-0.005	0.004	0.000
	1.039	1.054	1.035	1.031	1.035	0.995	0.952
	1.019	1.067	1.012	1.009	1.058	0.999	0.945
	0.020	-0.013	0.023	0.022	-0.023	-0.004	0.007
		WATER	1.075	1.074		1.020	0.958
			1.081	1.090	WATER	1.032	0.953
			-0.006	-0.026		-0.012	0.005
			1.086	1.097†	1.073	1.001	0.950
			1.054	1.104	1.086	0.989	0.945
			0.032	-0.007	-0.013	0.012	0.005
				WATER	1.039	0.968	0.935
					1.059	0.965	0.934
					-0.020	0.003	0.001
					0.990	0.943	0.921
					0.988	0.938	0.923
					0.002	0.005	-0.002
						0.922	0.908
						0.925	0.914
						-0.003	-0.006
							0.897
							0.903
							-0.006

XXX	Predicted Relative Power
YYY	Measured Relative Power
ZZZ	Predicted-Measured Values

$RMS_{\Delta RPD} = 0.013$.

*Measured and Predicted Powers are normalized to an assembly average power of 1.0.

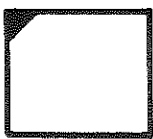
†Location of maximum measured and predicted pin power.

Table 6-4. Comparison of Normalized* Relative Power Density for Center Assembly, Core 5 – with Gd₂O₃

INCORE	0.993	0.952	0.189	0.976	1.045	1.068	1.077
DET	1.005	0.913	0.170	0.932	1.036	1.063	1.072
	-0.012	0.039	0.019	0.044	0.009	0.005	0.005
	1.006	1.001	0.975	1.019	1.090	1.094	1.084
	0.999	1.017	0.931	1.007	1.125	1.094	1.089
	0.007	-0.016	0.044	0.012	-0.035	0	-0.005
		WATER	1.009	1.060		1.120+	1.089
			0.988	1.087	WATER	1.158	1.100
			0.021	-0.027		-0.038	-0.011
			0.195	1.066	1.116	1.090	1.078
			0.181	1.050	1.131	0.088	1.086
			0.014	0.016	-0.015	0.002	-0.008
				WATER	1.048	0.033	1.057
					1.048	1.035	1.070
					0	-0.002	-0.013
					0.201	0.999	1.044
					0.187	0.963	1.054
					0.014	0.036	-0.010
						1.014	1.045
						1.018	1.060
						-0.004	-0.015
							1.052
							1.070
							-0.018

XXX
YYY
ZZZ

Predicted Relative Power
Measured Relative Power
Predicted-Measured Values



UO₂-Gd₂O₃ Fuel Rod Location

RMS_{ΔRPD} = 0.021

*Measured and predicted powers are normalized to an assembly average power of 1.0.
+Location of maximum and predicted pin power.

Table 6-5. Comparison of Measured and Predicted Fuel Rod
Relative Power Density Distribution along
Core Diagonal, Core 5

(Normalized to Center Fuel Assembly Power Density)

Fuel Rod Position	Relative Power Density		Deviation	% Deviation
	Measured	Calculated		
S1E1	0.999	1.006	0.007	0.70
S2E2	water	water	-	-
S3E3*	0.181	0.195	0.014	7.73
S4E4	water	water	-	-
S5E5*	0.187	0.201	0.014	7.49
S6E6	0.018	1.014	-0.004	-0.39
S7E7	1.070	1.052	-0.018	-1.68
S8E8	1.067	1.051	-0.016	-1.50
S9E9	1.018	1.009	-0.009	-0.88
S10E10*	0.187	0.199	0.012	6.42
S11E11	water	water	-	-
S12E12*	0.177	0.192	0.015	8.47
S13E13	water	water	-	-
S14E14	1.028	1.025	-0.003	-0.29
S15E15	water	water	-	-
S16E16	1.016	1.026	0.010	0.98
S17E17	water	water	-	-
S18E18	0.961	0.980	0.019	1.98
S19E19	water	water	-	-
S20E20	0.799	0.809	0.010	1.25
S21E21	0.728	0.704	-0.024	-3.30
S22E22	0.641	0.633	-0.008	-1.25
S23E23	0.590	0.565	-0.025	-4.24
S24E24	0.527	0.496	-0.031	-5.88
S25E25	0.439	0.425	-0.014	-3.19
S26E26	0.366	0.355	-0.011	-3.01
S27E27	0.293	0.290	-0.003	-1.02
S28E28	0.236	0.233	-0.003	-2.30
S29E29	0.193	0.191	-0.002	-1.04
S30E30	0.188	0.172	-0.016	-8.51
RMSΔRPD	-	0.015	-	-

*UO₂-Gd₂O₃ fuel rod.

NOTE: Fuel rod position indicators are described in section 4.

Table 6-6. Comparison of Normalized* Relative Power Densities for Center Assembly, Core 12 – without UO_2 - Gd_2O_3

Incore Det.	1.076	1.053	1.031	1.017	1.003	0.964	0.921
	1.075	1.041	1.006	1.019	1.000	0.960	0.923
	0.001	0.012	0.025	-0.002	0.003	0.004	-0.002
	1.091	1.102	1.069	1.055	1.055	0.993	0.927
	1.067	1.125	1.044	1.034	1.075	0.987	0.927
	0.024	-0.023	0.025	0.021	-0.020	0.006	0
		Water	1.117	1.107		1.022	0.930
			1.114	1.118	Water	1.034	0.942
			0.003	-0.011		-0.012	-0.012
			1.123	1.132+	1.094	0.992	0.917
			1.083	1.137	1.102	0.979	0.908
			0.040	-0.005	-0.008	0.013	0.009
				Water	1.045	0.945	0.894
					1.071	0.939	0.895
					-0.026	0.006	-0.001
					0.976	0.909	0.871
					0.958	0.900	0.883
					0.018	0.009	-0.012
						0.875	0.847
						0.884	0.856
						-0.009	-0.009
							0.824
							0.845
							-0.021

XXX Predicted Relative Power
 YYY Measured Relative Power
 ZZZ Predicted-Measured Power

RMS Δ RPD = 0.015

* Powers are normalized to an assembly average power of 1.0.

+ Location of maximum measured and predicted pin power.

Table 6-7. Comparison of Normalized* Relative Power Densities for Center Assembly, Core 14 - with Gd₂O₃

Incore Det.	1.070	1.029	0.169	1.022	1.054	1.045	1.024
	1.091	0.992	0.162	0.976	1.057	1.038	1.028
	-0.021	0.037	0.007	0.046	-0.003	0.007	-0.004
	1.085	1.086	1.051	1.069	1.111	1.077	1.031
	1.080	1.118	1.000	1.054	1.158++	1.091	1.028
	0.005	-0.032	0.051	0.015	-0.047	-0.014	0.003
		Water	1.094	1.121	Water	1.109	1.035
			1.072	1.138		1.140	1.038
			0.022	-0.017		-0.031	-0.003
			0.173	1.136	1.147+	1.072	1.019
			0.164	1.114	1.151	1.059	1.013
			0.009	0.022	-0.004	0.013	0.006
				Water	1.076	1.010	0.993
					1.080	1.011	1.003
					-0.004	-0.001	-0.010
					0.168	0.970	0.970
					0.162	0.942	0.976
					0.006	0.028	-0.006
						0.957	0.954
						0.965	0.978
						-0.008	-0.024
							0.941
							0.959
							-0.018

Indicates UO₂-Gd₂O₃ fuel

XXX	Predicted Relative Power
YYY	Measured Relative Power
ZZZ	Predicted-Measured Power

RMS ΔRPD = .022

* Normalized to an assembly average power of 1.0

† Location of maximum predicted pin power.

†† Location of maximum measured pin power.

Table 6-8. Midplane Relative Power Density Distribution
Along Core Diagonal, Core 14

(Normalized to Central Fuel Assembly Power Density)

Fuel Rod Position	Relative Power Density		Deviation	% Deviation
	Measured	Calculated		
S1E1	1.080	1.085	0.005	0.46
S2E2	water	water	-	-
S3E3*	0.164	0.173	0.009	5.49
S4E4	water	water	-	-
S5E5*	0.162	0.168	0.006	3.70
S6E6	0.965	0.957	-0.008	-0.83
S7E7	0.959	0.941	-0.018	-1.88
S8E8	0.917	0.902	-0.015	-1.64
S9E9	0.864	0.842	-0.022	-2.55
S10E10*	0.133	0.136	0.003	2.26
S11E11	water	water	-	-
S12E12*	0.113	0.117	0.004	3.54
S13E13	water	water	-	-
S14E14	0.663	0.654	-0.009	-1.36
S15E15	water	water	-	-
S16E16	0.470	0.422	-0.048	-10.21
S17E17	water	water	-	-
S18E18**	0.394	0.360	-0.034	-8.63
S19E19	water	water	-	-
S20E20**	0.303	0.272	-0.031	-10.23
S21E21**	0.273	0.228	-0.045	-16.48
S22E22**	0.238	0.198	-0.040	-16.81
S23E23**	0.201	0.172	-0.029	-14.43
S24E24**	0.174	0.146	-0.028	-16.09
S25E25**	0.145	0.123	-0.022	-15.17
S26E26**	0.119	0.100	-0.019	-15.97
S27E27**	0.094	0.080	-0.014	-14.89
S28E28**	0.073	0.063	-0.010	-13.70
S29E29**	0.059	0.050	-0.009	-15.25
S30E30**	0.055	0.043	-0.012	-21.82
RMSΔRPD	-	0.023	-	-

*UO₂-Gd₂O₃ rod.

**2.46 wt % enriched fuel rod.

Figure 6-1. Gadolinia Worth Measured Vs Calculated — No CRAs in Core

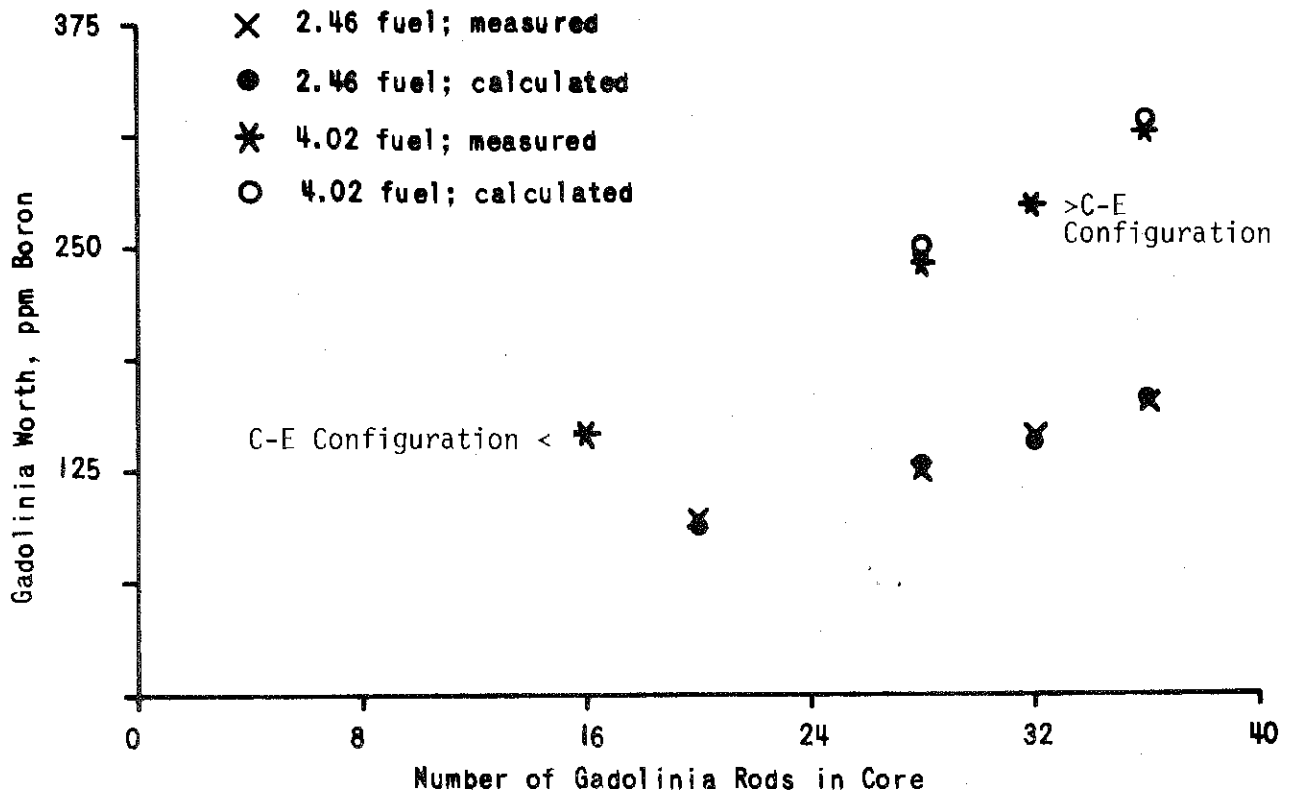


Figure 6-2. Measured and Calculated Control Rod Worth

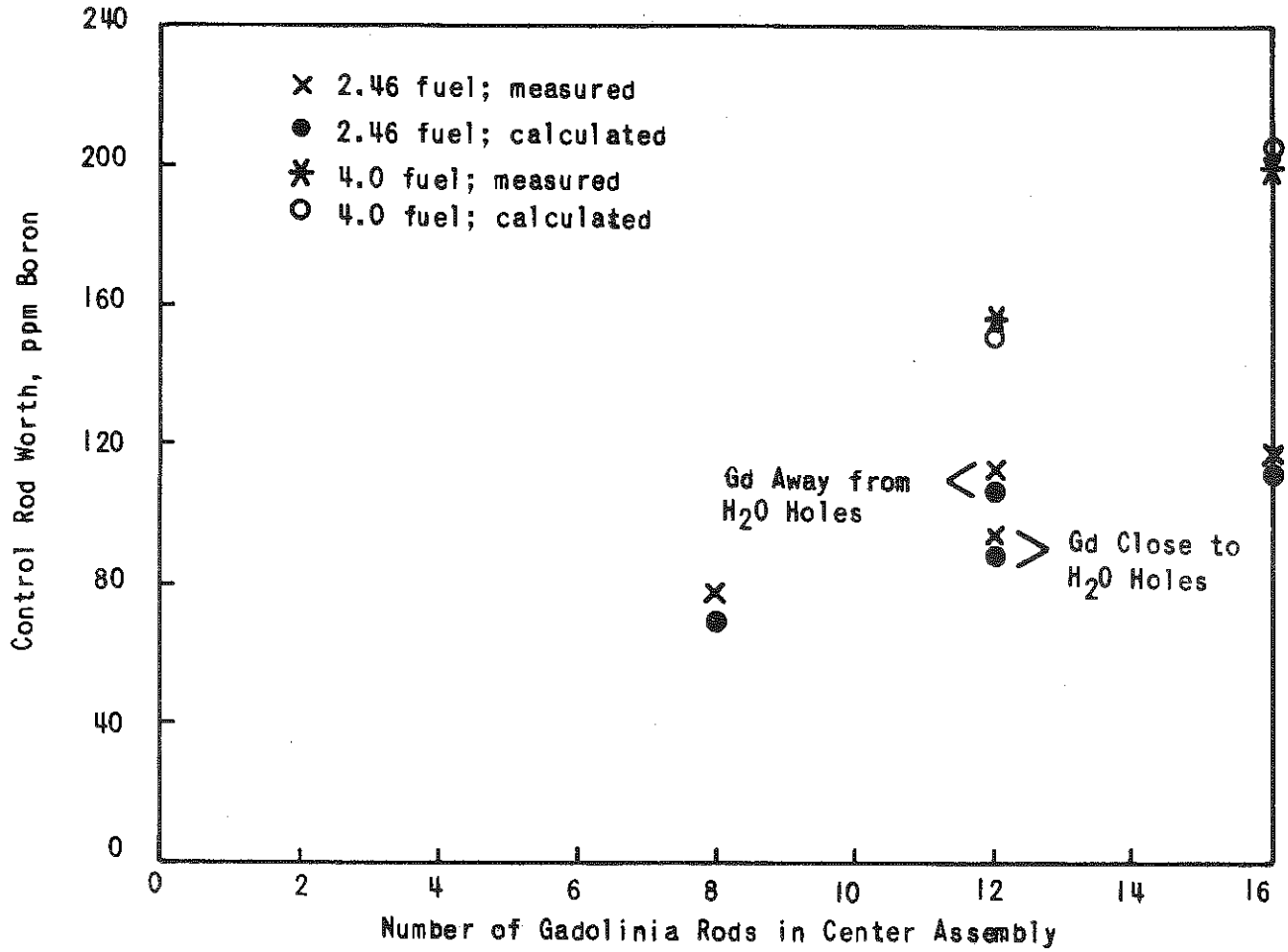


Figure 6-3. Radial Power Distribution Through UO₂ Fuel Pellet

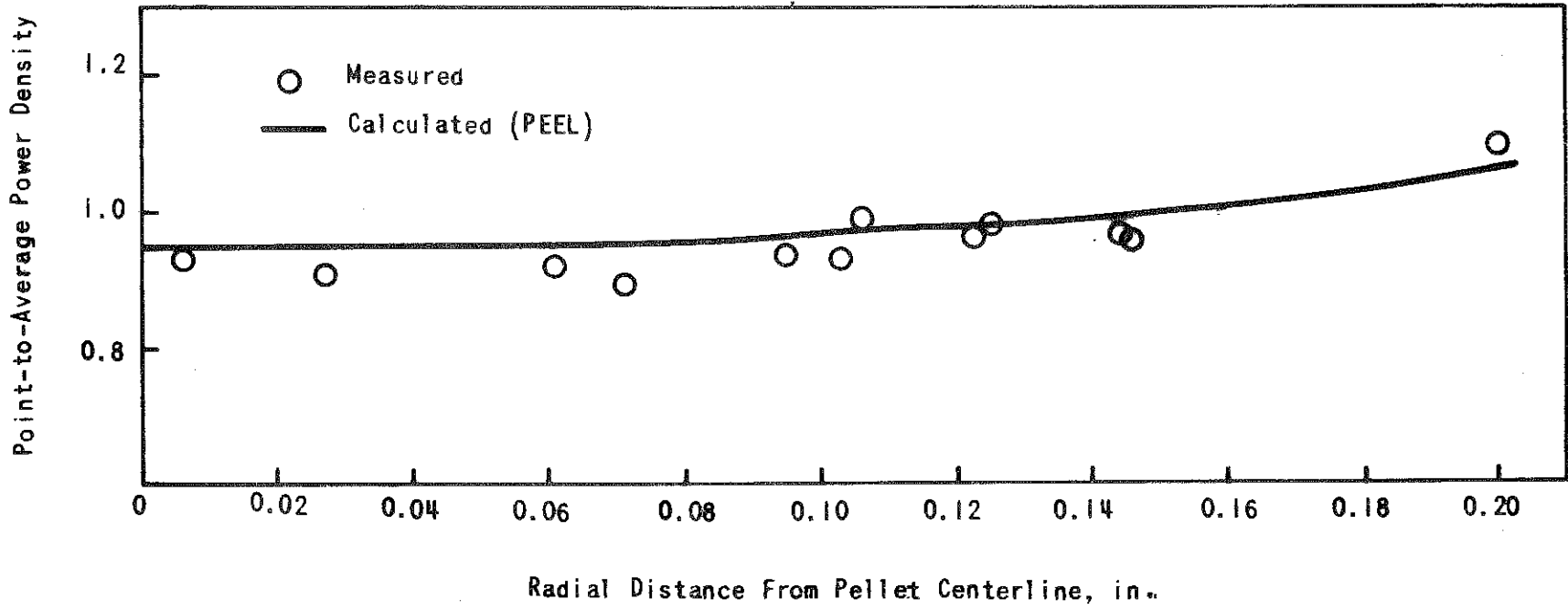


Figure 6-4. Radial Power Distribution Through UO_2 - Gd_2O_3 Fuel Pellet

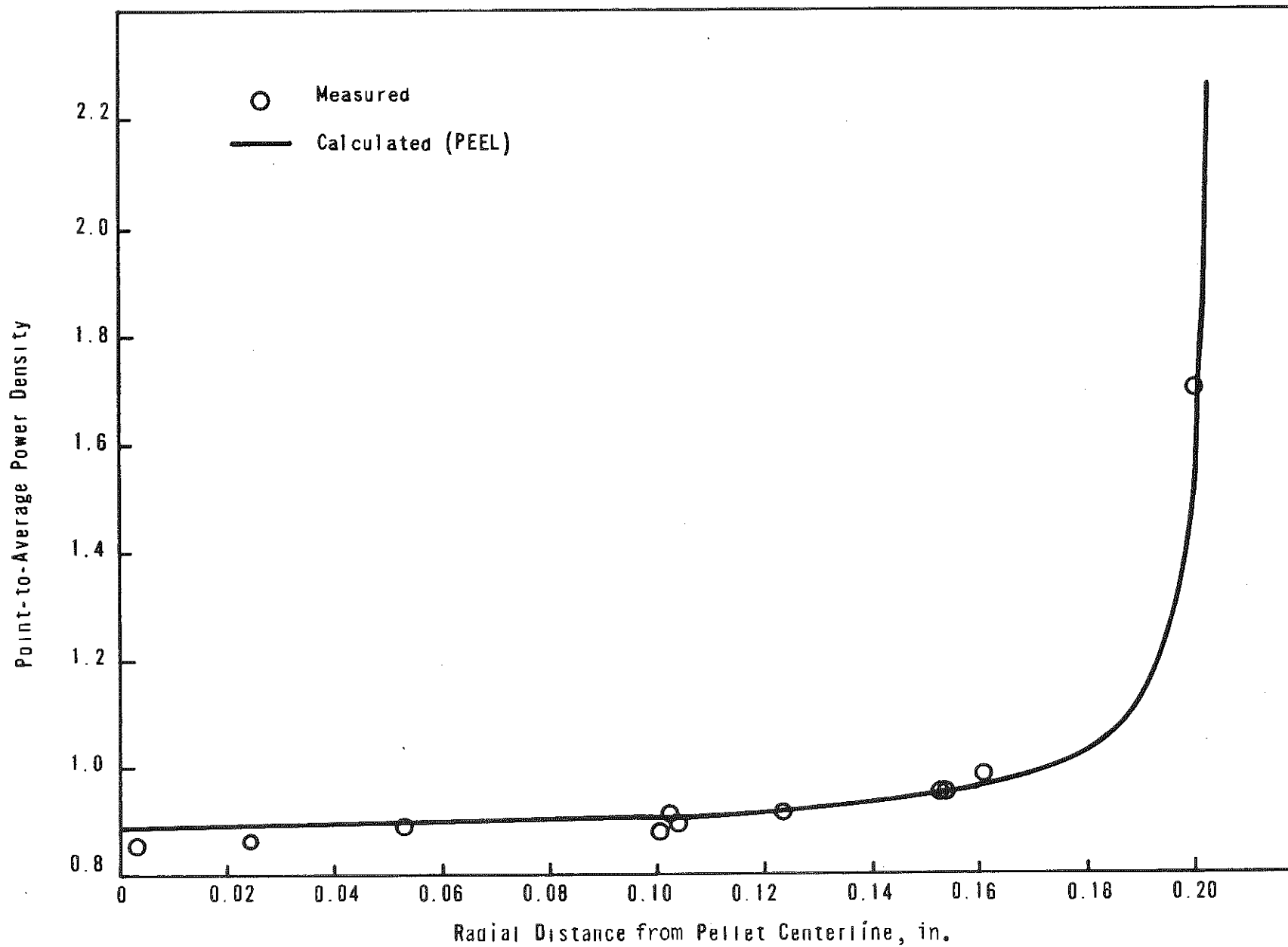


Figure 6-5. Comparison of Measured and Predicted Fuel Rod Powers Along Core 5 Diagonal

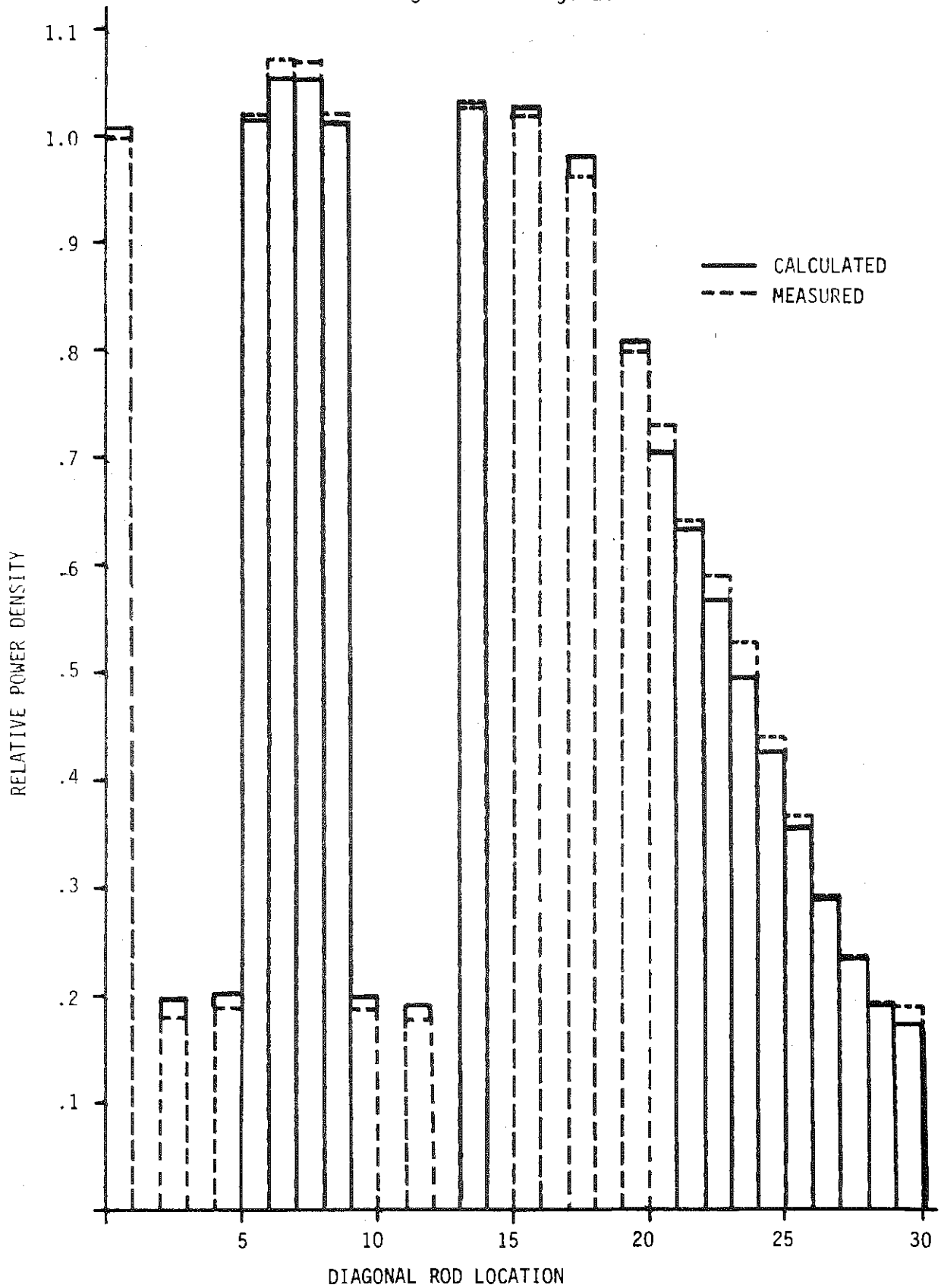
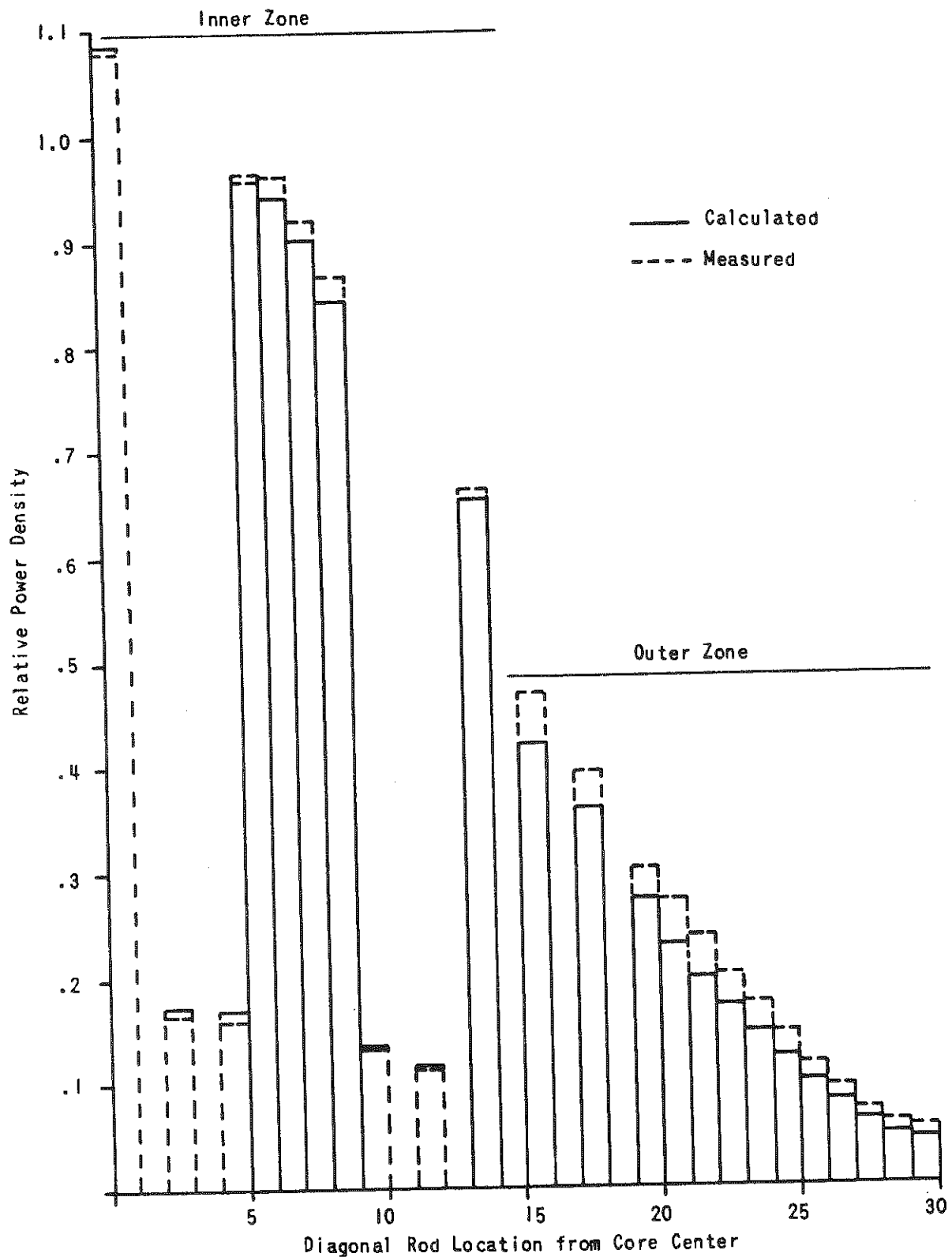


Figure 6-6. Comparison of Measured and Predicted Fuel Rod Powers Along Core 14 Diagonal



7. REFERENCES

1. L. W. Newman, et al., Development and Demonstration of an Advanced Extended-Burnup Fuel Assembly Design Incorporating Urania-Gadolinia: First Semi-Annual Progress Report, March - September 1981, BAW-1681-1, Babcock & Wilcox, Lynchburg, Virginia, February 1982.
2. L. W. Newman, et al., Development and Demonstration of an Advanced Extended-Burnup Fuel Assembly Design Incorporating Urania-Gadolinia: Second Semi-Annual Progress Report, October 1981 - March 1982, BAW-1681-2, Babcock & Wilcox, Lynchburg, Virginia, August 1982.
3. L. W. Newman, et al., Development and Demonstration of an Advanced Extended-Burnup Fuel Assembly Design Incorporating Urania-Gadolinia: Third Semi-Annual Progress Report, April - September 1982, BAW-1681-3, Babcock & Wilcox, Lynchburg, Virginia, September 1983.
4. L. W. Newman, et al., Development and Demonstration of an Advanced Extended-Burnup Fuel Assembly Design Incorporating Urania-Gadolinia: Fourth Semi-Annual Progress Report, October 1982 - March 1983, BAW-1681-4, Babcock & Wilcox, Lynchburg, Virginia, February 1984.
5. R. H. Clark and T. C. Engelder, Spectral Shift Control Reactor Basic Physics Program Critical Experiments Hazard Evaluation, BAW-1211, Babcock & Wilcox, Lynchburg, Virginia, September 1960 (also Supplement No. 1).
6. T. C. Engelder, et al., SSCR Basic Physics Program - Quarterly Technical Report No. 7, BAW-1259, Babcock & Wilcox, Lynchburg, Virginia, September 1962.
7. T. C. Engelder, et al., SSCR Basic Physics Program - Measurement and Analysis of Uniform Lattices of Slightly Enriched UO_2 Moderated by D_2O-H_2O Mixtures, BAW-1273, Babcock & Wilcox, Lynchburg, Virginia, November 1963.
8. R. M. Ball, et al., NMSR-MARTY Critical Experiments - Summary of 4% Enriched UO_2 Cores Studies, BAW-1216, Babcock & Wilcox, Lynchburg, Virginia, May 1961.
9. T. C. Engelder, et al., SSCR Basic Physics - Critical Experiments on Lattices Moderated by D_2O-H_2O Mixtures, BAW-1231, Babcock & Wilcox, Lynchburg, Virginia, December 1961.
10. E. Hellstrand, "Measurements of the Effective Resonance Integral in Uranium Metal and Oxide in Different Geometries," J. Appl. Phys., 28, 12, 1493 (1957). [Revised S. Pearlstein, ed., BNL-NCS 50-541, XVI, (1975)].
11. L. A. Hassler and N. M. Hassan, ANISNBW - A One-Dimensional Discrete Ordinate Transport Code, NPGD-TM-491, Rev. 2, Babcock & Wilcox, Lynchburg, Virginia, October 1980.

12. W. A. Wittkopf, et al., NULIF - A Neutron Spectrum Generator, Few-Group Constant Calculator, and Fuel Depletion Code, BAW-10115A, Babcock & Wilcox, Lynchburg, Virginia, February 1977.
13. BNC 325 Third Edition, June 1973.
14. R. T. Birge, Phy. Rev., 40, pp 207-227, (1932).
15. D. V. Huntsberger and P. Billingsley, Elements of Statistical Inference, Third Edition, Allyn and Bacon, Inc., (1973).
16. A. Z. Livolsi and W. A. Wittkopf, PEEL-A Transport Code for Spatial Depletion, BAW-1419, Babcock & Wilcox, Lynchburg, Virginia, October 1981.
17. M. N. Baldwin, et al., Critical Experiments Supporting Close Proximity Water Storage of Power Reactor Fuel, BAW-484-1, Babcock & Wilcox, Lynchburg, Virginia, May 1976.
18. M. N. Baldwin, Physics Verification Program - Summary Report, BAW-3647-37, Babcock & Wilcox, Lynchburg, Virginia, May 1976.
19. W. A. Wittkopf, J. M. Tilford, and G. Kirschner, ETOGM - Epithermal Cross Section Generation Code Using ENDF/B Data, BAW-10112, Babcock & Wilcox, Lynchburg, Virginia, October 1975.
20. J. B. Andrews, II, N. M. Hassan, and W. A. Wittkopf, THOR - Thermal Cross Section Generation Code Using ENDF/B Data, BAW-10113, Babcock & Wilcox, Lynchburg, Virginia, October 1975.
21. W. A. Wittkopf, J. M. Tilford and M. Furtney, PROLIB - Code to Create Production Library of Nuclear Data for Design Calculations, BAW-10114, Babcock & Wilcox, Lynchburg, Virginia, October 1975.
22. M. R. Gudorf, et al., Assembly Calculations and Fitted Nuclear Data, BAW-10116, Babcock & Wilcox, Lynchburg, Virginia, August 1976.
23. H. A. Hassan, et al., Babcock & Wilcox Version of PDQ07 - User's Manual, BAW-10117, Babcock & Wilcox, Lynchburg, Virginia, June 1976.
24. R. D. Mosteller, "An Automated Diffusion Theory Parameterization for Gadolinia-Loaded PWR Assemblies," Trans. Am. Nucl. Soc., 39, 906 (1981).
25. H. A. Hassan, et al., Power Peaking Nuclear Reliability Factors, BAW-10119A, Babcock & Wilcox, Lynchburg, Virginia, February 1979.
26. R. D. Mosteller, et al., "Design Implementation, Part I, Chapter 6 of the ARMP System Documentation," EPRI, CCM-3, (September 1977).
27. R. J. Breen, "A One-Group Model for Thermal Activation Calculation," Nuclear Science and Engineering, 9, 91 (1961).

APPENDIX
Gadolinia Critical Benchmark with EPRI-ARMP Codes

1.1. Introduction

The EPRI-ARMP codes were benchmarked to the data obtained from $\text{UO}_2\text{-Gd}_2\text{O}_3$ critical experiments. The facility, fuel, fuel placement within the core, and experiments were described in sections 3 and 4.

The design models for the EPRI-ARMP codes are described in section 1.2, while the measured-to-calculated comparisons are discussed in section 1.3 and 1.4. The comparisons are presented in the following order:

- o Gadolinia rod reactivity worths
- o Relative power density distributions

The results are summarized in section 1.5.

1.2. EPRI-ARMP Model Description

The ARMP PWR gadolinia model^{26,27} utilizes three computer codes: EPRI-CELL, GAD, and PDQ-7. The EPRI-CELL Model is used to obtain two energy group neutron cross sections for both the UO_2 and $\text{UO}_2\text{-Gd}_2\text{O}_3$ fuel cells plus the water regions such as guide tube cells and instrument cells. The GAD code is used to apply a transport-to-diffusion correction to the thermal group cross sections for the $\text{UO}_2\text{-Gd}_2\text{O}_3$ fuel cells obtained from EPRI-CELL. This correction factor is intended to preserve the cell/buffer reaction rate ratio from EPRI-CELL within the thermal group of the PDQ-7 assembly calculations. Finally, the resulting two-group cross sections are used in the two-dimensional PDQ-7 diffusion theory calculations for a quarter of the experimental core. All cross sections used in the comparisons were provided by Dr. R. D. Mosteller of S. Levy, Inc.

1.3. Reactivity Worth of $\text{UO}_2\text{-Gd}_2\text{O}_3$ Fuel Rods

Figure A-1 compares measured and calculated critical boron concentrations. The boron concentrations for cores 3, 5, 5A, 5B, and 8 were derived by matching the eigenvalue obtained from the core 1 calculation while varying the soluble boron concentration. The measured and calculated reactivity worths of the $\text{UO}_2\text{-Gd}_2\text{O}_3$ fuel rods are provided in Table A-1 and Figure A-2. The calculated and measured reactivity worths of the $\text{UO}_2\text{-Gd}_2\text{O}_3$ fuel rods are all within 2 ppm soluble boron -- the uncertainty associated with the soluble boron concentration measurement. Both the measured and calculated data display an approximately linear relationship between increases in reactivity worth and increases in the number of $\text{UO}_2\text{-Gd}_2\text{O}_3$ fuel rods in the core.

1.4. Relative Power Density Distribution

The measured and calculated normalized RPDs in the center assembly are compared in Figures A-3 and A-4 for cores 1 and 5, respectively. In addition, the normalized RPDs on the main diagonal of core 5 are included in Table A-2 and Figure A-5. The results of the EPRI-ARMP PDQ-7 calculations show the following:

1. The RMS differences of the RPDs in the center assembly of both cores 1 and 5 are small; however, the deviations in core 5 are larger than those exhibited in the core 1 comparison. The larger deviations are caused by the large Δ RPDs in the $\text{UO}_2\text{-Gd}_2\text{O}_3$ fuel rods and their surrounding fuel rods.
2. The location of the fuel rod having the maximum RPD is predicted correctly in both cores. The calculated RPD of this rod is within 0.016 RPD of the measured values in both cases.
3. The RPDs in the $\text{UO}_2\text{-Gd}_2\text{O}_3$ fuel rods are over-predicted by 0.025; the RPDs in the surrounding fuel rods are under-predicted by 0.02 and 0.03.

4. The RPDs on the main diagonal of core 5 are accurately predicted. The RPDs for fuel rods adjacent to water holes are, however, larger than those of the fuel rods not near water holes. This effect is consistent with the general behavior of pin-wise power distributions obtained from the ARMP model. Using mixed number density (MND)²³ thermal cross sections and generating fast water-hole cross sections with an infinite-medium spectrum combine to produce a conservative estimate of the power in pins adjacent to water holes (where the peak pin power normally occurs).

1.5. Summary

The ARMP PWR gadolinia model has predicted the gadolinium worth for each of the five geometries studies within the experimental uncertainty associated with the measurement (viz., 2 ppm). Furthermore, the predicted power distributions are in excellent agreement with the measured ones. These results provide added assurance that the ARMP system can be used with confidence for the analysis and design of gadolinia-loaded PWR assemblies.

Table A-1. Measured and Calculated Reactivity Worths
of Gadolinia-bearing Rods

Core	Gd rods, total No.	Moderator boron concentration ppm		Difference between core moderator boron concen- trations, ppm	
		(Meas.)	(Pred.)	(Meas.)	(Pred.)
1	0	1338	1338	0	0
3	20	1239	1239	99	99
5	28	1208	1206	130	132
5A	32	1191	1189	147	149
5B	28	1207	1206	131	132
8	36	1171	1170	167	168

Table A-2. RPDs on the Main Diagonals of Core 5

Position ^(a)	RPD ^(b)		Deviation
	(Meas.)	(Calc.)	
S1E1	0.999	1.021	0.022
S2E2		Water	
S3E3*	0.180	0.203	0.023
S4E4		Water	
S5E5*	0.187	0.211	0.024
S6E6	1.018	1.009	-0.009
S7E7	1.070	1.083	0.013
S8E8	1.067	1.082	0.015
S9E9	1.018	1.005	-0.013
S10E10*	0.187	0.210	0.023
S11E11		Water	
S12E12*	0.177	0.201	0.024
S13E13		Water	
S14E14	1.028	1.028	0.000
S15E15		Water	
S16E16	1.016	1.036	0.020
S17E17		Water	
S18E18	0.961	0.988	0.027
S19E19		Water	
S20E20	0.799	0.825	0.026
S21E21	0.728	0.721	-0.007
S22E22	0.641	0.654	0.013
S23E23	0.590	0.584	-0.006
S24E24	0.527	0.511	-0.016
S25E25	0.439	0.436	-0.003
S26E26	0.366	0.360	-0.006
S27E27	0.293	0.288	-0.005
S28E28	0.236	0.223	-0.013
S29E29	0.193	0.177	-0.016
S30E30	0.188	0.177	-0.011

(a) The coordinate SaEb indicates that the pin is located in a pin pitches south by b pitches east of the core center.

(b) The RPDs are the PDs relative to the PDs of the central assembly.

*UO₂-Gd₂O₃ fuel rods.

Figure A-1. Boron Concentration Measured Vs Calculated

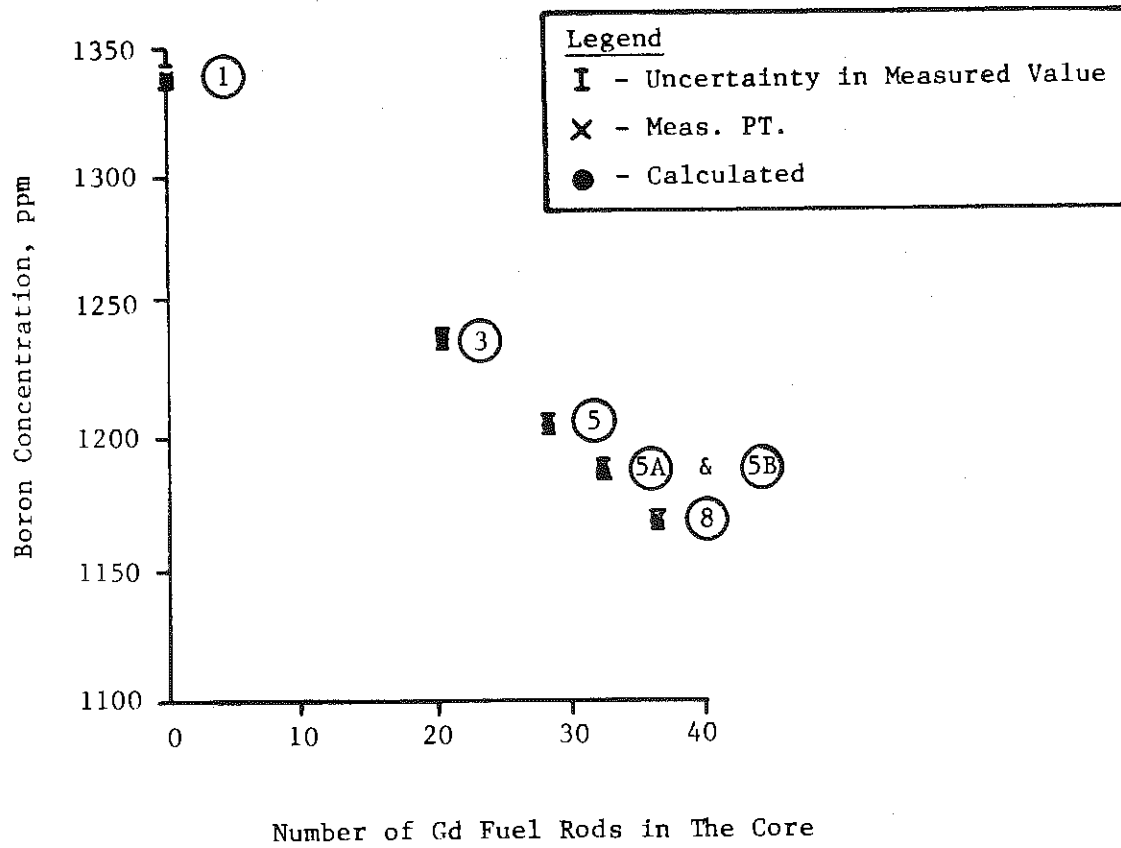


Figure A-2. Gd Worth Measured Vs Calculated

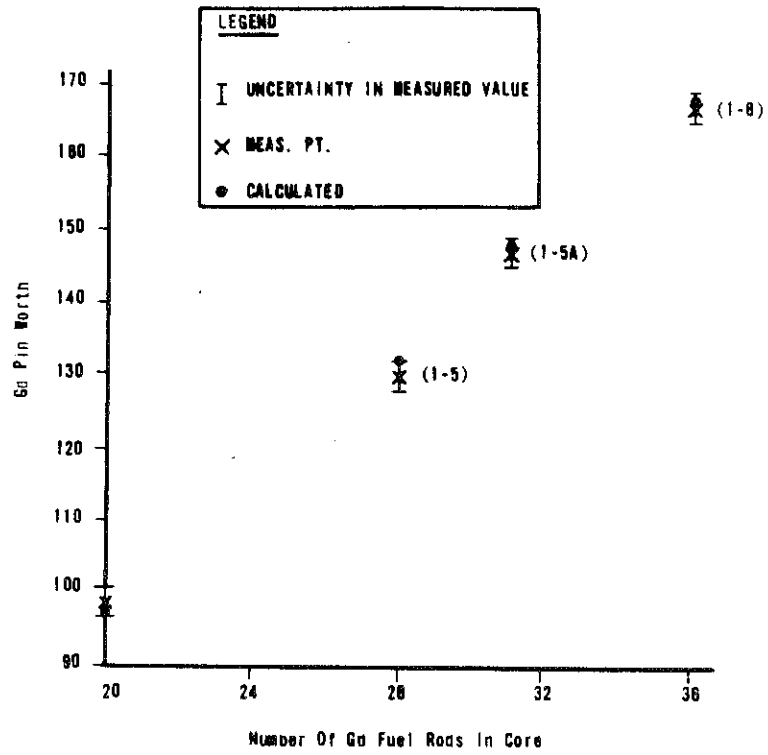


Figure A-3. Comparisons of Measured and Predicted Normalized Relative Power Densities for Core 1

IN CORE DETECTOR	1.018	1.011	.987	.981	.997	.966	.945
	1.038	.997	.979	.975	.978	.958	.936
	.020	-.014	-.008	-.006	-.019	-.008	-.009
	1.019	1.067	1.012	1.009	1.058	.999	.945
	1.035	1.069	1.015	1.012	1.054	.988	.941
	.016	.002	.003	.003	-.004	-.011	-.004
		WATER	1.081	1.090	WATER	1.032	.953
			1.087	1.089		1.045	.947
			.006	-.001		.013	-.006
			1.054	1.104*	1.086	.989	.945
			1.070	1.117*	1.100	.994	.939
			.016	.013	.014	.005	-.006
				WATER	1.059	.965	.934
					1.062	.957	.928
					.003	-.008	-.006
					.988	.938	.923
					.986	.937	.919
					-.002	-.001	-.004
				Measured RPD	.925	.914	
				Calculated RPD	.921	.911	
				Δ RPD	-.004	-.003	
						.903	
						.903	
						.000	

$RMS(\Delta RPD) = 0.008$

$Max (ABS(\Delta RPD)) = 0.020$

*Maximum power fuel rod predicted or measured.

Figure A-4. Comparisons of Measured and Predicted Normalized Relative Power Densities for Core 5

INCORE- DETECTOR	1.005	.913	.170	.932	1.036	1.063	1.072
	1.026	.886	.196	.903	1.045	1.077	1.090
	.021	-.027	.026	-.029	.009	.014	.018
	.999	1.017	.931	1.007	1.125	1.094	1.089
	1.021	1.012	.901	.997	1.135	1.112	1.096
	.022	-.005	-.030	-.010	.010	.018	.007
		WATER	.988	1.087		1.158*	1.100
			.962	1.073	WATER	1.174*	1.102
			-.026	-.014		.016	.002
			.181	1.050	1.131	1.088	1.086
			.203	1.035	1.158	1.105	1.090
			.022	-.015	.027	.017	.004
				WATER	1.048	1.035	1.070
					1.018	1.018	1.070
					-.030	-.017	.000
					.187	.963	1.054
					.211	.939	1.058
					.024	-.024	.004
				Measured RPD		1.018	1.060
				Calculated RPD		1.009	1.069
				Δ RPD		-.009	.009
							1.070
							1.083
							.013

UO₂-
Gd₂O₃

$$\text{RMS}(\Delta\text{RPD}) = 0.018$$

$$\text{Max}(\text{ABS}(\Delta\text{RPD})) = 0.030$$

*Maximum power fuel rod predicted or measured.

Figure A-5. Comparison of Measured and Predicted Relative Fuel Rod Powers Along Core Diagonal

